**UNIVERSITY OF MANITOBA**

# Gradient Flow in Holographic Superconductors

by

Paul Mikula

A thesis submitted to the Faculty of Graduate Studies of
UNIVERSITY OF MANITOBA
in partial fulfilment of the requirements of the degree of
DOCTOR OF PHILOSOPHY

Faculty of Science
Department of Physics and Astronomy

UNIVERSITY OF MANITOBA

# *Abstract*

Faculty of Science
Department of Physics and Astronomy

Doctor of Philosophy

by Paul Mikula

We study the gradient flow equations derived from an Einstein-Maxwell-Higgs model in 3+1 dimensions. We see how this model relates to a phenomenological description of a superconductor in two ways. In flat spacetime the model is equivalent to the Ginzburg-Landau theory of superconductivity and describes a 3 dimensional superconductor. In curved spacetime with negative cosmological constant, we can apply the AdS/CFT correspondence to obtain a 2 dimensional theory on the boundary that describes a superconductor. The gradient flow equations in both cases are a system of parabolic partial differential equations analagous to the heat equation. The flow describes a non-isolated system where energy is allowed to dissipate as the system evolves towards thermal equilibrium. In the first case the gradient flow gives rise to the time-dependent Ginzburg-Landau equations, and we study the formation and interaction of superconducting vortices. In the second case, the flow in the bulk describes the formation of scalar hair around a black hole, which corresponds to the formation of a superconducting condensate on the boundary. The flow in the bulk creates an equivalent flow on the boundary that can be thought of as an extension of the AdS/CFT correspondence to non-equilibrium configurations.

# *Acknowledgements*

I would like to thank my supervisors Gabor Kunstatter and Margaret Carrington for their guidance and advice throughout my graduate studies. I would also like to thank all those involved at the physics departments at the University of Winnipeg and Brandon University.

This thesis was possible in part due to the funding support from the University of Manitoba Graduate Fellowship, and the Natural Sciences and Engineering Research Council of Canada.

# Contents

# List of Figures

# Chapter 1

# Introduction

## 1.1 Overview

The study of systems away from equilibrium, and in particular how systems return to equilibrium is a subject of great interest in physics. Tools from perturbation theory can be used to study systems very close to equilibrium but not systems far from equilibrium. In order to understand a field theory far from equilibrium it is helpful to study how its free energy depends on the fields. Gradient flow is a potential tool for studying non-equilibrium physics because it defines a path through the field space along lines of steepest descent of the free energy. Gradient flow can be used to understand not just the evolution of the state of a system as it equilibrates, but can also provide information about the timescales at which the process occurs. In this thesis we use gradient flow to study equilibration in two different contexts: vortices in planar Ginzburg-Landau theory and the flow of boundary operator expectation values in a holographic superconductor. The gradient flow equations describing both these systems are derivable from the free energy of Einstein-Maxwell-Higgs theory. The remainder of Chapter 1 will provide some

background on superconductors, AdS/CFT correspondence, and gradient flow in general. Chapter 2 expands upon these concepts in the context of the Einstein-Maxwell-Higgs action in particular. In Chapter 3 the gradient flow is applied to a superconductor described by Ginzburg-Landau theory to obtain the time dependent Ginzburg-Landau equations [1]. In Chapter 4 the gradient flow is applied to a system describing a superconductor through the AdS/CFT correspondence, providing a possible extension of the correspondence to non-equilibrium states [2].

## 1.2 Superconductors

A superconductor is a material that allows electrical current to flow with zero resistance. Superconductivity was first found by Kammerlingh Onnes in 1911 by cooling mercury to the temperature of liquid helium (approximately 4 K). Superconductivity has since been observed in many metal elements and alloys. The critical temperature ($T_c$) at which they transition from the normal metal phase to a superconducting phase is a property of the material. Superconductors carry current with zero resistance and without loss of energy or heat production, which means they can carry much larger currents than a conventional conductor and maintain them without additional energy input. The main use of superconductors today is in superconducting electromagnets, which are typically made from a Neobium-Titanium alloy that has $T_c \approx 10K$. Since the magnetic field produced by an electromagnet is proportional to the current in the wire, superconducting electromagnets are much stronger than conventional electromagnets. However, since the temperatures required for superconductivity are so low, superconducting electromagnets are mainly used in highly specialized applications such as MRI machines and high energy particle colliders. It is difficult to predict the technological advancements that could arise from the discovery of room temperature superconductivity, but the search for materials with

higher $T_c$ has been ongoing for the last century. In 1986 a major breakthrough occured when superconductivity was discovered in cuprates [3], which were the first of the so-called "high temperature superconductors". Although the critical temperature of high temperature superconductors is still far below room temperature, some cuprates have $T_c > 77K$ which means that they become superconducting at the temperature of liquid nitrogen. This eliminates the need for helium, which is scarce and expensive, in the cooling process. In 2008 high temperature superconductivity was also discovered in iron pnictides [4], and presently cuprates and iron pnictides are active areas of experimental research on high temperature superconductivity. Although significant experimental progress has been made in finding new materials with higher critical temperatures, we still do not have a good theoretical understanding of the mechanisms behind the onset of superconductivity, or how to predict the critical temperature of high temperature superconductors. Understanding the mechanisms behind high temperature superconductivity could pave the way to the discovery of superconductors with even higher critical temperatures.

There are currently two theoretical models for superconductivity, a microscopic theory and a macroscopic phenomenological theory. The microscopic theory of superconductivity, BCS theory, was first proposed in 1957 by Bardeen, Cooper and Schrieffer [5]. The phenomenological theory of superconductivity, Ginzburg-Landau (GL) theory, was proposed in 1950 by Ginzburg and Landau. The two theories work well to describe conventional superconductors, and it has been shown that GL theory is a limiting case of BCS theory valid near the critical temperature. We will discuss GL theory in more detail in Chapters 2 and 3. BCS theory describes superconductivity as being the result of the condensation of electrons into pairs called Cooper pairs. Electrons will begin to condense into Cooper pairs as long as there is an attractive potential between two electrons that exceeds the Coulomb repulsion. For conventional superconductors BCS theory describes how this potential arises from interactions between the negatively charged electrons and

the positively charged atomic lattice. The first electron attracts nearby positive ions in the lattice, which creates a region of increased positive charge that attracts the second electron.

Superconductivity in high temperature superconductors is still expected to be the result of the formation of Cooper pairs, but the mechanism that causes the condensation is not well understood. While cuprates and iron pnictides are quite different in terms of elemental composition, they are both layered superconductors. In these materials the atomic lattice consists of superconducting layers (copper and oxygen layers in cuprates or iron pnictide layers in iron pnictides) and spacing layers. The layered structure means that the electron interactions in the layers are described by 2+1 dimensional quantum electrodynamics (QED). The difficulty in understanding these systems theoretically arises because in 2 dimensions QED becomes strongly coupled at low energies, and strongly coupled systems are much harder to deal with mathematically.

## 1.3 Holographic Principle

The holographic principle is the idea that all of the information in our 3 dimensional universe is contained on a 2 dimensional surface at the boundary. The idea was originally proposed by 't Hooft and further developed in the context of string theory by Susskind in 1995 [6]. The holographic principle became a subject of great interest in 1999 when Maldacena proved the equivalence between a string gravity theory in $AdS_5 \times S_5$ containing $N$ branes and a super symmetric Yang-Mills (SYM) field theory with $\mathcal{N} = 4$ supersymmetries, and gauge group $SU(N)$ in 3+1 dimensions in the limit where $N$ is large [7]. He conjectured that the equivalence would be very general, and different compactifications of the gravity theory would be equivalent to different conformal field theories (CFTs) on the boundary. This equivalence is often referred to as the AdS/CFT correspondence or

gauge/gravity duality. Typically the AdS spacetime is called "the bulk" and the gravity theory in AdS space is called "the bulk theory" and the conformal gauge field theory on the boundary is "the boundary theory".

The main appeal of the AdS/CFT correspondence is that a strongly coupled theory is in the large $N$ limit equivalent to a 'corresponding' weakly coupled theory. This makes it possible to study a strongly coupled system indirectly by working with a weakly coupled theory, which is in general much easier to deal with mathematically. The main downside of the correspondence is that standard model physics is not supersymmetric nor does it have a large number $N$ of gauge groups. Nevertheless, there has been a great deal of interest in the AdS/CFT correspondence as a computational tool for dealing with strongly coupled field theories. Due to the weak/strong nature of the correspondence, we can study strongly coupled field theories indirectly by looking at weakly coupled gravity theories. This allows us to avoid a full string theoretical description and work instead with classical Einstein gravity in the bulk.

It is not clear to what extent the AdS/CFT correspondence can accurately describe the behaviour of a physical system that is strongly coupled. Some generic properties of strongly coupled systems can be found by studying systems with gravity duals, and these properties can be tested experimentally. One particular success of this approach was the calculation of the ratio of the shear viscosity to the entropy density ($\eta/s$) in quark-gluon plasma [8]. By studying a broad class of strongly coupled plasmas using their weakly coupled gravitational duals a lower bound for $\eta/s$ was conjectured. The value of $\eta/s$ determined in experiments at the Large Hadron Collider was very close to this bound, suggesting that quark gluon plasmas described with quantum chromodynamics may be well approximated by plasmas described by a gravitational dual in one higher dimension through the AdS/CFT correspondence. In addition to its applications to quark gluon

plasma, the AdS/CFT correspondence has been applied to many other problems, such as relativistic hydrodynamics, dark matter, and superconductivity.

As we mentioned in the previous section, it is thought that high temperature superconductors will require a strongly coupled description due to their layered structure. It is often sufficient to consider only a single layer and neglect the effect of interactions between layers. Since each superconducting layer can be described using 2+1 dimensional QED they can be studied using a gravity theory in 3+1 dimensional AdS spacetime. A superconductor described through the AdS/CFT correspondence is called a holographic superconductor. A minimal bulk theory that describes a 2+1 dimensional superconductor on the boundary is discussed in more detail in Chapter 2.

## 1.4 Gradient Flow

Gradient flows are a method for describing the evolution (or "flow") of fields with respect to a flow parameter $\tau$ based on the steepest descent curves of a generating functional. In terms of a physical field theory the functionals of interest are the action or free energy, and the equations of motion of a system are obtained from the requirement that the fields extremize the action. The gradient flow equations are partial differential equations that evolve the fields from a specified starting point along a path that attempts to minimize the free energy as fast as possible.

Gradient flows have many applications in both mathematics and physics. There are two notable and particularly relevant applications of gradient flow in mathematics. The first is the use of the gradient flow of the Yang-Mills functional, or Yang-Mills Flow, to study the topology of Riemann surfaces [9]. The second is Ricci flow, which was shown by Perelman in 2003 to be the gradient flow of a modified Einstein-Hilbert action and was

the key to his proof of Thurston's geometrization conjecture [10]. Gradient flows have also been used in applications in other areas such as image processing [11] and machine learning [12].

In general, if we have some energy functional $\mathcal{E}(\Phi^I)$ that depends on a set of fields $\Phi^I$, and an inner product for our fields

$$\langle \delta\Phi | \delta\Phi \rangle \quad := \quad \int dx\, G_{IJ}\, \delta\Phi^I(x) \delta\Phi^J(x)\,. \tag{1.1}$$

We can define the gradient flow equations

$$\frac{d\Phi^I(x)}{d\tau} = -G^{IJ} \frac{\delta\mathcal{E}}{\delta\Phi^J(x)}\,. \tag{1.2}$$

The flow equations (1.2) are not necessarily gauge invariant, so extra terms that fix the gauge along the flow are required. Extra terms of this type are known as "deTurck terms". Suppose the energy is invariant under the infinitesmal transformation:

$$\delta\Phi^I(x) = K^I_\alpha(x)\xi^\alpha(x) \tag{1.3}$$

for a set of arbitrary parameters $\xi^\alpha(x)$ so that:

$$\delta\mathcal{E} = \int dx \frac{\delta\mathcal{E}}{\delta\Phi^I(x)} K^I_\alpha(x)\xi^\alpha(x) = 0\,. \tag{1.4}$$

The $K$'s generally involve differential operators and functions of the fields. For example, in the case of Yang-Mills theory a gauge transformation of the vector potential is

$$\delta A^a_\mu(x) = \partial_\mu \chi^a(x) - igf^a_{bc} A^b_\mu(x)\chi^c(x)\,. \tag{1.5}$$

Using the notation in (1.3) we have

$$K^I_\alpha(x) \to \delta^a_c \partial_\mu - igf^a_{bc} A^b(x)_\mu, \tag{1.6}$$

$$\xi^\alpha(x) \to \chi^c(x), \tag{1.7}$$

so that the index $I$ includes the indices $a$ and $\mu$, and the fact that the covariant derivative involves the gauge field $A$; the index $\alpha$ becomes $c$; and the generic parameter $\xi$ is called $\chi$. The general form of the flow equations, including the required deTurck term is:

$$\frac{d\Phi^I}{d\tau} + K^I_\alpha \xi^\alpha = G^{IJ} \frac{\delta \mathcal{E}}{\delta \Phi^J}\,. \tag{1.8}$$

The role of the deTurck term is to ensure that any change in gauge along the flow can be compensated by a corresponding change in the parameters $\xi^\alpha$. To see how the deTurck term preserves gauge invariance along the flow we write the rate of change of the energy with respect to the flow parameter $\tau$ as

$$\frac{d\mathcal{E}}{d\tau} = \int dx \, \frac{\delta \mathcal{E}}{\delta \Phi^J(x)} \frac{d\Phi^J(x)}{d\tau}, \tag{1.9}$$

and substituting (1.8) into (1.9) we obtain

$$\begin{aligned} \frac{d\mathcal{E}}{d\tau} &= \int dx \, \frac{\delta \mathcal{E}}{\delta \Phi^I(x)} \left( G^{IJ} \frac{\delta \mathcal{E}}{\delta \Phi^J(x)} - K^I_\alpha \xi^\alpha \right) \\ &= \int dx \, \frac{\delta \mathcal{E}}{\delta \Phi^I(x)} G^{IJ} \frac{\delta \mathcal{E}}{\delta \Phi^J(x)}\,. \end{aligned} \tag{1.10}$$

where we have used (1.4) in the last step.

One simple example of a gradient flow is the heat equation of classical physics which can be derived from the Dirichlet energy functional.

$$\mathcal{E}(u) = \frac{1}{2}\int d^3x \vec{\nabla}u \cdot \vec{\nabla}u \tag{1.11}$$

$$\delta\mathcal{E}(u) = \int d^3x \left(-\nabla^2 u\right)\delta u, \tag{1.12}$$

where $u(\vec{x})$ is a scalar field that represents the temperature. The general structure of inner product for our field can be determined from the energy functional, and we introduce a diffusion constant $k_u$

$$\langle u|u\rangle = k_u^2 \int d^3x u^2\,, \tag{1.13}$$

$$G_{uu} = k_u^2. \tag{1.14}$$

Since we are working in flat spacetime with a single scalar field, the simple form of $G_{IJ}$ is expected. This gives us the gradient flow equation from equation (1.2)

$$\frac{\partial u}{\partial \tau} = -k_u^2 \frac{\delta \mathcal{E}}{\delta u} = k_u^2 \nabla^2 u. \tag{1.15}$$

This is the heat equation, where $k_u^2$ is the thermal diffusivity of the material and the flow parameter $\tau$ is time. In general when dealing with only a single field, the overall factor of $k_u^2$ can be absorbed into the flow parameter $\tau \to \tau/k_u^2$, but with multiple fields that diffuse at different rates, this is not generally possible as shown in Chapter 3.

The heat equation takes regions where the temperature varies rapidly and spreads it out into large regions of slowly varying temperature. Ricci flow acts in a similar way on a manifold, taking regions of high curvature and spreading them out into larger regions of lower curvature. This type of behaviour is typical of parabolic partial differential equations in general, and gradient flows derived from a physical action or free energy

functional are usually parabolic.

# Chapter 2

# Einstein-Maxwell-Higgs Theory in 3+1 Dimensions

## 2.1 The Action

Einstein-Maxwell-Higgs theory describes a gravity theory (Einstein) coupled with matter fields that contains electrodynamics (Maxwell) with a charged scalar field (Higgs). These require a metric $g_{\mu\nu}$, a gauge vector field $A_\mu$ and a complex scalar field $\phi$ respectively. The complete action is given by

$$S[g_{\mu\nu}, A_\mu, \phi] = \int d^4x\sqrt{-g}\left[\frac{c^4}{16\pi G}\left(R - 2\Lambda\right) - \frac{1}{4}F^{\mu\nu}F_{\mu\nu} - (D^\mu\phi)^\dagger D_\mu\phi - V(\phi^\dagger\phi)\right] \quad (2.1)$$

The first two terms are the gravity part of the action, and the remaining terms are referred to as the matter part of the action. We will introduce each of the terms in the action as we proceed through this section. The action functional can be expressed in terms of a

Lagrangian density $\mathcal{L}$ as

$$S = \int d^4x\sqrt{-g}\mathcal{L}. \tag{2.2}$$

After performing the Wick rotation into Euclidean space and expressing $\mathcal{L}$ in terms of the new Euclidean time $t_E$ we can express the free energy of the system as

$$\mathcal{E} = -\int d^3x\sqrt{-g}\mathcal{L}(t_E), \tag{2.3}$$

where the integral is over the spatial dimensions only. We write $\mathcal{L}(t_E)$ to emphasize that we are using the Euclidean time but recall $\mathcal{L}$ in general depends on our metric $g_{\mu\nu}$ and our matter fields, $A_\mu$ and $\phi$.

The action can be separated into a matter part and a gravitational part as

$$S[A,\phi] = \int d^4x\sqrt{-g}\left[\mathcal{L}_{GR} + \mathcal{L}_M\right], \tag{2.4}$$

where we define the gravity and matter Lagrangian densities as

$$\mathcal{L}_{GR} = \frac{c^4}{8\pi G}\frac{1}{2}\left(R - 2\Lambda\right), \tag{2.5}$$

$$\mathcal{L}_M = -\frac{1}{4}F^{\mu\nu}F_{\mu\nu} - (D^\mu\phi)^\dagger D_\mu\phi - V(\phi^\dagger\phi). \tag{2.6}$$

The gravity Lagrangian density consists of the Ricci scalar of the metric, $R$, and the cosmological constant $\Lambda$. The overall factor of $\frac{c^4}{8\pi G}$ that depends on the speed of light (c) and Newton's gravitational constant (G) is called Einstein's constant. Typically this constant can be set to 1 by an appropriate choice of units. $R$ is derived from the Ricci

curvature tensor $R_{\mu\nu}$ and depends only on the spacetime metric $g_{\mu\nu}$,

$$R_{\mu\nu} = \partial_\lambda \Gamma^\lambda_{\mu\nu} - \partial_\mu \Gamma^\lambda_{\lambda\nu} + \Gamma^\gamma_{\mu\nu}\Gamma^\lambda_{\lambda\gamma} - \Gamma^\gamma_{\lambda\nu}\Gamma^\lambda_{\mu\gamma} \tag{2.7}$$

$$R = g^{\mu\nu} R_{\mu\nu} = g^{\mu\nu}\left(\partial_\lambda \Gamma^\lambda_{\mu\nu} - \partial_\mu \Gamma^\lambda_{\lambda\nu} + \Gamma^\gamma_{\mu\nu}\Gamma^\lambda_{\lambda\gamma} - \Gamma^\gamma_{\lambda\nu}\Gamma^\lambda_{\mu\gamma}\right) \tag{2.8}$$

using the Christoffel symbols $\Gamma^\lambda_{\mu\nu}$ which are defined in terms of the metric as

$$\Gamma^\lambda_{\mu\nu} = \frac{g^{\lambda\gamma}}{2}\left(\partial_\mu g_{\gamma\nu} + \partial_\nu g_{\gamma\mu} - \partial_\gamma g_{\mu\nu}\right). \tag{2.9}$$

While the value of $\Lambda$ can typically be interpreted as the length scale of the gravity theory, the sign of $\Lambda$ leads to three distinct spacetime geometries.

$$\Lambda < 0: \quad \text{anti-deSitter spacetime} \tag{2.10}$$

$$\Lambda = 0: \quad \text{flat spacetime} \tag{2.11}$$

$$\Lambda > 0: \quad \text{deSitter spacetime} \tag{2.12}$$

Current astronomical observations suggest our universe has either zero or positive cosmological constant. The case $\Lambda \geq 0$ is of interest in astronomical applications such as studying the early universe through the cosmic microwave background radiation or studying compact objects using gravitational waves. There has also been a great deal of recent research into spacetimes with $\Lambda < 0$ since through the AdS/CFT we can use these spacetimes to study strongly coupled physical systems such as those arising in high energy particle collisions at the Large Hadron Collider or in condensed matter systems.

The matter Lagrangian density depends on the gauge field $A_\mu$ through the electromagnetic tensor $F_{\mu\nu}$, and gauge-covariant derivative $D_\mu$

$$F_{\mu\nu} = \partial_\mu A_\nu - \partial_\nu A_\mu, \tag{2.13}$$

$$D_\mu = \partial_\mu - iqA_\mu. \tag{2.14}$$

$V(\phi^\dagger\phi)$ is some potential for the scalar field. We are mainly interested in potentials with a quadratic mass term and a quartic interaction term

$$V(\phi^\dagger\phi) = m^2\phi^\dagger\phi + \lambda(\phi^\dagger\phi)^2, \tag{2.15}$$

where $m$ and $\lambda$ are constant parameters of the theory. The matter Lagrangian is invariant under a local $U(1)$ gauge transformation.

$$\phi \rightarrow \phi e^{\imath\chi}, \tag{2.16}$$

$$A_\mu \rightarrow A_\mu + \frac{1}{q}\partial_\mu\chi. \tag{2.17}$$

The spontaneous symmetry breaking of gauge symmetries leads to a great deal of interesting physics, including superconductivity and mass generation for quarks through the Higgs mechanism. In many models the spontaneous symmetry breaking is due to a potential function like equation (2.15) with $m^2 < 0$. This is the type of symmetry breaking we will consider in the next section and in Chapter 3. In Chapter 4 the potential $V$ is only the mass term and the symmetry breaking is due to the effects of curved spacetime near a black hole event horizon.

The equations of motion for this model can be derived in the usual way from the variational principle. We vary the action with respect to the matter fields $A_\mu$, $\phi$ and $\phi^\dagger$ as

well as the metric $g_{\mu\nu}$. This leads to the following equations of motion

$$0 = \frac{1}{\sqrt{-g}}\partial_\nu(\sqrt{-g}F^{\nu\mu}) - 2q^2\phi\phi^\dagger A^\mu - iq(\phi^\dagger\partial^\mu\phi - \phi\partial^\mu\phi^\dagger), \tag{2.18}$$

$$0 = \frac{1}{\sqrt{-g}}D_\nu(g^{\mu\nu}\sqrt{-g}(D_\mu\phi)^\dagger) - \frac{\partial V}{\partial\phi}, \tag{2.19}$$

$$0 = -R_{\mu\nu} - \frac{1}{2}g_{\mu\nu}(R - 2\Lambda) - T_{\mu\nu}, \tag{2.20}$$

where $T_{\mu\nu}$ is the stress-energy tensor of the matter fields

$$T_{\mu\nu} = -\frac{1}{2}g_{\mu\nu}\mathcal{L}_M - \frac{1}{2}g^{\delta\lambda}F_{\mu\delta}F_{\nu\lambda} - (D_\mu\phi)^\dagger D_\nu\phi. \tag{2.21}$$

In general this is a system of nine coupled non-linear partial differential equations which is difficult to solve without some simplifying assumptions. The equations for the metric are greatly simplified by considering a limit where the matter fields do not backreact on the metric. In this limit we start with the vacuum solutions to these equations, namely $A_\mu = \phi = \phi^\dagger = 0$. This gives $T_{\mu\nu} = 0$ and the remaining equation (2.20) is just the Einstein equations in the vacuum. The solution to the Einstein equations depends on the choice of the cosmological constant $\Lambda$.

For $\Lambda = 0$ the simplest solution is the Minkowski metric

$$ds^2 = -dt^2 + dz^2 + d\Omega_{R^2}^2, \tag{2.22}$$

where $d\Omega_{R^2}^2$ is the metric in flat 2 dimensional space. We will consider two possible forms for $d\Omega_{R^2}^2$,

$$d\Omega_{R^2}^2 = dx^2 + dy^2 \quad \text{and} \tag{2.23}$$

$$d\Omega_{R^2}^2 = d\rho^2 + \rho^2 d\theta^2, \tag{2.24}$$

which will be referred to as the translationally symmetric and axially symmetric configurations, respectively. In flat space, the AdS/CFT correspondence does not apply, but this action still exhibits superconducting behaviour. Although there are other possible solutions for $g_{\mu\nu}$, to describe a superconductor the Minkowski metric is the most physically relevant choice. More details on how this action describes superconductivity are given in section 2.2 and the gradient flow equations are discussed in Chapter 3.

For $\Lambda < 0$ the simplest solution is anti-deSitter space. It is convenient to rewrite the cosmological constant in terms of a length scale $L$

$$\Lambda = \frac{-3}{L^2}. \tag{2.25}$$

$L$ is referred to as the AdS radius. The metric for AdS space can be written in terms of $L$ as

$$ds^2 = \frac{r^2}{L^2}\left(-dt^2 + d\Omega_{R^2}^2\right) + \frac{L^2}{r^2}dr^2, \tag{2.26}$$

where $r \in [0, \infty)$ is the AdS radial coordinate. In this case we can use the AdS/CFT correspondence to describe a superconductor using a field theory on the $r \to \infty$ boundary. A more general solution to the Einstein equations with negative cosmological constant is the planar AdS Schwarzchild black hole

$$ds^2 = -f(r)dt^2 + \frac{dr^2}{f(r)} + \frac{r^2}{L^2}d\Omega_{R^2}^2 \tag{2.27}$$

where

$$f(r) = \frac{r^2}{L^2} - \frac{M}{r} + \frac{Q^2}{r^2}, \tag{2.28}$$

where $M$ and $Q$ are constants that are related to the mass and charge respectively. This

metric has an event horizon at radius $r_0$ such that $f(r_0) = 0$. To study the theory on the boundary, we only need to consider the bulk theory outside the black hole horizon $r \in [r_0, \infty)$. The gradient flow equations for the matter fields with an AdS background metric are discussed in Chapter 4.

## 2.2 Superconductor Phenomenology

Many important properties of superconductors can be described as being the result of the spontaneous symmetry breaking of the $U(1)$ gauge symmetry in the electromagnetic field $A_\mu$. The main phenomenological description of superconductors comes from the Ginzburg-Landau theory. GL theory is based on a power series expansion of the Gibbs free energy in terms of a complex order parameter $\phi$ representing the density of superconducting electron pairs:

$$\mathcal{E}[A_i, \phi] = \int d^3x \left[\frac{1}{4}F^{ij}F_{ij} + (D^i\phi)^\dagger(D_i\phi) + V(\phi^\dagger\phi)\right], \tag{2.29}$$

with

$$V = \frac{\lambda}{4}\left(\phi^\dagger\phi - \frac{v^2}{2}\right)^2 + \mathcal{O}\left((\phi^\dagger\phi)^3\right). \tag{2.30}$$

This free energy is the time independent case of the action (2.1) in flat spacetime with $\Lambda = 0$ and $g_{ij} = \delta_{ij}$. Normally a theory describing electrons would require a Dirac spinor field, but Cooper pairs are formed from electrons with opposite spin and it is therefore natural to describe Cooper pairs as a complex scalar field. The potential $V$ allows for symmetry breaking as long as $v^2 > 0$. The broken symmetry can be interpreted as the development of a condensate in a superconducting state. In order for this interpretation to make sense for a physical system, the model should be temperature dependent with

a critical temperature $T_c$ above which superconductivity does not occur. In the GL model the temperature dependence comes from the parameter $v$ which gives the vacuum expectation value of the scalar field

$$v = v(0)\left(1 - \frac{T}{T_c}\right)^{-\frac{1}{2}} . \tag{2.31}$$

From (2.31) we can see that for $T > T_c$ we will have $v^2 < 0$ and there will be no symmetry breaking, while for $T < T_c$ the symmetry can be broken.

A superconductor has two standard length scales, the coherence length ($\xi$) and the London penetration depth ($\Lambda_L$). The coherence length is the scale over which the order parameter changes at the boundary of a superconducting material. The London penetration depth is the scale over which magnetic fields can penetrate the superconductor. These length scales can be written in terms of the parameters of the GL theory

$$\xi = \frac{2}{v\sqrt{\lambda}} \text{ and } \Lambda_L = \frac{1}{qv} . \tag{2.32}$$

Both length scales are temperature dependent, but we can define a dimensionless, temperature independent ratio called the Ginzburg-Landau parameter $\kappa$

$$\kappa^2 = \frac{\Lambda_L^2}{\xi^2} = \frac{\lambda}{4q^2} . \tag{2.33}$$

It is possible to rescale the fields such that the GL equations depend only on $\kappa$. In the GL model, $\kappa_c^2 = 1/2$ is a critical value that divides two physically distinct regions in the phase space that correspond to type I superconductors ($\kappa < \kappa_c$) and type II superconductors ($\kappa > \kappa_c$). Typically, conventional superconductors are type I, while high-temperature superconductors are type II. The main distinction between the two types is that type II superconductors allow sufficiently strong magnetic fields to penetrate the superconductor,

creating a superconducting vortex. A superconducting vortex is a small region in the superconductor where the material is in the normal metal phase and a quantized amount of magnetic flux passes through the material.

The equations of motion (2.18) and (2.19) after the appropriate simplifications become the Ginzburg-Landau equations:

$$0 = \nabla^2\phi - 2\imath q\vec{A}\cdot\vec{\nabla}\phi - q^2\vec{A}\cdot\vec{A}\phi - \left(\frac{\lambda}{2}\phi^\dagger\phi - \frac{v^2\lambda}{4}\right)\phi, \tag{2.34}$$

$$0 = \nabla^2\vec{A} - \imath q\left(\phi^\dagger\vec{\nabla}\phi - \phi\vec{\nabla}\phi^\dagger\right) - 2q^2\vec{A}\phi^\dagger\phi. \tag{2.35}$$

Since we are working in flat 3-dimensional space we use vector notation where

$$\vec{A} = \begin{pmatrix} A_x \\ A_y \\ A_z \end{pmatrix} \quad \text{and} \quad \vec{\nabla} = \begin{pmatrix} \partial_x \\ \partial_y \\ \partial_z \end{pmatrix}. \tag{2.36}$$

The GL equations can be solved analytically in some special cases that demonstrate the two length scales of the superconductor. To find the coherence length we look at the case with no magnetic fields $\vec{A} = 0$, and consider the scalar field to be a function of $x$ only. In order for the order parameter to have non trivial $x$-dependence there must be some inhomogeneity in the superconductor itself. We can consider an interface at $x = 0$ between a superconductor for $x > 0$ and a normal material for $x < 0$. In this case we anticipate that deep inside the superconductor $x \to \infty$ the order parameter approaches its maximum, and at the boundary $x = 0$ the order parameter should approach 0. With $\vec{A} = 0$ (2.35) becomes

$$\phi\vec{\nabla}\phi^\dagger = \phi^\dagger\vec{\nabla}\phi. \tag{2.37}$$

This means that the phase of the scalar field is constant. Therefore we can make a gauge transformation to make $\phi$ real. We are left with one equation from (2.34)

$$0 = \nabla^2\phi - \left(\frac{\lambda}{2}\phi^2 - \frac{v^2\lambda}{4}\right)\phi. \tag{2.38}$$

This can be solved analytically for $\phi(x)$:

$$\phi(x) = \frac{v}{\sqrt{2}}\tanh\left(x\sqrt{\frac{v^2\lambda}{8}}\right) = \frac{v}{\sqrt{2}}\tanh\left(\frac{x}{\sqrt{2}\xi}\right), \tag{2.39}$$

where we have used the coherence length $\xi$ from equation (2.32).

The other superconducting length scale, the London penetration depth, can be determined using a similar configuration with the inclusion of a magnetic field outside the superconductor. For $x < 0$ (outside the superconductor) we take $A_y = Bx + c_0$, $B$ will be the strength of an external magnetic field pointing along the $z$-axis, and $c_0$ is a constant whose value is chosen such that $\vec{A(x)}$ is continuous. If we consider the case where $\xi \ll \Lambda_L$ then we can assume that $\phi$ is approximately constant and has reached its vacuum expectation value such that $\phi\phi^\dagger = \frac{v^2}{2}$. In this case the GL equation (2.35) becomes

$$0 = \nabla^2\vec{A} - q^2v^2\vec{A}. \tag{2.40}$$

Asssuming $\vec{A}$ has only one component, $A_y(x)$, we can solve the equation along with the boundary condition $A_y(x=0) = c_0$,

$$A_y(x) = c_+\exp(xqv) + c_-\exp(-xqv) \text{ with} \tag{2.41}$$

$$c_0 = c_+ + c_-. \tag{2.42}$$

The term proportional to $c_+$ increases exponentially for $x > 0$, therefore it is not a physical solution inside the superconductor and we will take $c_+ = 0$. This gives the solution for

$A_y$ inside the superconductor

$$A_y(x) = c_0 \exp(-xqv) = c_0 \exp\left(\frac{-x}{\Lambda_L}\right), \tag{2.43}$$

using the London penetration depth $\Lambda_L$ from equation (2.32). The exponential decay of magnetic fields inside a superconductor leads to one of their defining characteristics, the Meissner effect. The Meissner effect is the expulsion of magnetic fields from a material as it undergoes the phase transition into a superconducting state. While the Meissner effect tends to prevent any magnetic fields from penetrating a superconductor, in situations where magnetic flux does pass through a superconductor it is found that the flux is quantized. The requirement that magnetic flux is quantized can be seen in the GL equations. We can calculate the magnetic flux through an area as the loop integral of $\vec{A}$. Since $\phi$ must be single valued, the phase of the scalar field around a loop can only change by $2n\pi$ where $n$ is an integer. This means equation (2.35) suggests the integral of $\vec{A}$ around a loop and therefore the magnetic flux must also be some multiple of $n$.

We note that in our definition of the London penetration depth we required $\xi \ll \Lambda_L$ which means that the GL parameter is small: $\kappa \ll 1$. When the two length scales are of similar magnitude, magnetic fields do not decay as quickly inside the superconductor. This is the basis for the separation of superconductors into type I and type II. In type II superconductors $\xi > \frac{1}{2}\Lambda_L$, and there is not a complete Meissner effect, but a lattice of superconducting vortices forms in the material. These vortices are studied in greater depth in Chapter 3.

## 2.3 The AdS/CFT Dictionary

In order to describe a holographic superconductor, we first need to understand the "AdS/CFT dictionary" which describes how the fields in the bulk AdS theory correspond to values in the CFT on the boundary. We will look at the action (2.1) as our bulk theory in 3+1 dimensions, and consider a 2+1 dimensional theory on the boundary.

The properties of the boundary theory are determined by the asymptotic behaviour of the bulk fields at the AdS boundary. With the cosmological constant $\Lambda$ given in terms of the AdS radius $L$ as in equation (2.25), we can set $L = 1$, which is equivalent to using the AdS radius as our choice of length units. If we separate the AdS radial coordinate from the other 2+1 dimensions, a bulk metric in AdS space that solves the Einstein equations (2.20) can be written in general as

$$ds^2 = \frac{\tilde{g}_{\bar{\mu}\bar{\nu}}(x^{\bar{\rho}}, u)dx^{\bar{\mu}}dx^{\bar{\nu}} + du^2}{u^2}, \tag{2.44}$$

where $u$ is the radial AdS coordinate defined so that $u = 0$ is the boundary of AdS space. The barred greek indices run over the bulk coordinates except for the radial AdS coordinate $u$, and emphasize that $\tilde{g}_{\bar{\mu}\bar{\nu}}$ is not the full bulk metric $g_{\mu\nu}$. The 2+1 dimensional metric $\tilde{g}_{\bar{\mu}\bar{\nu}}$ is a function of all 3+1 bulk coordinates, and must approach the 2+1 dimensional Minkowski metric at the AdS boundary, $u = 0$, in order for the bulk to be asymptotically AdS space

$$\tilde{g}_{\bar{\mu}\bar{\nu}}(x^{\bar{\rho}}, 0) = \eta_{\bar{\mu}\bar{\nu}}. \tag{2.45}$$

From the boundary behaviour of $\tilde{g}_{\bar{\mu}\bar{\nu}}$ we obtain the expectation value of the energy-momentum tensor in the field theory [13]

$$\langle T_{\bar{\mu}\bar{\nu}}(x^{\bar{\rho}})\rangle = \frac{N_c^2}{2\pi^2}\partial_u^4 \tilde{g}_{\bar{\mu}\bar{\nu}}(x^{\bar{\rho}}). \tag{2.46}$$

where $N_c$ is the number of colors (i.e. the dimension of the gauge group) in the field theory. Starting with an energy-momentum tensor in the boundary theory that corresponds to a thermal state with temperature $T$, we can solve the Einstein equations in the bulk with a boundary condition given by (2.46). The solution for the metric in the bulk is a planar AdS black hole with Hawking temperature $T$. So thermal states in the boundary theory correspond to black holes in the bulk theory with the same temperature.

The free energy of the superconductor is related to the Euclidean on-shell action in the bulk. We obtain the Euclidean action from a Wick rotation of the Lorentzian action

$$S_E(t_E, x) = -S(t = -\imath t_E, x)\,. \tag{2.47}$$

After the Wick rotation we define a Euclidean time coordinate $t_E$. When the AdS space-time contains a black hole, $t_E$ must be periodic, with period $\beta = 1/T$, inversely proportional to the temperature of the black hole [14]. In this thesis we will be mainly concerned with static field configurations such that the Euclidean action is proportional to energy of the bulk system. In the absence of time dependence in the fields, we can integrate over the time coordinate and write

$$S_E = \beta\mathcal{E} = \frac{\mathcal{E}}{T}. \tag{2.48}$$

Note that the free energy $\mathcal{E}$ involves an integral over the spatial coordinates only.

The correspondence also links the scalar field in the bulk and an operator in the boundary

theory that we will take to represent the superconducting condensate. The dimension and expectation value of this operator is determined by the fall off of the scalar field $\phi$ at the AdS boundary $u = 0$.

The dimension of the operator will depend on our choice of mass for the scalar field. From the Klein-Gordon equation with the metric (2.44) near $u = 0$ where $\tilde{g}_{\bar{\mu}\bar{\nu}}(x^{\bar{\rho}}, u) \approx \eta_{\bar{\mu}\bar{\nu}}$,

$$u^2\partial_u^2\phi - 2u\partial_u\phi - m^2\phi + u^2\eta^{\bar{\mu}\bar{\nu}}\partial_{\bar{\mu}}\partial_{\bar{\nu}}\phi = 0 \tag{2.49}$$

the asymptotic behaviour of $\phi$ has two possible fall off rates $\Delta_\pm$:

$$\phi(u) = c_- u^{\Delta_-}\left(1 + \mathcal{O}(u^2)\right) + c_+ u^{\Delta_+}\left(1 + \mathcal{O}(u^2)\right) \quad \text{where} \tag{2.50}$$

$$\Delta_\pm = \frac{1}{2}\left(3 \pm \sqrt{9 + 4m^2}\right) . \tag{2.51}$$

In Chapter 4 we consider only the case $m^2 = -2$. Although it appears that we have started with an instability that will produce the condensate we are looking for, Breitenlohner and Freedman (BF) showed that $\mathrm{AdS}_{d+1}$ spacetime is stable if the scalar field mass satisfies $m^2 > -d^2/(4)$ [15]. Note that this bound is equivalent to the requirement that $\Delta_\pm$ is real. In our calculation ($d = 3$), this BF bound requires $m^2 > -2.25$ and is therefore satisfied by our choice. For masses near the BF bound, $-d^2/4 + 1 > m^2 > -d^2/4$ both terms in (2.50) are normalizable [16], but if both coefficients are nonzero the theory is unstable in the asymptotic region [17]. For $m^2 = -2$ there are two possible operators, $\mathcal{O}_2$ and $\mathcal{O}_1$, in the boundary theory with scaling dimension given by $\Delta_+ = 2$ and $\Delta_- = 1$, respectively. To determine the expectation values of the operators we write the asymptotic behaviour of the scalar field in terms of the radial coordinate $r$ used in the metric (2.27)

$$\phi(r) = \frac{\langle\mathcal{O}_-\rangle}{r^{\Delta_-}} + \frac{\langle\mathcal{O}_+\rangle}{r^{\Delta_+}} + \cdots . \tag{2.52}$$

We also introduce a finite charge density and chemical potential, which are obtained from the scalar potential $A_t$ in the boundary theory [18]. The motivation is that an additional scale is necessary to produce a superconducting instability at low temperatures. For $u \to 0$ we write

$$A_t(u) = \mu - \bar{\rho} u + \cdots , \tag{2.53}$$

where $\mu$ and $\bar{\rho}$ are, respectively, the chemical potential and charge density in the boundary theory (note that we use $\bar{\rho}$ for the charge density because $\rho$ will be used as a radial coordinate when studying solutions with axial symmetry). From the spatial components of the gauge vector we can obtain the magnetic vector potential and current on the boundary

$$A_i(u) = \bar{A}_i - J_i u + \cdots . \tag{2.54}$$

This means we can find the magnetic field on the boundary to be

$$\vec{B} = \vec{\nabla} \times \bar{A}_i \, . \tag{2.55}$$

Although we will be working in only 2 dimensions on the boundary, the vectors in (2.55) should be 3 dimensional, since we will consider external magnetic fields that are perpendicular to the 2 dimensional superconductor.

## 2.4 The Gradient Flow Equations

### 2.4.1 Matter Flows

In order to obtain the gradient flow equations for the bulk action (2.1) we need the configuration space metric $G_{IJ}$ for our fields. The structure of $G_{IJ}$ for the matter fields can be read off the gradient terms for our fields in the action. Given

$$S = \int d^4x H_{IJ} \partial_\mu \Phi^I \partial^\mu \Phi^J + \cdots , \tag{2.56}$$

for our matter fields

$$\left(\Phi^I\right) = \begin{pmatrix} A_\mu \\ \phi \\ \phi^\dagger \end{pmatrix} \tag{2.57}$$

from the action (2.1) we obtain

$$H_{IJ} = \begin{bmatrix} \sqrt{-g}g^{\mu\nu} & 0 & 0 \\ 0 & 0 & \sqrt{-g} \\ 0 & \sqrt{-g} & 0 \end{bmatrix} . \tag{2.58}$$

The action has two types of matter field, the vector field $A_\mu$ and the scalar field $\phi$. Introducing diffusion constants $k_A^2$ and $k_\phi^2$ which in the case of GL theory are the inverse conductivity and the normal state diffusion respectively, we obtain the field space metric

$$G_{IJ} = \begin{bmatrix} k_A^{-2}\sqrt{-g}g^{\mu\nu} & 0 & 0 \\ 0 & 0 & k_\phi^{-2}\sqrt{-g} \\ 0 & k_\phi^{-2}\sqrt{-g} & 0 \end{bmatrix} . \tag{2.59}$$

Using $G_{IJ}$ we can find the gradient flow equations for the matter fields:

$$\frac{\partial A_\mu}{\partial \tau} = \frac{k_A^2 g_{\mu\rho}}{\sqrt{-g}}\partial_\nu(\sqrt{-g}F^{\nu\rho}) - 2q^2\phi\phi^\dagger A_\mu - iq(\phi^\dagger\partial_\mu\phi - \phi\partial_\mu\phi^\dagger), \tag{2.60}$$

$$\frac{\partial \phi}{\partial \tau} = \frac{k_\phi^2}{\sqrt{-g}}D_\nu^\dagger(g^{\mu\nu}\sqrt{-g}D_\mu\phi) - \frac{\partial V}{\partial \phi^\dagger}, \tag{2.61}$$

$$\frac{\partial \phi^\dagger}{\partial \tau} = \frac{k_\phi^2}{\sqrt{-g}}D_\nu(g^{\mu\nu}\sqrt{-g}(D_\mu\phi)^\dagger) - \frac{\partial V}{\partial \phi}. \tag{2.62}$$

Since our action is invariant under a gauge transformation of our fields, given by

$$\phi \rightarrow \phi e^{\imath\chi} \tag{2.63}$$

$$A_\mu \rightarrow A_\mu + \frac{1}{q}\partial_\mu\chi, \tag{2.64}$$

we will want to include additional 'DeTurck' terms in our flow equations to ensure any initial gauge choice is preserved. The impact of the DeTurck terms becomes more obvious after a reparameterization of the scalar field. The complex field $\phi$ can be written in terms of two real fields as

$$\phi = \frac{1}{\sqrt{2}}pe^{\imath\theta}, \tag{2.65}$$

where $p$ is the modulus and $\theta$ is the phase. In terms of these fields the flow equations are

$$\frac{\partial A_\mu}{\partial \tau} = \frac{g_{\mu\rho}}{\sqrt{-g}}\partial_\nu(\sqrt{-g}F^{\nu\rho}) - p^2q(qA_\mu - \partial_\mu\theta) \tag{2.66}$$

$$\frac{\partial p}{\partial \tau} = \frac{1}{\sqrt{-g}}\partial_\nu(g^{\mu\nu}\sqrt{-g}\partial_\mu p) - pg^{\mu\nu}(qA_\mu - \partial_\mu\theta)(qA_\nu - \partial_\nu\theta) - m^2p \tag{2.67}$$

$$\frac{\partial \theta}{\partial \tau} = \frac{1}{\sqrt{-g}}\partial_\nu(g^{\mu\nu}\sqrt{-g}p^2(qA_\mu - \partial_\mu\theta)). \tag{2.68}$$

In this case, the value of the field $\theta$ can be fixed by a gauge transformation. Therefore we can choose our DeTurck term to set

$$\frac{\partial\theta}{\partial\tau} = 0 \tag{2.69}$$

so that the phase of the scalar field is constant along the flow.

### 2.4.2 Metric Flows

In order to extend the gradient flow to include the metric as well as the matter fields we need an inner product for $g_{\mu\nu}$. Since the action depends on second order derivatives of the metric through $R$ we can not simply read the inner product off of the gradient terms in the action. Consider the inner product

$$\langle \delta g_{\mu\nu} | \delta g_{\gamma\lambda} \rangle \quad := \quad \int dx \, \sqrt{-g} g^{\gamma\mu} g^{\lambda\nu} \delta g_{\mu\nu} \delta g_{\gamma\lambda}, \tag{2.70}$$

which is the simplest choice to ensure the gradient flow equations are covariant. This leads to the flow equation for the metric

$$\frac{\partial g_{\mu\nu}}{\partial\tau} \quad = \quad -R_{\mu\nu} - \frac{1}{2} g_{\mu\nu}(R + \frac{6}{L^2}) - T_{\mu\nu}, \tag{2.71}$$

where $T_{\mu\nu}$ is the stress-energy tensor of the matter fields (2.21).

We also need to consider the DeTurck terms for the metric flow since the coordinate invariance in general relativity means we can change coordinates on the metric $g_{\mu\nu}$ without changing the curvature scalar $R$. To remedy this, we introduce a new term to the flow equations to account for a gauge choice that may depend on the flow parameter $\tau$. The

new equations are

$$\frac{\partial g_{\mu\nu}}{\partial \tau} = -R_{\mu\nu} - \frac{1}{2} g_{\mu\nu}(R + \frac{6}{L^2}) + \mathcal{L}_X g_{\mu\nu} - T_{\mu\nu} \tag{2.72}$$

and the new term is just the Lie derivative along a vector $X$ that generates the coordinate transformation along $\tau$.

The flow equations obtained for the metric are not quite Ricci flow equations, they contain several additional terms. The cosmological constant term and the stress-energy tensor term are unavoidable consequences of our physical model, but the $g_{\mu\nu}R$ term may not be necessary. We note that without this extra term the pure gravitational part of the gradient flow is just Ricci flow, therefore we would like to understand how Ricci flow can be derived as a gradient flow. To do this we consider Perelman's functional [10]

$$\mathcal{F} = -\int dx^4 \sqrt{-g} e^{-f} 2 \left[R + |\nabla f|^2\right]. \tag{2.73}$$

This metric can be interpreted physically as gravity coupled with a dilaton field $f$. If we find the gradient flow of the metric associated with this action, we get

$$\frac{\partial g_{\mu\nu}}{\partial \tau} = -2 \left(R_{\mu\nu} + \nabla_\mu \nabla_\nu f\right). \tag{2.74}$$

The flow for $f$ is not determined by the gradient of the action, instead we must impose the condition that the measure $\sqrt{-g}e^{-f}$ does not change along the flow which gives

$$\frac{\partial f}{\partial \tau} = -R - \nabla^2 f. \tag{2.75}$$

We notice that $-2\nabla_\mu \nabla_\nu f = \mathcal{L}_X g_{\mu\nu}$ where $X = \nabla_\mu f$. Comparing this with (2.72) we see that this gradient flow is in fact Ricci flow with a particular DeTurck term. We

can interpret this as working in a gauge where the measure is independent of the flow parameter $\tau$. Perelman's method could be applied to our action to obtain simpler flow equations for the metric, at the cost of introducing another field into the action.

There is another method to obtain Ricci flow as the gradient flow of our gravitational action [19]. By considering a more general form of the field space metric $G_{IJ}$ for $g_{\mu\nu}$, there is a one parameter family of gradient flows of the Einstein-Hilbert action. One of these flows is Ricci flow without an extra DeTurck term.

In this thesis we focus on the gradient flows of the matter fields with fixed background metrics.

# Chapter 3

# Flat Spacetime

## 3.1 Ginzburg-Landau Theory

As we discussed in the previous chapter, the free energy in the GL model is equivalent to the negative of the matter part of the action (2.1) in a flat ($\Lambda = 0, g_{ij} = \delta_{ij}$) spacetime with 3 spatial dimensions. In order to allow for symmetry breaking our potential takes the form

$$V = \frac{\lambda}{4}(\phi^\dagger\phi - \frac{v^2}{2})^2 \,. \tag{3.1}$$

Since the gravity part of the action is trivial in flat spacetime, we work with a simplified free energy

$$\mathcal{E} = \int d^3x \left[\frac{1}{4}F^{ij}F_{ij} + (D^i\phi)^\dagger(D_i\phi) + \frac{\lambda}{4}(\phi^\dagger\phi - \frac{v^2}{2})^2\right] \tag{3.2}$$

Notice that this potential includes a constant term $\frac{\lambda v^4}{16}$ which corresponds to the energy of the symmetric false vacuum state. In the context of superconductivity this is the normal

metal state. The superconducting state is the result of spontaneous symmetry breaking, where the symmetric $\phi = 0$ state decays into the energetically favored $\phi = \frac{ve^{\imath\theta}}{\sqrt{2}}$ for some phase $\theta$. Recall that in the GL model $v$ is temperature dependent, and above a critical temperature $T_c$, $v^2 < 0$ and no symmetry breaking occurs. We will confine our interest to temperatures below the critical value.

## 3.2 Gradient Flow and the Time-Dependent Ginzburg-Landau Equations

In order to obtain the gradient flow equations for the GL model, we first need an inner product on our field space. Here we only have two fields, a vector potential $A_i$ and a complex scalar field $\phi$. Using the field space metric from (2.59) the inner product for the vector potential is

$$\langle \delta A | \delta A \rangle = \frac{1}{k_A^2} \int d^3x \delta^{ij} \delta A_i \delta A_j \,, \tag{3.3}$$

and for a complex scalar $\phi$ we have

$$\langle \delta\phi | \delta\phi \rangle = \frac{1}{k_\phi^2} \int d^3x \delta\phi^\dagger \delta\phi \,. \tag{3.4}$$

Recall that $k_\phi$ is the diffusion constant and $k_A$ is the inverse conductivity which will be defined in terms of physical quantities in equations (3.20), (3.21). We will show below that the GL flow equations depend only on the ratio of these parameters. The flow

equations have the form:

$$\frac{\partial A_i}{\partial \tau} = \frac{k_A^2 g_{ij}}{\sqrt{g}} \frac{\delta \mathcal{E}}{\delta A^j} = -\frac{k_A^2}{\sqrt{g}} \left( -\partial^j (\sqrt{g} F_{ji}) + iq \left( (D_i \phi)^\dagger \phi - \phi^\dagger D_i \phi \right) \right) \tag{3.5}$$

$$\frac{\partial \phi}{\partial \tau} = \frac{k_\phi^2}{\sqrt{g}} \frac{\delta \mathcal{E}}{\delta \phi^\dagger} = k_\phi^2 \left[ \left( D_j D^j \phi \right) - \frac{dV}{d\phi^\dagger} \right] \tag{3.6}$$

$$\frac{\partial \phi^\dagger}{\partial \tau} = \frac{k_\phi^2}{\sqrt{g}} \frac{\delta \mathcal{E}}{\delta \phi} = k_\phi^2 \left[ \left( D_j D^j \phi \right)^\dagger - \frac{dV}{d\phi} \right] . \tag{3.7}$$

We define dimensionless variables as follows. We consider all lengths in units of the coherence length $\xi$, that is, we write

$$X = \tilde{X} \xi \,, \quad \text{or} \quad \tilde{X} = \frac{v\sqrt{\lambda}}{2} X \,, \quad X \in \{x, y, z, \rho\} \,. \tag{3.8}$$

The scalar field is written in terms of its vacuum expectation value:

$$\phi = \tilde{\phi} v = \frac{v}{\sqrt{2}} (\tilde{\phi}_1 + i \tilde{\phi}_2) \,, \tag{3.9}$$

and the gauge field is scaled so that

$$g^{ij} A_i A_j = \frac{v^2 \lambda}{4q^2} \tilde{g}^{ij} \tilde{A}_i \tilde{A}_j \,. \tag{3.10}$$

In Cartesian coordinates this can be written as

$$A_i = \frac{v\sqrt{\lambda}}{2q} \tilde{A}_i = \xi H_{c2} \tilde{A}_i, \tag{3.11}$$

where $H_{c2}$ denotes the upper critical field of the superconductor, using the notation of [20].

In order to interpret the flow parameter as a physical time we must consider time dependent gauge transformations. The flow equations are not invariant under time dependent gauge transformations. However, we can replace the $\tau$ derivatives with the appropriate gauge invariant derivatives by including additional deTurck terms

$$\frac{\partial \vec{\tilde{A}}}{\partial \tau} \to \frac{\partial \vec{\tilde{A}}}{\partial \tau} - q\vec{\nabla} Q \quad \text{and} \quad \frac{\partial \tilde{\phi}}{\partial \tau} \to \frac{\partial \tilde{\phi}}{\partial \tau} + iq\, Q \tilde{\phi}\,, \tag{3.12}$$

where $Q$ is a scalar that transforms as

$$Q \to Q - q\partial_\tau \chi \tag{3.13}$$

under the gauge transformation given in (3.30). $Q$ can be interpreted as the scalar potential $A_0$. In section 3.4 we consider an axially symmetric situation that allows us to work with explicitly gauge invariant quantities. In section 3.5 we use a two dimensional Cartesian coordinate system and work in the gauge where $Q = 0$. In both cases the flow equations are equivalent to the usual TDGL equations for superconductors as proposed in [21] and [22].

We rewrite the flow parameter in terms of a dimensionless variable and a characteristic timescale which is defined as

$$t_0 = \frac{\Lambda_L^2(0)}{k_A^2} = \frac{\Lambda_L^2}{k_A^2}\frac{v^2}{v(0)^2}\,. \tag{3.14}$$

The rescaled flow parameter is denoted $t$ and defined

$$\tau = t\; t_0 \frac{v^2(0)}{v^2}. \tag{3.15}$$

When working in terms of the rescaled fields and units, it will also be useful to define a rescaled version of the free energy:

$$\mathcal{E} = \tilde{\mathcal{E}} v^2 \,. \tag{3.16}$$

The fully rescaled flow equations have the form

$$\frac{\partial \tilde{\phi}_1}{\partial t} = \frac{k_\phi^2 \kappa^2}{k_A^2} \left[ \nabla^2 \tilde{\phi}_1 - \tilde{\phi}_1 (\tilde{\phi}_1^2 + \tilde{\phi}_2^2 - 1) - \vec{\tilde{A}}^2 \tilde{\phi}_1 - 2\vec{\tilde{A}} \cdot \vec{\nabla} \tilde{\phi}_2 - \tilde{\phi}_2 \vec{\nabla} \cdot \vec{\tilde{A}} \right] \tag{3.17}$$

$$\frac{\partial \tilde{\phi}_2}{\partial t} = \frac{k_\phi^2 \kappa^2}{k_A^2} \left[ \nabla^2 \tilde{\phi}_2 - \tilde{\phi}_2 (\tilde{\phi}_1^2 + \tilde{\phi}_2^2 - 1) - \vec{\tilde{A}}^2 \tilde{\phi}_2 + 2\vec{\tilde{A}} \cdot \vec{\nabla} \tilde{\phi}_1 + \tilde{\phi}_1 \vec{\nabla} \cdot \vec{\tilde{A}} \right] \tag{3.18}$$

$$\frac{\partial \vec{\tilde{A}}}{\partial t} = \kappa^2 \left[ \nabla^2 \vec{\tilde{A}} - \vec{\nabla} (\vec{\nabla} \cdot \vec{\tilde{A}}) \right] - \left[ \tilde{\phi}_1 \vec{\nabla} \tilde{\phi}_2 - \tilde{\phi}_2 \vec{\nabla} \tilde{\phi}_1 + \vec{\tilde{A}} (\tilde{\phi}_1^2 + \tilde{\phi}_2^2) \right] . \tag{3.19}$$

The parameters $k_\phi$ and $k_A$ are related to the normal state diffusion constant, $D$, and the conductivity, $\sigma$, determined from BCS theory as follows:

$$D = k_\phi^2 = \frac{\xi^2(0)}{12 t_{GL}} \,, \tag{3.20}$$

$$\sigma^{-1} = k_A^2 = \frac{\Lambda_L^2(0)}{t_{GL}} \,. \tag{3.21}$$

Equations (3.17 - 3.19) depend only on the ratio of $k_\phi$ and $k_A$, and from (2.33) we obtain immediately $k_A^2/k_\phi^2 = 12\kappa^2$. Our equations (3.17 - 3.19) correspond to Eq. (8) of [20], without the random force term, and identifying $t_0$ in equation (3.14) with the Ginzburg-Landau timescale $t_{GL}$, in the notation of [20]. Also, since we work with fixed temperature $T$, we have rescaled by the temperature dependent quantities, rather than their values at $T = 0$.

## 3.3 Superconductor Vortices

Superconductor vortices are created when magnetic flux penetrates the superconductor, creating a region of normal material surrounded by a circulating current. It was shown by Nielsen and Olesen that the GL model has classical vortex solutions [23]. Exact solutions were obtained in [24] for $\kappa = 1/2$. In this case, the GL equations reduce to first-order Bogomolnyi equations [25–27]. We comment that in physical systems the behaviour at the critical point ($\kappa = 1/2$) is actually quite complicated, and very different states can appear. These systems can be studied using extensions of Ginzburg-Landau theory [28–33]. The near critical regime is therefore both interesting and very complicated.

In bulk physical systems, the sub-critical and super-critical cases exhibit distinctly different behaviour, in agreement with the predictions of the GL theory. In type I superconductors ($\kappa < \kappa_c$) there are no stable vortices. The magnetic flux is expelled via induced surface currents. In type II superconductors ($\kappa > \kappa_c$), there are stable solutions containing multiple vortices with flux number $n = 1$. A lattice of flux vortices forms which is known as an Abrikosov lattice [34]. The stability of these solutions was proven in the GL model by Gustafson [35].

## 3.4 Axially symmetric vortices

In this section we work in cylindrical coordinates and use an axially symmetric ansatz that reduces the problem to a 1-dimensional calculation. We parametrize the complex scalar field using two real functions that correspond to the magnitude and phase of the complex field. We define the components of the scalar field as

$$\frac{\phi}{v} = \tilde{\phi} = \frac{f}{\sqrt{2}} e^{i\omega} . \tag{3.22}$$

We use the ansatz

$$A_\rho = 0\,, \quad A_z = 0\,, \quad \tilde{A}_\theta = \tilde{A}_\theta(\tilde{\rho})\,, \quad f = f(\tilde{\rho}) \quad \omega = -n\theta\,, \tag{3.23}$$

and therefore (3.10) with

$$\tilde{g}^{\theta\theta} = \frac{1}{\tilde{\rho}^2} \qquad \text{gives} \qquad \tilde{A}_\theta = qA_\theta. \tag{3.24}$$

We define a new field $B$ as

$$B = -(\tilde{A}_\theta + \partial_\theta\omega\,) = -(\tilde{A}_\theta - n\,). \tag{3.25}$$

In order for the field $\phi$ to be single valued we require $n$ to be an integer, which is known as the winding number. The free energy in terms of these variables is given by

$$\tilde{\mathcal{E}} = \pi \int d\tilde{\rho} \left[\frac{1}{\tilde{\rho}}(\kappa^2 B'^2 + f^2 B^2) + f'^2\tilde{\rho} + \frac{\tilde{\rho}}{2}(f^4 - 2f^2 + 1)\right], \tag{3.26}$$

where we have performed the integration over $d\theta$, and the flow equations have the form

$$\frac{\partial B}{\partial t} = \kappa^2\left(B'' - \frac{B'}{\tilde{\rho}}\right) - f^2 B\,, \tag{3.27}$$

$$\frac{\partial f}{\partial t} = \frac{1}{12}\left[f'' + \frac{f'}{\tilde{\rho}} - \frac{fB^2}{\tilde{\rho}^2} - f(f^2-1)\right], \tag{3.28}$$

$$\frac{\partial \omega}{\partial t} = \frac{-1}{\tilde{\rho}}\partial_\theta\left(\frac{fB}{\tilde{\rho}}\right). \tag{3.29}$$

where the prime denotes differentiation with respect to $\tilde{\rho}$. Using (3.23) the right side of (3.29) is zero, and therefore $\omega$ is constant along the flow.

The energy is invariant under a transformation which has the form in tilde variables

$$\tilde{\phi} \to e^{iq\chi}\tilde{\phi}\,, \quad \tilde{A}_\theta \to \tilde{A}_\theta - q\partial_\theta\chi\,. \tag{3.30}$$

Using the axially symmetric ansatz (3.23) this transformation takes the form

$$\omega \to \omega + q\chi\,, \quad \tilde{A}_\theta \to \tilde{A}_\theta - q\partial_\theta\chi \tag{3.31}$$

which shows that the field $B$ in (3.25) is gauge invariant. In the rest of this section, we suppress the tildes.

We start by looking at the fixed points of the flow, which are the axially symmetric vortex solutions. It can be shown that for $\frac{\partial B}{\partial t} = \frac{\partial f}{\partial t} = 0$ (3.27) and (3.28) can be integrated to find first order equations of the form

$$f' - c_1\frac{Bf}{\rho} = 0, \tag{3.32}$$

$$\frac{1}{\rho}B' - c_2(f^2 - c_3) = 0, \tag{3.33}$$

where the parameters $c_i$ are constants of integration. Differentiating (3.32) and (3.33) and rearranging, one finds that the resulting second order differential equations are equivalent to the original equations (3.27, 3.28) if

$$c_1 = \pm 1\,, \quad c_2 = \pm 1\,, \quad c_3 = 1\,, \quad \kappa^2 = \frac{1}{2}\,. \tag{3.34}$$

We choose the upper (positive) solution in order to obtain finite energy, as explained below. We can obtain a decoupled second order equation for $B$ if we differentiate (3.33), and then use (3.32) to eliminate $f'$ and (3.33) to remove $f^2$. The result of this procedure

is the set of equations

$$B'' + 2\frac{BB'}{\rho} - \frac{B'}{\rho} - B = 0\,, \tag{3.35}$$

$$f^2 = 1 - 2\frac{B'}{f}\,, \tag{3.36}$$

which can be solved analytically [24].

In order to solve the general flow equations, we must choose the initial configurations from which to start the flow. We require these configurations to give finite energy, which restricts the behaviour of the fields in the limit $\rho \to \infty$. We also want the flow to preserve the form of the initial configurations at $\rho \ll 1$. We discuss below how to choose boundary conditions so that these conditions are satisfied.

A pure superconducting state given by

$$f = 1\,, \qquad \vec{A} = 0 \qquad \text{and} \qquad n = 0 \tag{3.37}$$

has zero free energy (from equation (3.26)). If the fields approach (3.37) as $\rho \to \infty$ then the energy will be finite. We therefore use the boundary condition

$$\lim_{\rho\to\infty} f \to 1\,, \quad \lim_{\rho\to\infty} B \to 0\,. \tag{3.38}$$

In the small $\rho$ limit we assume an expansion of the form

$$B = b_0 + b_2\rho^2 + b_4\rho^4 + \cdots \tag{3.39}$$

$$f = \rho^\gamma(a_0 + a_2\rho^2 + a_4\rho^4 + \cdots)\,. \tag{3.40}$$

Substituting (3.40) into the right side of (3.28) we obtain

$$\dot{f} = \rho^{\gamma-2} a_0(\gamma^2 - b_0^2) + \rho^{\gamma}\big(a_2((2+\gamma)^2 - b_0^2) + a_0(\kappa^2 - 2b_0 b_2) + \big) + \mathcal{O}(\rho^{\gamma+2})\,. \tag{3.41}$$

If the flow preserves the boundary conditions, we need the forms of (3.40) and (3.41) to be the same, which means that the coefficient of the term of order $\rho^{\gamma-2}$ must be zero, from which we have

$$\gamma^2 = b_0^2\,. \tag{3.42}$$

Substituting (3.39) into the right side of (3.27) gives

$$\dot{B} = 8\rho^2 b_4 - \rho^{2\gamma}\big(a_0^2 b_0 + a_0(2a_2 b_0 + a_0 b_2)\rho^2 + \mathcal{O}(\rho^4)\big)\,. \tag{3.43}$$

The consistency of (3.39) and (3.43) requires $\gamma$, and hence $b_0$ to be an integer greater than or equal to one. The natural choice is to take $b_0 = n$ (see equation (3.25)). Equations (3.39) and (3.40) therefore give $B(0) = n$ and $f(0) = 0$.

The results of the previous two paragraphs give the complete set of boundary conditions on the flow as

$$B(0) = n\,, \quad f(0) = 0\,, \tag{3.44}$$

$$\lim_{\rho\to\infty} B(\rho) = 0\,, \quad \lim_{\rho\to\infty} f(\rho) = 1\,. \tag{3.45}$$

We will solve the flow equations by choosing initial configurations for the fields that satisfy these conditions. We also require that the fields are constant in time at the spatial boundaries, which means that (3.44) is enforced at every step $dt$ throughout the flow. We

start at $t = 0$ with the configurations

$$B(\rho) = ne^{-\rho^2} + g_1(\rho) \tag{3.46}$$

$$f(\rho) = 1 - e^{-\rho|n|} + g_2(\rho) \tag{3.47}$$

where the $g_i$ are arbitrary functions with compact support such that

$$g_1(0) = g_2(0) = 0\,. \tag{3.48}$$

Without loss of generality we can consider $n \geq 0$, which gives vortices with flux in the positive $z$ direction. Negative vortices differ only by an overall sign.

The constraint that the scalar field must be single valued means that the winding number must be an integer. Since the flow is continuous, the winding number does not change from its initial value during the flow (it is topologically conserved). The energy and flux do change under the flow but, as shown in Fig. 3.1, both flow rapidly to their asymptotic values, with very little dependence on the choice of the initial configuration from which the flow begins. The same behaviour was found in Ref. [36].

To check our method we look at $\kappa = \kappa_c$, where the energy and flux of the vortices can be determined analytically [24]:

$$\mathcal{E}_\infty = n\pi\,, \qquad \Phi_\infty = 2\pi n\,. \tag{3.49}$$

The results are shown in Fig. 3.1 for $n = 1$. The asymptotic value of the flux is reached numerically in the limit of long flow times. The correct asymptotic value of the energy is also reached numerically. We see from Fig. 3.1 that even when the functions $g_i$ introduce large perturbations, there is little effect on the time required to converge to the solution.

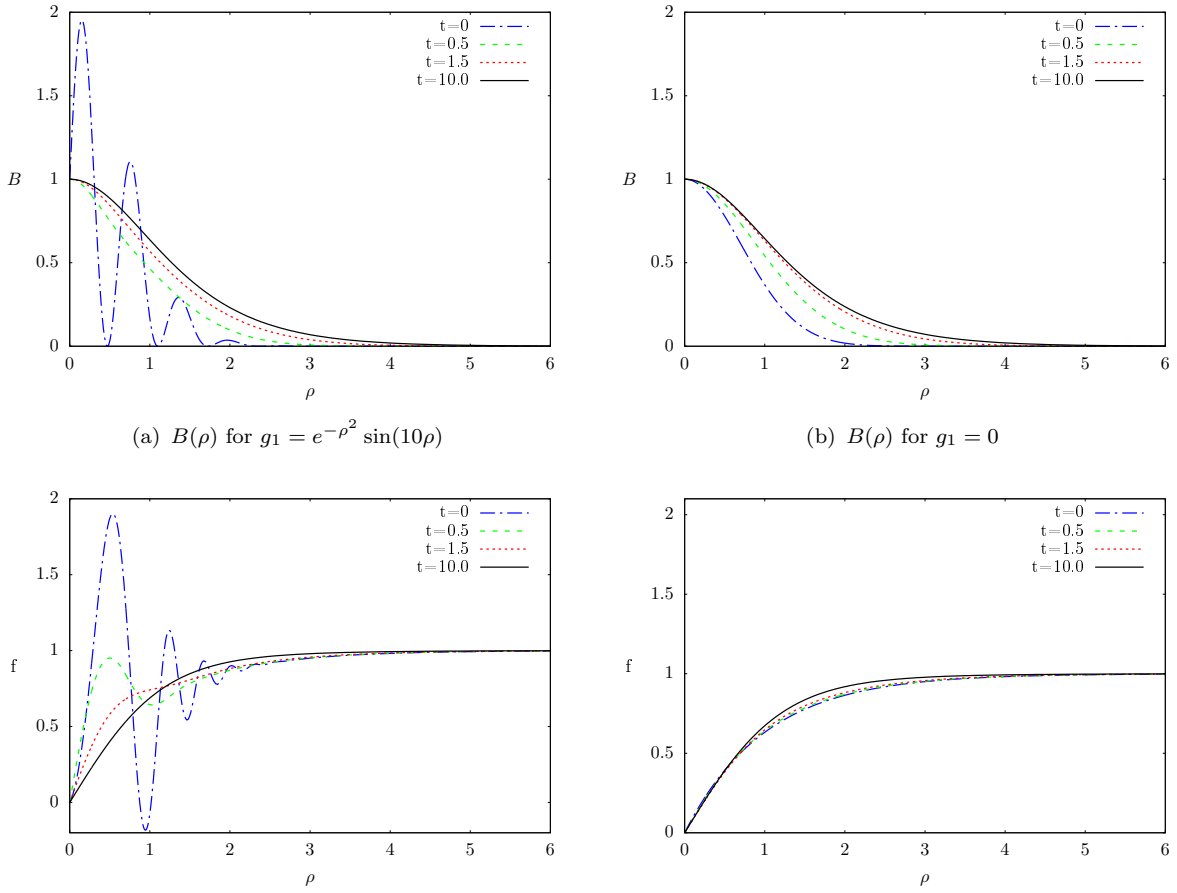


(a) $B(\rho)$ for $g_1 = e^{-\rho^2}\sin(10\rho)$

(b) $B(\rho)$ for $g_1 = 0$

(c) $f(\rho)$ for $g_2 = 2e^{-\rho^2}\sin(5\rho^2)$

(d) $f(\rho)$ for $g_2 = 0$

FIGURE 3.1: At $t = 10$ the flow with $\kappa = \kappa_c$ has converged to the solution for $n = 1$.

We also calculate the energy for different values of $\kappa$ and $n$. The energy of the vortices for $\kappa$ on either side of the critical value is summarized in equation (3.50):

$$\begin{aligned} \kappa > \kappa_c \quad &\rightarrow \quad n\mathcal{E}_1 < \mathcal{E}_n \\ \kappa = \kappa_c \quad &\rightarrow \quad n\mathcal{E}_1 = \mathcal{E}_n \\ \kappa < \kappa_c \quad &\rightarrow \quad \mathcal{E}_n < n\mathcal{E}_1 \,. \end{aligned} \tag{3.50}$$

These results verify that for $\kappa > \kappa_c$ the system is unstable to decay into 1-vortices, and when $\kappa < \kappa_c$ the $n$-vortex is stable. Fitting the data we find that the energy of an

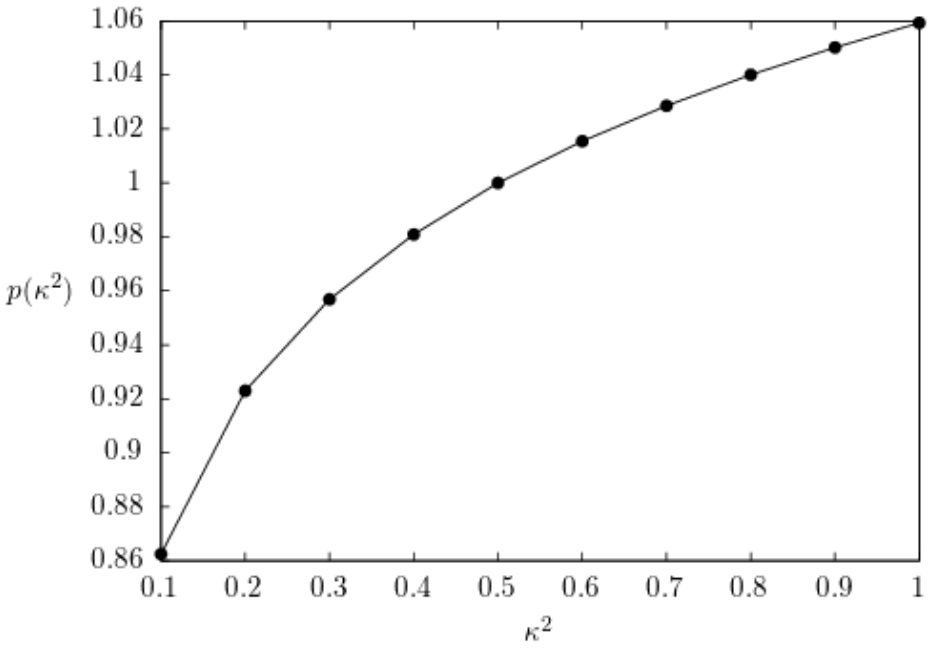


FIGURE 3.2: The exponent $p(\kappa^2)$ of the power law defined in (3.51).

$n$-vortex relative to that of $n$ 1-vortices obeys a power law of the form,

$$\mathcal{E}_n = \mathcal{E}_1 \, n^{p(\kappa^2)} \, . \tag{3.51}$$

The exponent $p(\kappa^2)$ is plotted in Fig. 3.2 for a range of $\kappa$'s in the neighborhood of the critical value. Note that each vortex energy is itself a function of $\kappa^2$ (the notation $\mathcal{E}_n$ means $\mathcal{E}_n(\kappa^2)$). At the critical value $p(\kappa_c^2) = 1$, in agreement with [24]. The function $p(\kappa^2)$ increases with $\kappa^2$ but is only weakly $\kappa^2$ dependent. The approximate solution of [23] predicts an $n^2$ dependence which agrees with the heuristic arguments of [37]. We find that the exponent increases slowly and does not appear to approach 2 in the asymptotic limit: for example, $p(1000) = 1.58$. Further discussion of the vortex energy and the static interaction energy between two vortices can be found in [38].

We would like to study numerically the stability of $n$-vortices under arbitrary perturbations. This is impossible using axial symmetric vortices in polar coordinates, since any

axially symmetric vortex in polar coordinates will be located at the origin. In order to study the stability of $n$-vortices, we consider the flow equations in a Cartesian coordinate system. This is the subject of the next section.

## 3.5 Two dimensional vortices

### 3.5.1 Ansatz for Cartesian Coordinates

We would like to study the interaction of vortices at different locations. In this case there is no overall axial symmetry, and therefore it is no longer advantagous to work in polar coordinates. The reason is as follows: (1) in polar coordinates, the preferred center of an axially symmetric system is the origin, but we want mutiple distinct vortex centers; (2) an $n$-vortex is indistinguishable from $n$ 1-vortices, if all are located at the origin. To avoid this problem we work in 2-dimensional Cartesian coordinates. The flow equations are given in equations (3.17-3.19), and as in section 3.4 we will suppress the tildes.

We consider axially symmetric vortices which can be shifted so that their centers are not at the origin. Since we work on a square lattice, the boundaries themselves break the axial symmetry, but we choose initial conditions so that the vortices are located far enough from the boundaries that the flow is unaffected by this asymmetry. A similar method was used in [39, 40]. The phase of the scalar field will not be a constant along the flow, as was the case using axial symmetry. We want to start with a configuration for the scalar field that is single valued, so that we obtain an integer winding number which will then be conserved (topologically) by the flow. We therefore define the following scalar field configuration corresponding to a single vortex with winding number $n = 1$ centered

at the point $(x_i, y_i)$:

$$\phi(x, y; x_i, y_i) = f(x, y; x_i, y_i)\, e^{i\omega(x,y;x_i,y_i)}, \tag{3.52}$$

where

$$\omega(x, y; x_i, y_i) = -\arctan\left(\frac{y - y_i}{x - x_i}\right), \quad \lim_{\vec{r}\to\infty} f(x, y; x_i, y_i) \to 1\,. \tag{3.53}$$

Parametrizing the complex scalar in terms of a real ($\phi_1$) and imaginary ($i\phi_2$) field equation (3.52) becomes

$$\phi_1(x, y; x_i, y_i) = f(x, y; x_i, y_i)\, \cos\left(-\arctan\left(\frac{y - y_i}{x - x_i}\right)\right) \tag{3.54}$$

$$\phi_2(x, y; x_i, y_i) = f(x, y; x_i, y_i)\, \sin\left(-\arctan\left(\frac{y - y_i}{x - x_i}\right)\right), \tag{3.55}$$

and thus we have

$$\lim_{\vec{r}\to\infty} \arctan\frac{\phi_1}{\phi_2} = -\arctan\frac{y}{x} \quad \text{or} \quad \lim_{\vec{r}\to\infty} \omega = -\theta\,, \tag{3.56}$$

which shows that the winding number is one (see equation (3.23)).

In the two sections below we will consider two different situations: the formation of vortices, and the interaction of vortices.

### 3.5.2 Vortex Formation

We initialize the scalar field using (3.52) centered at the origin with $f = 1$ and $\omega = -\theta$. We set the vector potential (and magnetic field) to zero ($\vec{A} = 0$) and evolve the configuration for various values of $\kappa$. We calculate the evolution of the fields and the corresponding

energy and flux. Note that the energy density in the $(x, y)$ plane of the initial configuration is constant, which leads to infinite energy if we consider the entire $(x, y)$ plane (see equations (3.26) and (3.38)). The initial energy is regulated by the size of the finite lattice in our numerical calculation. We have checked that the final energy is not affected by the finite size of the box, as long as the vortex centers are not close to the edges. We have also checked that when $\kappa = \kappa_c$ the energy approaches the correct finite value for a 1-vortex $\lim_{t\to\infty} \mathcal{E} = \pi$, as given in equation (3.49). In Fig. 3.3(a) we show the energy as a function of the flow parameter for several values of $\kappa^2$. The figure shows that the

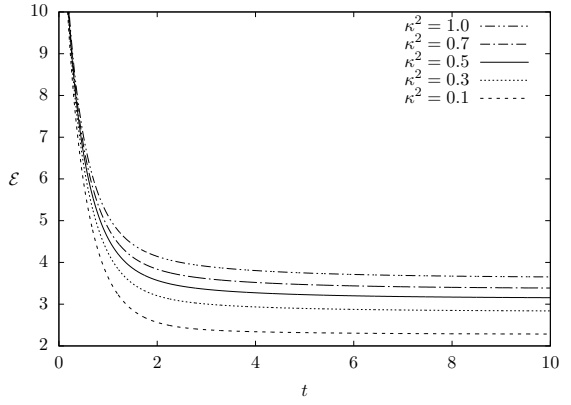


(a) The energy of configurations where a 1-vortex forms at the origin. Larger values of $\kappa^2$ correspond to larger final energies.

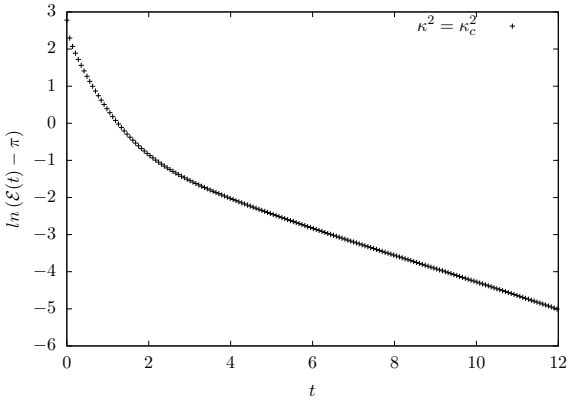


(b) $\ln(\mathcal{E}(t) - \pi)$ with $\kappa = \kappa_c$. The nonlinear behaviour is clear for early $t$, but the time dependence becomes linear as the flow progresses.

FIGURE 3.3: Energy of a configuration where a single vortex forms at the origin.

energy of a vortex increases with $\kappa$, but the evolution in time is similar for all values of $\kappa$. In Fig. 3.3(b) we see that $\ln(\mathcal{E}(t) - \pi)$ is nonlinear initially but becomes linear as the flow progresses. This suggests the existence of two distinct time scales in the vortex formation, a short time scale when the configuration is initially far from equilibrium and a longer time scale as the vortex settles to equilibrium.

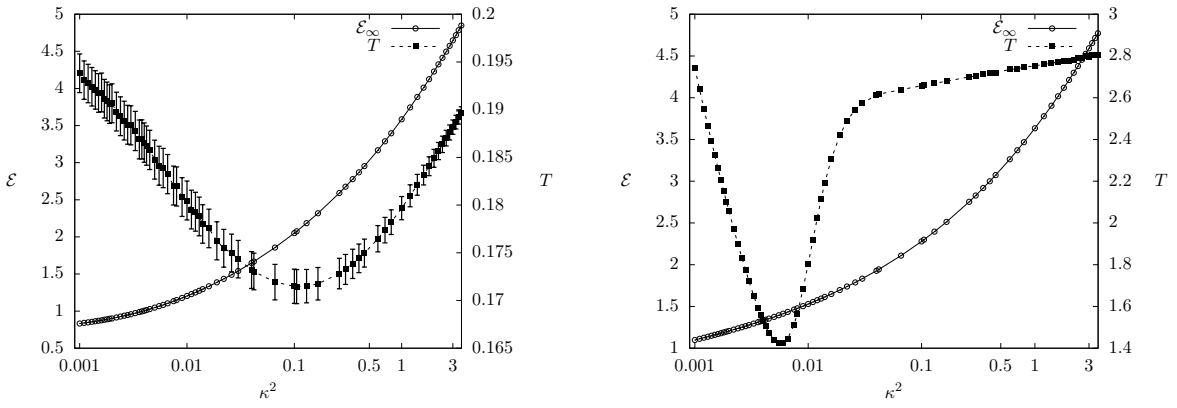


(a) $T$ and $\mathcal{E}_\infty$ for $0 < t < 5$

(b) $T$ and $\mathcal{E}_\infty$ for $5 < t < 15$

FIGURE 3.4: Parameters obtained by fitting the data to equations (3.57) in (a) and (3.58) in (b) for different values of $\kappa$.

In order to quantify the effect of $\kappa$ on the timescales for vortex formation, we fit the energy for $0 < t < 5$ to a function of the form

$$\mathcal{E}(t) = \mathcal{E}_\infty + (\Delta\mathcal{E})e^{-\sqrt{t/T}}\,, \tag{3.57}$$

where we allow $\mathcal{E}_\infty$, $\Delta\mathcal{E}$, and $T$ to vary. For $5 < t < 15$ we fit to a function of the form

$$\mathcal{E}(t) = \mathcal{E}_\infty + (\Delta\mathcal{E})e^{-t/T}\,. \tag{3.58}$$

The results are shown in Figs. 3.4(a) and 3.4(b). The parameter $\mathcal{E}_\infty$ is a non-linear increasing function of $\kappa$ and the values obtained from the two fits agree within 3%. For early times, $T$ varies very little as a function of $\kappa$, but has a minimum near $\kappa^2 = 0.1$ as shown in Fig. 3.4(a). In Fig. 3.4(b) we see that for later times $T$ has a minimum near $\kappa^2 = 0.0055$, and increases as $\kappa \to 0$ or $\kappa \to \infty$. The graphs show the asymptotic standard error from the fits for the $T$ data points.

We also considered the net magnetic flux $\Phi(t)$, starting from an initial configuration with zero flux $\Phi(0) = 0$. We expect that $\lim_{t\to\infty}\Phi = 2\pi$ (see equation (3.49)) since the

magnetic flux of a vortex is independent of $\kappa$. In fact, we found that $\Phi(t)$ is independent of $\kappa$ to numerical accuracy at all points along the flow.

### 3.5.3 Vortex Interactions

To study the interaction of vortices we want to start with field configurations that are closer to vortex solutions, so that they can properly be considered vortices. We start once again with a discussion of a 1-vortex, but this time not centered at the origin. We choose initial conditions so that the magnitude of the scalar potential satisfies the condition $\lim_{\vec{r}\to\infty} f = 1$, and the two components of the vector potential satisfy the flux quantization condition ($\Phi = 2\pi$). We define $r_i = \sqrt{(x-x_i)^2 + (y-y_i)^2}$ and choose

$$f(x, y; x_i, y_i) = \left(1 - e^{-4\sqrt{\kappa^2}\, r_i^2}\right) \tag{3.59}$$

and

$$\begin{aligned} A_x(x, y; x_i, y_i) &= -(y - y_i)\left(\frac{1 - e^{-r_i^2}}{r_i^2}\right) \\ A_y(x, y; x_i, y_i) &= (x - x_i)\left(\frac{1 - e^{-r_i^2}}{r_i^2}\right), \end{aligned} \tag{3.60}$$

which gives a flux

$$\Phi = \int_{-\infty}^{\infty} dx \int_{-\infty}^{\infty} dy\, (\partial_x A_y - \partial_y A_x) = \oint \vec{A} \cdot d\vec{l} = 2\pi\,, \tag{3.61}$$

where the line integral is taken around a square at infinity. Numerically we use a finite range for the variables $x$ and $y$ but, because of the exponential factors in (3.60), $\Phi/(2\pi)$ is still approximately one as long as the vortex center is not close to the edges of the region of integration.

Now we want to construct the fields that correspond to a superposition of vortices centered at different locations with winding numbers not necessarily equal to one. We use $(x_i^-, y_i^-)$ and $(x_i^+, y_i^+)$ to denote the initial coordinates of the centres of the negative and positive vortices respectively. In order to construct a superposition of 1-vortex configurations, the new vector field $\vec{A}$ is given by the sum of the component vector fields, while the new scalar field $\phi$ is given by the product of the component scalar fields. In this way, different gauge transformations acting on each of the vortices can be combined into a single gauge transformation of the composite fields. If we choose all $(x_i, y_i)$ distinct, the initial configuration corresponds to $n$ 1-vortices at different locations. If we choose coordinates so that two vortices are centered at the same location, we have effectively a 2-vortex at this position. We show below that the total winding number is equal to the sum of the component winding numbers. Our initial configurations are

$$A_x = \sum_i^{n^+} A_x(x, y; x_i^+, y_i^+) - \sum_i^{n^-} A_x(x, y; x_i^-, y_i^-) \tag{3.62}$$

$$A_y = \sum_i^{n^+} A_y(x, y; x_i^+, y_i^+) - \sum_i^{n^-} A_y(x, y; x_i^-, y_i^-) \tag{3.63}$$

$$\phi_1(x, y) = f \ \cos(\omega) \tag{3.64}$$

$$\phi_2(x, y) = f \ \sin(\omega) \tag{3.65}$$

where

$$f = \prod_i^{n^+} f(x, y; x_i^+, y_i^+) \prod_i^{n^-} f(x, y; x_i^-, y_i^-) \tag{3.66}$$

$$\omega = \sum_{i=1}^{n_-} \arctan\left(\frac{y - y_i^-}{x - x_i^-}\right) - \sum_{i=1}^{n_+} \arctan\left(\frac{y - y_i^+}{x - x_i^+}\right) \tag{3.67}$$

and $\omega$ satisfies

$$\lim_{\vec{r}\to\infty} \omega = -(n_+ - n_-)\theta \,. \tag{3.68}$$

We consider initial configurations with an $n$-vortex and a 1-vortex separated by a distance large enough that they do not significantly overlap. We find numerically that if $\kappa > \kappa_c$, the $n$-vortex decays into $n$ 1-vortices. This is shown in Fig. 3.5. For $\kappa < \kappa_c$ an $n$-vortex is stable, which means that the two vortices in the initial configuration will attract each other. In both the stable and unstable cases, the graph for the magnetic field has the same structure as the corresponding plots of the scalar field. At the critical value of the coupling $\kappa = \kappa_c$ the vortices do not interact, and the locations of the vortices do not deviate from those specified in the initial configuration. In this case we can find numerically stable solutions for any number of vortices, at any locations.

We would like to obtain some quantitative information about the timescales of vortex interactions. We consider three different cases.

**Two 1-Vortices**

In order to study the timescale of vortex interactions, we look at the interaction of two 1-vortices similar to the study in [38]. We find again the existence of two timescales with the best fit obtained using equation (3.57) for early times, and equation (3.58) for later times. We discuss below the physical interpretation of these timescales.

In section 3.5.2 we studied vortex formation and showed that in the early part of its evolution, a field configuration approaches equilibrium quite rapidly, with a characteristic timescale that is of order 0.2 and only weakly $\kappa$ dependent. This initial period of rapid change is followed by a longer period of slower evolution characterized by a timescale $\sim 2$. This separation of scales can be seen qualitatively from the early (steeper) and later (flatter) regions of the curve in Fig. 3.3(b).

A plot of $\ln[E(t) - E_\infty]$ versus $t$ for two approximate 1-vortices which start at (-1,0) and (0,1) is shown in Fig 3.6. The curve shows the same separation into two steep/flat regions which correspond to different characteristic timescales. We will show below that

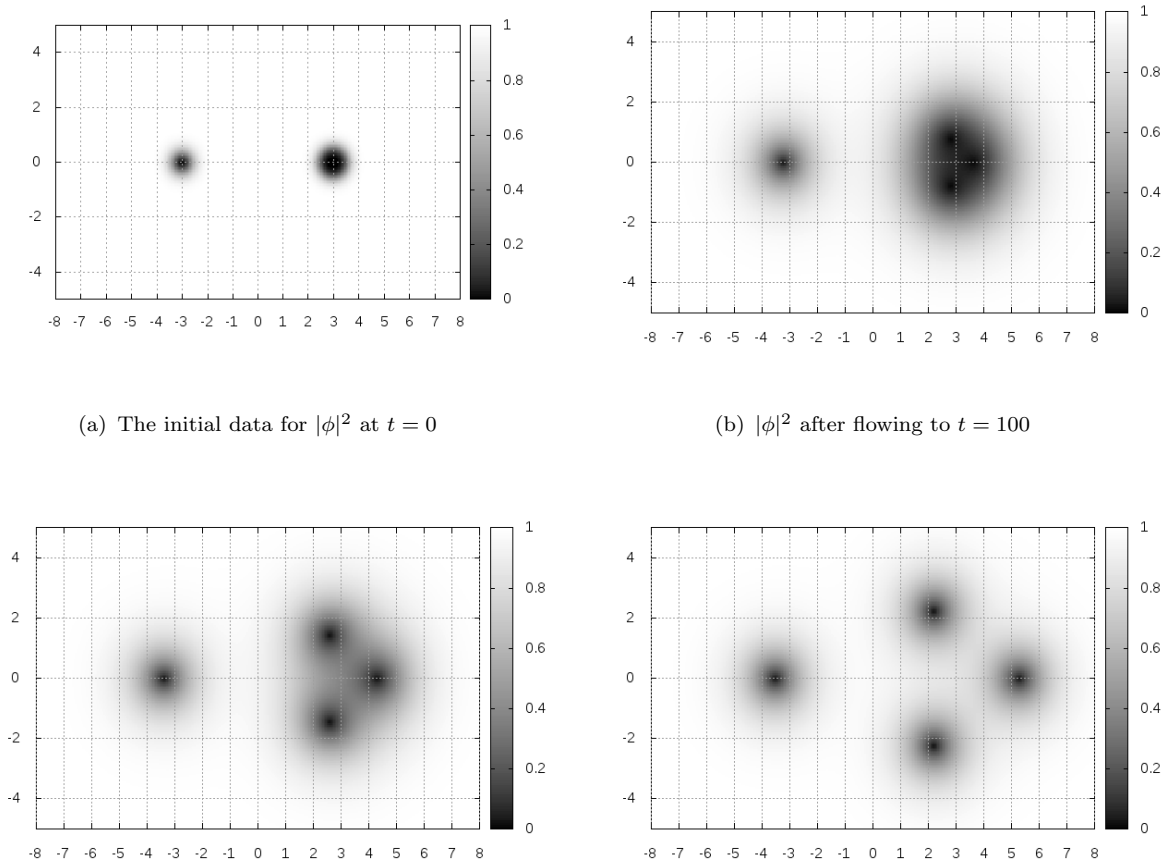

(a) The initial data for $|\phi|^2$ at $t = 0$

(b) $|\phi|^2$ after flowing to $t = 100$

(c) $|\phi|^2$ after flowing to $t = 200$

(d) $|\phi|^2$ after flowing to $t = 320$

FIGURE 3.5: Decay of a 3-vortex initially located at $(3, 0)$ with $\kappa = 1$, in the presence of a 1-vortex at $(-3, 0)$.

the results from fitting to (3.57, 3.58) produce a typical short timescale that is the same order of magnitude as in section 3.5.2, but the long timescale is orders of magnitude greater. We interpret these results by concluding that what we are seeing is a brief initial period during which the vortices form, followed by a longer phase that is dominated by the interaction of the formed vortices. The short and long timescales are therefore characteristic of vortex formation and vortex interactions, respectively. The key point is our assumption that the two timescales which are clearly seen in Fig 3.6 can be associated with the two distinct physical processes of formation and interaction. This assumption

seems justified for four reasons:

1. The simulations in section 3.4 showed that the timescale for vortex formation is largely insensitive to the initial configuration (see Fig. 3.1).

2. The short timescale has the same $\sqrt{t}$ dependence that was found in section 3.5.2 where vertex formation was studied.

3. The numerical values obtained for the short timescale are close to the numerical values for the short timescale for vortex formation from Fig. 3.4(a).

4. The interaction timescale depends strongly on $\kappa$ but the short timescale has a much weaker $\kappa$ dependence, in agreement with Figs. 3.4(a) and 3.4(b).

These last two points are explained in more detail in the last paragraph of this section.

We consider an initial configuration of two approximate vortices separated by a distance $d = 3.0$. We expect different asymptotic configurations in the cases $\kappa > \kappa_c$ and $\kappa < \kappa_c$. For $\kappa > \kappa_c$ the vortices repel and we expect the flow to move towards a configuration of two 1-vortices with large separation, and therefore we fit using $\mathcal{E}_\infty = 2\mathcal{E}_1$ where $\mathcal{E}_1$ is the energy of a single vortex for the appropriate $\kappa$. For $\kappa < \kappa_c$ the vortices attract and we expect the flow to move towards a single 2-vortex centered at the midpoint between the two initial vortices, so we fit using $\mathcal{E}_\infty = \mathcal{E}_2$ where $\mathcal{E}_2$ is the energy of a single 2-vortex for each $\kappa$ considered.

The results of the fits to (3.57) and (3.58) are summarized in Figure 3.7. In order to separate as cleanly as possible the formation timescale from the interaction timescale, we obtain the former from the region $t \in (0, 5)$ and the latter from $t \in (25, 60)$. Figure 3.7 shows clearly that $T_{\text{short}} \ll T_{\text{long}}$. We therefore conclude that the vortex formation timescale is generically faster than the vortex interaction timescale. As expected, the

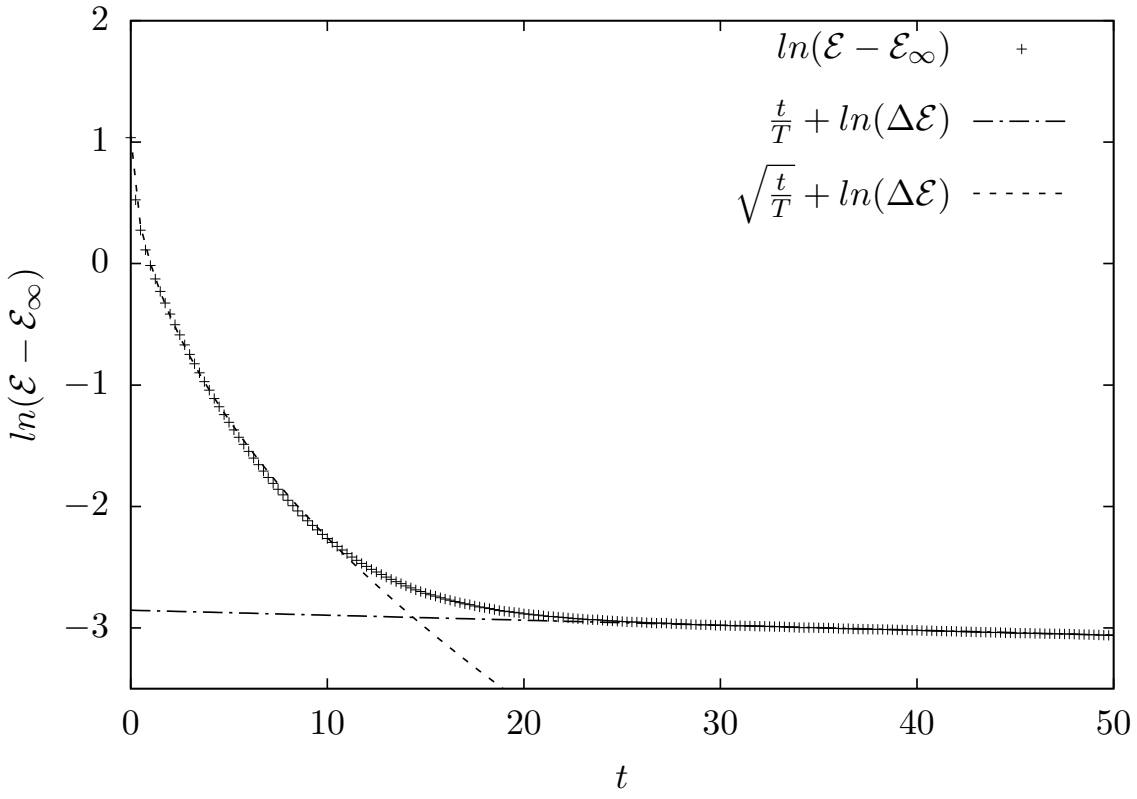


FIGURE 3.6: $\ln[\mathcal{E}(t)-\mathcal{E}_\infty]$ with $\kappa^2=0.7$ for two approximate 1-vortices which start at $(-1,0)$ and $(1,0)$. The dotted lines are the fits to equations (3.57) and (3.58). (Not all data points are plotted so that the fit lines can be clearly seen.)

interaction timescale diverges at $\kappa_c$ where the vortices do not interact, and decreases as we move away from $\kappa_c$ in either direction, and the vortex interactions become stronger. The $\kappa$ dependence of the formation timescale is weaker, which similar to what we found for the 1-vortex case (see Figs. 3.4(a) and 3.4(b)). We note also that the numerical values of the formation timescale differ from what was obtained in section 3.5.2. From Fig. 3.4(a) we find $T_{\text{short}}\sim 0.18$ for a single vortex centered at the origin, while Fig. 3.7 shows that for the configuration used in this section $0.3<T_{\text{short}}<0.8$. These differences are expected, since different initial conditions are used in the two different calculations. The important point is that we find consistently $T_{\text{long}}\gg T_{\text{short}}$.

**A 1-Vortex and a (-1)-Vortex**

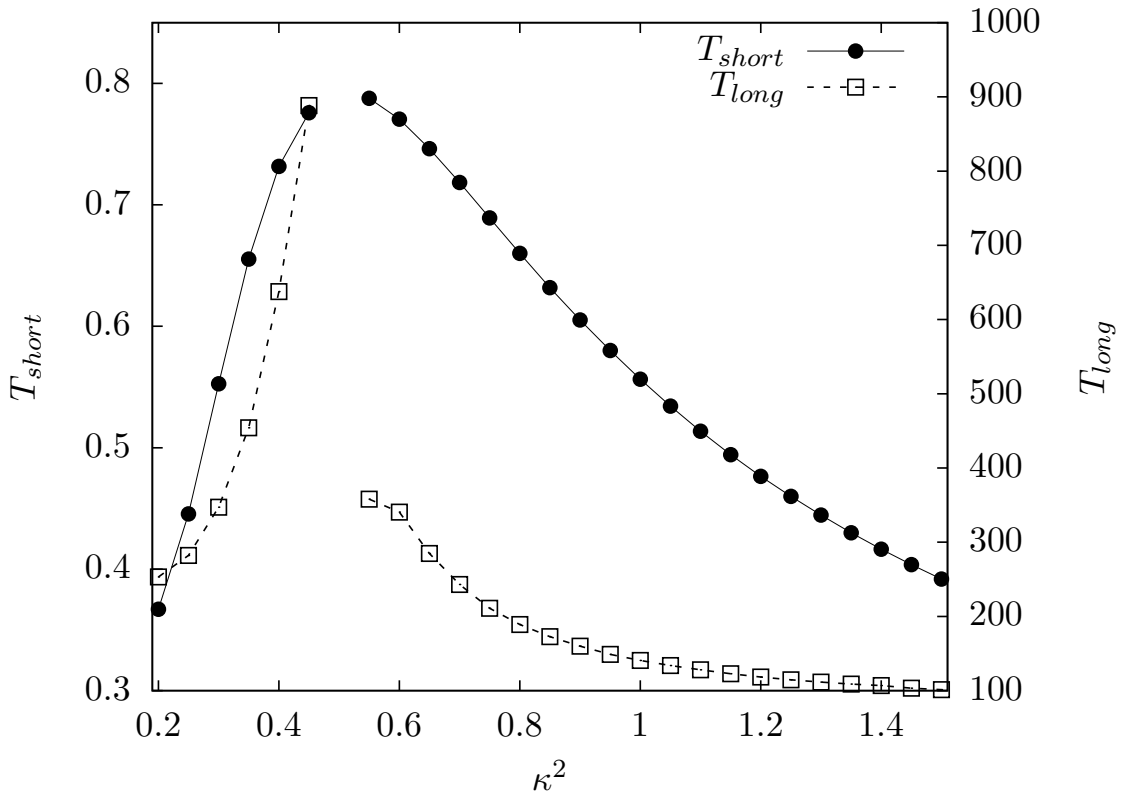


FIGURE 3.7: A plot of the fit parameters $T_{\text{short}}$ and $T_{\text{long}}$ for several values of $\kappa^2$. Near $\kappa_c^2$ the vortex interactions are very weak and the fits used to determine $T_{\text{long}}$ become more uncertain. For $\kappa_c^2$ the vortices do not interact so we exclude this point from the graph.

We also look at the interaction between a 1-vortex and a (-1)-vortex. In this case we have an overall winding number of zero, and we expect the two vortices to attract each other and cancel when they merge. In Fig 3.8 we plot the energy for $\kappa = \kappa_c$ and $\kappa = 1$. We note that vortices with opposite sign will interact in the $\kappa = \kappa_c$ case, and we can clearly see the point where the vortices merge. For $\kappa = 1$ the vortices move together rather than apart.

### Multiple Vortices

Finally, we can also study the energy of multiple vortex configurations as a function of $t$ for different values of $\kappa$. We consider two different configurations, both of which have

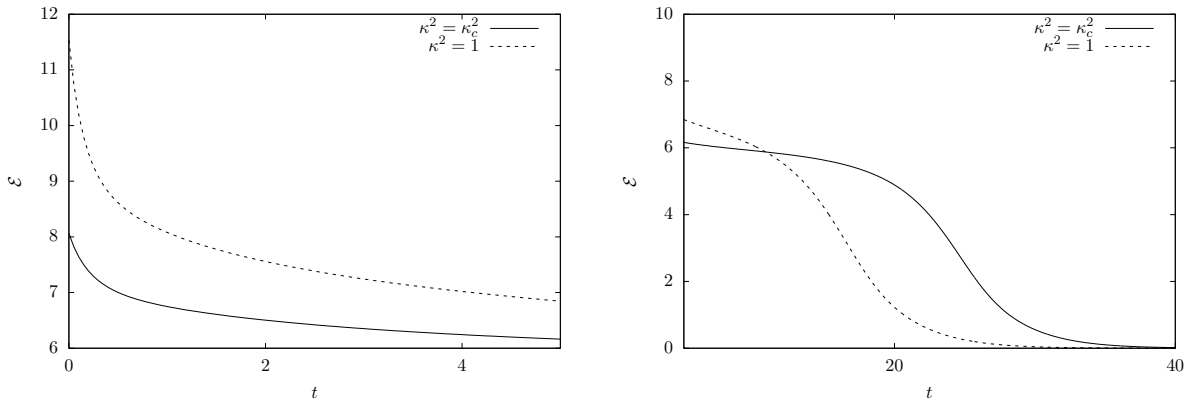


(a) The short time behaviour of $\mathcal{E}$.

(b) The long time behaviour of $\mathcal{E}$.

FIGURE 3.8: The energy of a 1-vortex and a (-1)-vortex. We start with vortices initially located at $(1.5, 0)$ and $(-1.5, 0)$, and show $\kappa^2 = \kappa_c^2$ and $\kappa^2 = 1$. For $0 < t < 5$ we see behaviour similar to the vortex interactions in both cases, but at longer times we see the vortices will attract and merge for any $\kappa$

total winding number 4. The first configuration is a 3-vortex at (3,0) and a 1-vortex at (-3,0). The second has 4 distinct 1-vortices in symmetric locations about the origin: (1,1), (1,-1), (-1,1), (-1,-1). The results are shown in Fig. 3.9. The energy $\mathcal{E}(t)$ is a monotonically decreasing function. Initially the energy decreases rapidly as the flow moves from a configuration of approximate initial vortices to true vortices. Then there is a region where the energy evolves through vortex interactions. The vortices move together or apart depending on the value of $\kappa$. For large $t$ there is an asymptotic region where the vortices have reached a stable configuration either because they are too far apart to interact strongly, or because they have merged into a single vortex. From Fig. 3.9 it is clear that the two configurations have similar short time behaviour even with different initial energies, but there is a noticeable difference in their behaviour in the region where the 3-vortex is splitting into 3 1-vortices. The asymptotic behaviour is, as expected, the same in both cases.

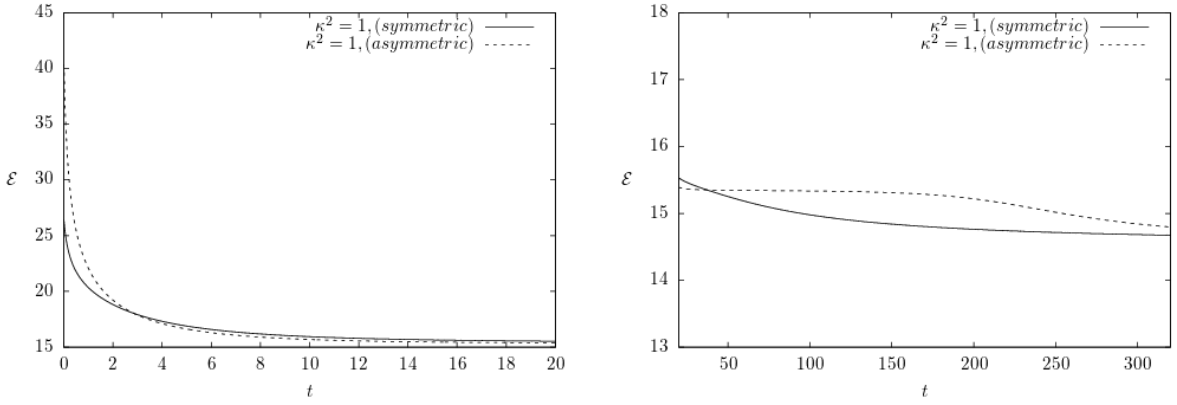


(a) The short time behaviour of $\mathcal{E}$.

(b) The long time behaviour of $\mathcal{E}$.

FIGURE 3.9: Comparison of the energy of two different configurations with total winding number $n = 4$. The symmetric configuration contains 4 1-vortices and the asymmetric one is a 3-vortex in the presence of an additional 1-vortex (see text for details). The mid range behaviour of $\mathcal{E}$ is altered by the breakup of the 3-vortex in the asymmetric case.

# Chapter 4

# Curved Spacetime

## 4.1 The Holographic Superconductor

In the previous chapter we demonstrated how the matter part of our bulk action (2.1) can describe a superconductor when the system undergoes spontaneous symmetry breaking. In this chapter we would like to use the AdS/CFT correspondence to describe a strongly coupled superconducting field theory on the 2+1 dimensional boundary of our bulk action.

To study the superconductor at some finite temperature we will need a black hole background. We start with the simplest case, a planar Schwarzschild anti-deSitter black hole with mass $M$ and $Q = 0$ we have the metric (2.27)

$$ds^2 = -f(r)dt^2 + \frac{dr^2}{f(r)} + r^2 d\Omega_{R^2}^2 \quad \text{with} \quad f(r) = \frac{r^2}{L^2} - \frac{M}{r}. \tag{4.1}$$

The mass $M$ is related to the Hawking temperature of the black hole $T = 3M^{1/3}/(4\pi L^{4/3})$, which also gives the temperature of the superconductor. Recall that $d\Omega_{R^2}^2$ is the metric on flat 2 dimensional space and we will consider $d\Omega_{R^2}^2$ in both polar and cartesian coordinates.

Once again the interesting physics in this model arises from spontaneous symmetry breaking in the scalar field. In this case the symmetry breaking of the scalar field is a result of the black hole geometry, so our potential only needs a mass term

$$V(\phi^\dagger\phi) = m^2\phi^\dagger\phi, \tag{4.2}$$

The bulk action is therefore

$$S[A,\psi] = \int d^4x\sqrt{-g}\left[\frac{c^4}{16\pi G}\left(R + \frac{6}{L^2}\right) - \frac{1}{4}F^{\mu\nu}F_{\mu\nu} - (D^\mu\phi)^\dagger D_\mu\phi - m^2\phi^\dagger\phi\right]. \tag{4.3}$$

In the context of the gravity theory, the symmetry breaking corresponds to a static non-zero scalar field outside the black hole horizon. While the formation of scalar hair suggests a contradiction to black hole no hair theorems, this is not necessarily the case in AdS spacetimes. These theorems are based on the idea that matter outside a black hole wants to either fall into the black hole, or radiate out to infinity in the asymptotically flat case. The proof is formulated in terms of a black hole uniqueness theorem, which says that when gravity is coupled to matter fields, a stationary black hole solution is uniquely characterised by its conserved charges. However, there is no completely general no hair theorem, and counter examples have been known since the 1990's [41].

In our problem, the formation of scalar hair is possible because we work in AdS space, where the negative cosmological constant acts like a confining box that prevents the charged particles from escaping to infinity. It is easy to see why the vacuum in the theory defined in (4.3) might be unstable to the formation of scalar hair. The effective mass of the scalar field is $m^2_{\text{eff}} = m^2 + g^{tt}q^2A_t^2 + \cdots$. Since $g_{tt} = -f(r) < 0$ it is possible that the effective mass becomes sufficiently negative near the horizon to destabilize the scalar field.

We can also see that the formation of the instability could be temperature dependent. Rewriting $f(r)$ from equation (4.1) in terms of the temperature and horizon radius $r_0$, defined from the equation $f(r_0) = 0$, we obtain

$$f(r) \;=\; L^2 \left(\frac{4\pi T}{3}\right)^2 \frac{r^2}{r_0^2}\left(1 - \frac{r_0^3}{r^3}\right) = L^2\alpha^2 \frac{r^2}{r_0^2}\left(1 - \frac{r_0^3}{r^3}\right) \tag{4.4}$$

where $r_0 = (ML^2)^{1/3} = \frac{4\pi L^2}{3}T$ is the radius of the event horizon and $\alpha := 4\pi T/3$ is the temperature. From this expression we see that as the temperature decreases, $|g_{tt}|$ decreases at fixed $r$ and therefore $|g^{tt}|$ increases, which means that the potential instability becomes stronger at low temperature.

It is useful to write the metric in terms of an inverse radial coordinate $u = r_0/r$. Using this notation the metric takes the form

$$ds^2 = \frac{L^2\alpha^2}{u^2}\left(-h(u)dt^2 + d\Omega_{R^2}^2\right) + \frac{L^2 du^2}{u^2 h(u)} \quad \text{with} \quad h(u) = 1 - u^3\,. \tag{4.5}$$

In these coordinates the black hole horizon is located at $u = 1$ and the boundary of AdS space is $u = 0$. Since we are not concerned with the physics inside the black hole horizon, we only need to consider $u \in [0, 1]$.

It will be convenient to write the complex scalar field $\phi$ in terms of two real scalar fields, $p$ and $\omega$

$$\phi = \frac{p}{q\sqrt{2}} e^{i\omega}. \tag{4.6}$$

We will also rescale our vector field $\tilde{A}_\mu = qA_\mu$ which gives

$$\tilde{F}_{\mu\nu} = qF_{\mu\nu} = \partial_\mu \tilde{A}_\nu - \partial_\nu \tilde{A}_\mu \quad \text{and} \quad \tilde{D}_\mu = \partial_\mu - i\tilde{A}_\mu\,. \tag{4.7}$$

Using this notation the action becomes

$$S = \int d^4x\sqrt{-g}\,(\mathcal{L}_{GR} + \frac{1}{q^2}\mathcal{L}_M). \tag{4.8}$$

In order to avoid considering backreactions of the matter fields on the metric we will consider the "probe limit." Mathematically we reach the probe limit by taking $q \to \infty$ in equation (4.8), so that the gravity part of the action decouples from the matter part. Physically this means that we neglect backreaction of the gauge and scalar fields on the geometry itself. The basis of the approximation is the assumption that the terms containing the matter fields are negligible in the equations of motion for the metric components, which can then be solved to obtain the metric in (4.1). The equations of motion for the matter fields are then calculated after we substitute the metric in equation (4.1) into the action, which means physically that we study the dynamics of the matter fields within a background AdS blackhole metric.

We will also redefine the free energy to include only the matter part

$$\tilde{\mathcal{E}} = -\int dx^3\sqrt{-g}\,\mathcal{L}_M\,, \tag{4.9}$$

which in the case of static fields only is

$$\begin{aligned}\tilde{\mathcal{E}} = \int d^3x \Bigg[&\frac{g^{tt}}{2}(\partial^i\tilde{A}_t\partial_i\tilde{A}_t + \frac{1}{4}\tilde{F}^{ij}\tilde{F}_{ij} + \frac{g^{tt}}{2}\tilde{A}_t^2p^2 \\ &+\frac{p^2}{2}(\tilde{A}^i - \partial^i\omega)(\tilde{A}_i - \partial_i\omega) + \frac{1}{2}\partial^ip\partial_ip + \frac{1}{2}m^2p^2\Bigg]\,,\end{aligned} \tag{4.10}$$

where the $i, j$ indices are summed over spatial dimensions only. From this point forward we drop the tildes that were introduced in equations (4.7, 4.9).

## 4.2 Properties of Holographic Superconductors

Generally the solutions to the equations of motion for (4.3) must be found numerically. The gradient flow can be used to find solutions numerically, and also to study the stability of the solutions. This section will discuss several properties of holographic superconductors determined by the fixed points of the gradient flow without going into detail about the flow itself.

The most important property of the holographic superconductor is the critical temperature $T_c$. The critical temperature can be determined by studying the stability of the $p = 0$ vacuum solution. Below the critical temperature the solution is unstable to the formation of scalar hair, and above the critical temperature the solution is stable.

By varying $\alpha = 4\pi T/3$ we can determine the critical value below which the vacuum becomes unstable. We start with an initial perturbation of the scalar field and solve the flow numerically. If the vacuum is stable the flow will move towards $p(u) = 0$, otherwise the system will flow towards a stable fixed point, where $p(u \to 0) = c_2 u^2 + \cdots$ determines the expectation value of the condensate operator on the boundary. To compare with the results of [42], we recall $\langle \mathcal{O}_\pm \rangle = \alpha^{\Delta_\pm} c_\pm$ and plot $\langle O_2 \rangle$ versus $T$. The parameter $c_2$ is obtained from a second derivative of the scalar field [see equation (2.50)]. The result is shown in Fig. 4.1(a), and agrees well with figure 1b in Ref. [42]. In Fig. 4.1(b) we show the same data using different variables: using $\alpha = 4\pi T/3 = r_0/L^2$ we plot $c_2$ versus $\alpha^2$. From Fig. 4.1(b) we see that the critical temperature is approximately $\alpha_c^2 \approx 0.059$ or $T_c \approx 0.058$.

We can also determine the coherence length of the holographic superconductor. Starting with a configuration similar to the coherence length calculation in section 2.2, we can find the length scales over which the condensate operator and the charge density change. Further details of the calculation will be provided in section 4.3.4.

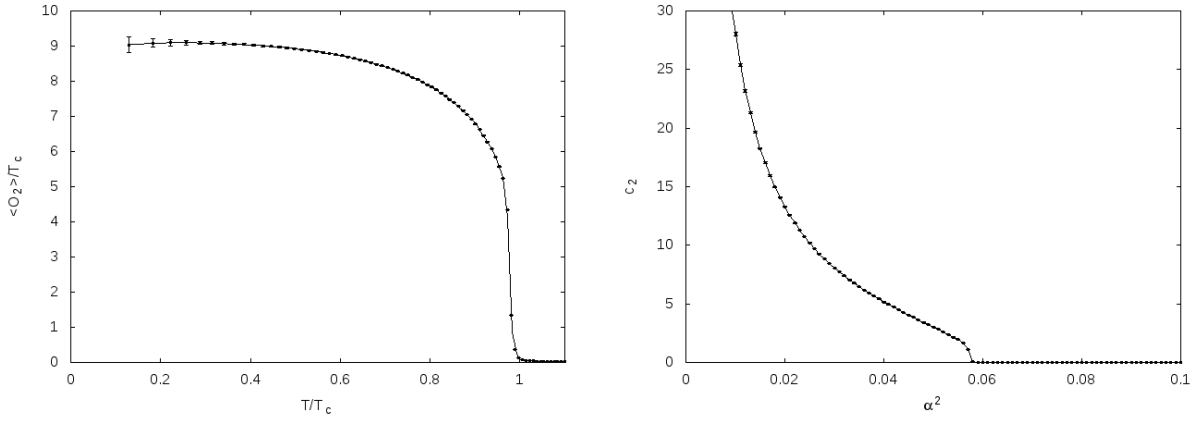


(a) $\langle O_2 \rangle$ as a function of $T$

(b) $c_2$ as a function of $\alpha^2$

FIGURE 4.1: The dependence of the condensate on temperature for spatially independent fields.

Recall that in the Ginzburg-Landau (GL) theory of superconductivity there is an exact solution for the order parameter $\phi_{Gl}$

$$\phi_{Gl} = \phi_\infty \tanh\left(\frac{x}{\sqrt{2}\xi}\right), \tag{4.11}$$

where $\phi_\infty$ is the value of the order parameter in the pure superconducting phase, and $\xi$ is the coherence length.

Our numerical results indicate that the boundary operator has a similar $x$ dependence, and we can therefore fit to a function of the same form as equation (4.11) to determine the coherence length of the holographic superconductor. We can see in Fig. 4.2(b) that, as expected, the coherence length diverges proportional to $1/\sqrt{1-\alpha/\alpha_c} = 1/\sqrt{1-T/T_c}$ as we approach the critical temperature. We note that due to this divergence, the condition $x_{\max}/\xi > 1$ cannot be satisfied very close to the critical temperature and for this reason we have considered only $T \leq 0.93 T_c$.

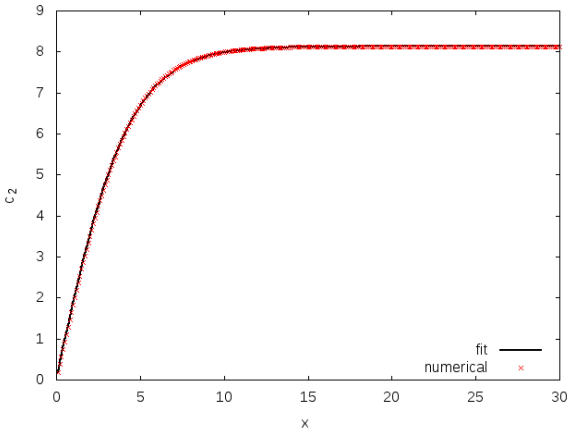


(a) For $\alpha^2 = 0.03$ we fit the boundary values $c_2(x)$ to a hyperbolic tanh function for the soliton fixed point (see equation (4.11)).

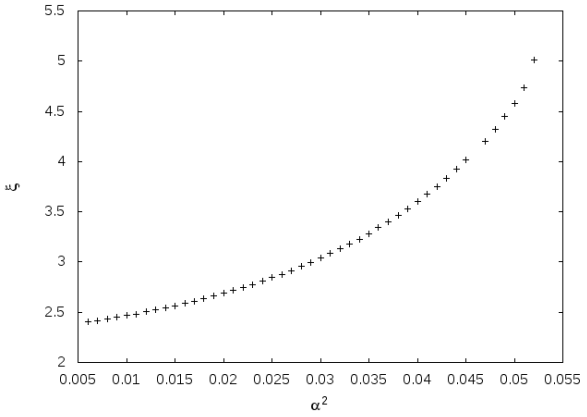


(b) The coherence length as a function of $\alpha^2$ for the superconductor. For the range of $\alpha$'s in the figure we have $\xi \ll x_{\max} = 30$, as discussed in the text under equation (4.11).

FIGURE 4.2: Measuring the coherence length of the holographic superconductor by considering an inhomogeneous configuration with $B = 0$

In the GL theory the charge density is proportional to $\phi^2$

$$\bar{\rho} \propto \phi^2 \propto \tanh^2\left(\frac{x}{\sqrt{2}\xi}\right) = 1 - \operatorname{sech}^2\left(\frac{x}{\sqrt{2}\xi}\right). \tag{4.12}$$

We can therefore find a characteristic length for the charge density $\bar{\rho}(x)$ by fitting to $\operatorname{sech}^2(\frac{x}{\sqrt{2}\xi_q})$. Contrary to what we expect from GL theory, we find that the two length scales are different. The difference between $\xi$ and $\xi_q$ increases as we move further from the critical temperature, as can be seen in Fig. 4.3. This result agrees with what was found in [43] (apart from a difference in how coherence length is defined in the GL compared to Gross-Pitaevskii equations).

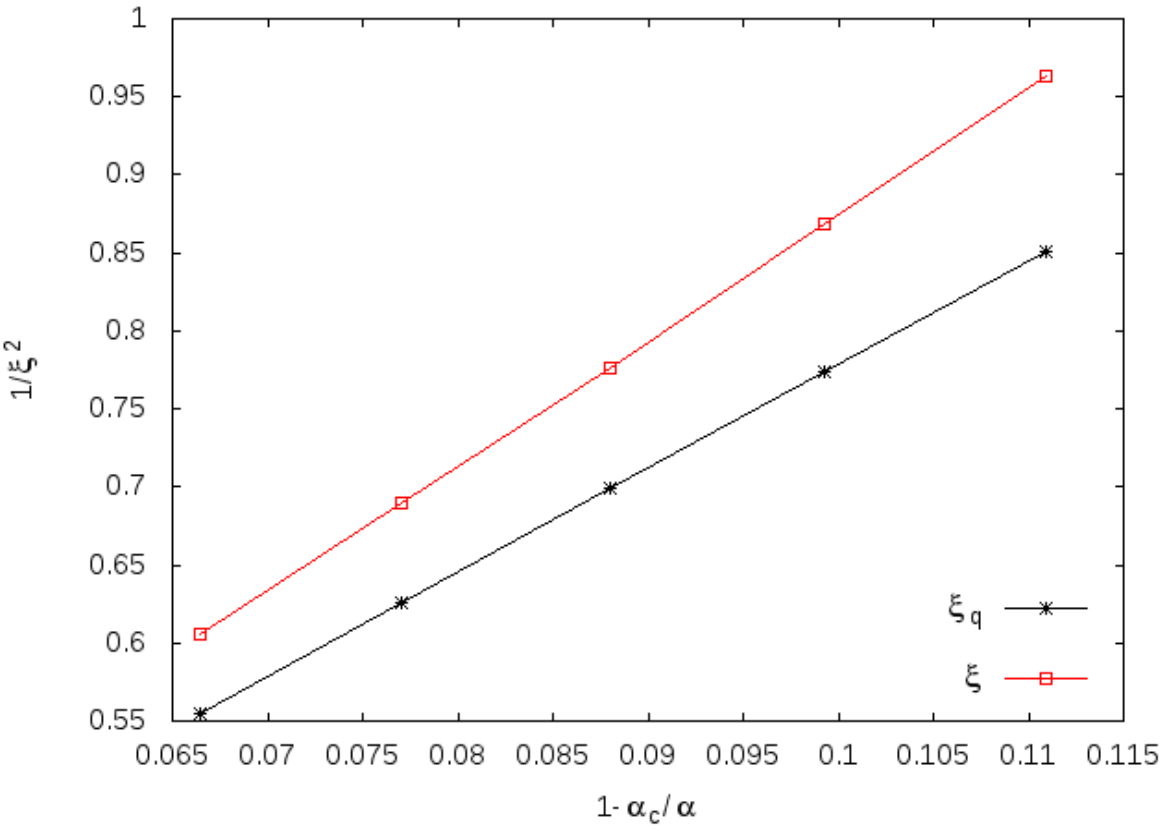


FIGURE 4.3: The two coherence lengths $\xi$ (for the scalar field) and $\xi_q$ (for the charge density) as a function of the deviation from the critical temperature for soliton solutions.

## 4.3 The Gradient Flow

### 4.3.1 Gauge Choice and Ansätze

We will consider three separate cases, with different symmetries on the boundary.

#### Spatially Independent Case

We use coordinates in which $d\Omega_{R^2}^2 = dx^2 + dy^2$. We will simplify the equations by setting $A_u = A_x = A_y = \omega = 0$. We will also take $A_t$ and $p$ to be functions of $u$ only. The

complete set of conditions we impose are

$$A_u = A_x = A_y = \omega = 0 \tag{4.13}$$

$$A_t = A_t(u)\,,\ p = p(u)\,. \tag{4.14}$$

The free energy obtained from (4.10) is

$$\mathcal{E} = \frac{1}{2}\int du\left[-\alpha(\partial_u A_t)^2 + \frac{\alpha^3 h(u)}{u^2}(\partial_u p)^2 + p^2\left(\frac{m^2\alpha^3}{u^4} - \frac{\alpha A_t^2}{u^2 h(u)}\right)\right]. \tag{4.15}$$

The flow equations for the fields in (4.13) become $\dot{A}_u = \dot{A}_x = \dot{A}_y = \dot{\omega} = 0$, where the dots denote derivatives with respect to the flow parameter. Thus the conditions in (4.13) are preserved by the flow. We also note that these conditions give $\chi = 0$, which means that the deTurck term does not contribute. The flow equations for the non-zero fields are

$$\dot{A}_t = \frac{u^2 h}{L^2}\partial_u^2 A_t - p^2 A_t \tag{4.16}$$

$$\dot{p} = \frac{u^2}{L^2}\left[u^2\partial_u(\frac{h}{u^2}\partial_u p) - p\left(\frac{-A_t^2}{\alpha^2 h} + \frac{L^2 m^2}{u^2}\right)\right]. \tag{4.17}$$

Since the metric depends only on the coordinate $u$, the conditions in (4.14) are also preserved by the flow. Equations (4.16, 4.17) give a closed set of equations for two fields that depend on two spatial dimensions, $x$ and $u$, and the flow parameter.

### Translational Symmetry

We again consider coordinates in which $d\Omega_{R^2}^2 = dx^2 + dy^2$ and simplify the equations by setting $A_u = A_x = \omega = 0$. We will now take $A_t$, $A_y$ and $p$ to be functions of $x$ and $u$ only, so our problem has a translational symmetry along the $y$ axis. The complete set of

conditions we impose are

$$A_u = A_x = \omega = 0 \tag{4.18}$$

$$A_t = A_t(u,x)\,,\ A_y = A_y(u,x)\,,\ p = p(u,x)\,. \tag{4.19}$$

It is easy to see that with these conditions, the flow equations for the fields in (4.18) become $\dot{A}_u = \dot{A}_x = \dot{\omega} = 0$, which shows that the conditions in (4.18) are preserved by the flow. We also note that these conditions again give $\chi = 0$, so that the deTurck term does not contribute. The free energy (4.10) in this case is:

$$\mathcal{E} = \frac{1}{2}\int dudx \left[-\alpha(\partial_u A_t)^2 + \alpha h(\partial_u A_y)^2 - \frac{(\partial_x A_t)^2}{h\alpha} + \frac{(\partial_x A_y)^2}{\alpha} + \frac{\alpha}{u^2}(\partial_x p)^2 \right.$$
$$\left. + \frac{\alpha^3 h(u)}{u^2}(\partial_u p)^2 + p^2\left(\frac{m^2\alpha^3}{u^4} + \frac{\alpha A_y^2}{u^2} - \frac{\alpha A_t^2}{u^2 h(u)}\right)\right]. \tag{4.20}$$

The flow equations for the non-zero fields are

$$\dot{A}_t = \frac{u^2 h}{L^2}\partial_u^2 A_t + \frac{u^2}{L^2\alpha^2}\partial_x^2 A_t - p^2 A_t \tag{4.21}$$

$$\dot{A}_y = \frac{u^2}{L^2}\partial_u(h\partial_u(A_y)) + \frac{u^2}{L^2\alpha^2}\partial_x^2 A_y - p^2(A_y) \tag{4.22}$$

$$\dot{p} = \frac{u^2}{L^2}\left[\frac{1}{\alpha^2}\partial_x^2 p + u^2\partial_u\left(\frac{h}{u^2}\partial_u p\right) - p\left(\frac{-A_t^2}{\alpha^2 h} + \frac{(A_y)^2}{\alpha^2} + \frac{L^2 m^2}{u^2}\right)\right]. \tag{4.23}$$

Since the metric depends only on the coordinate $u$, the right sides of these equations are independent of $y$ and $t$, which shows that the conditions in (4.19) are also preserved by the flow. Equations (4.21 - 4.23) give a closed set of equations for three fields that depend on two spatial dimensions, $x$ and $u$, and the flow parameter.

We note that using these coordinates the magnetic field in the boundary theory is obtained from equation (2.55) as

$$B(x) = \partial_x A_y(u = 0, x)\,. \tag{4.24}$$

### Axial Symmetry

We will also consider coordinates where $d\Omega_{R^2}^2 = d\rho^2 + \rho^2 d\theta^2$. One motivation is that rotational symmetry allows us to study completely localized solutions that could be created in a lab. When working with axial symmetry one typically looks for solutions where the phase of the complex scalar field can be written $\omega = n\theta$, and $n$ is interpreted as an integer winding number. The value of the winding number is an important property of vortex solutions and leads to flux quantization in superconductors. We will once again take $\omega = 0$, which can be thought of as a gauge choice as before, but since we impose axial symmetry on the remaining fields, it also restricts us to solutions with zero winding number. We will further take $A_u = A_\rho = 0$, and assume that our remaining fields are functions of $u$ and $\rho$ only. The complete set of conditions we use is

$$A_u = A_\rho = 0 \tag{4.25}$$

$$\omega = n\theta\,,\ n = 0 \tag{4.26}$$

$$A_t = A_t(u,\rho)\,,\ A_\theta = A_\theta(u,\rho)\,,\ p = p(u,\rho)\,. \tag{4.27}$$

The free energy (4.10) becomes

$$\mathcal{E} = \frac{1}{2}\int du\, d\rho\, \rho \left[-\alpha(\partial_u A_t)^2 + \alpha h(\partial_u A_\theta)^2 - \frac{(\partial_r A_t)^2}{h\alpha} + \frac{(\partial_r A_\theta)^2}{\rho^2\alpha} + \frac{\alpha}{u^2}(\partial_r p)^2 \right.$$
$$\left. + \frac{\alpha^3 h(u)}{u^2}(\partial_u p)^2 + p^2\left(\frac{m^2\alpha^3}{u^4} + \frac{\alpha A_\theta^2}{\rho^2 u^2} - \frac{\alpha A_t^2}{u^2 h(u)}\right)\right]. \tag{4.28}$$

We note that the flow equations again give $\dot{A}_u = \dot{A}_\rho = \dot{\omega} = 0$ so that the conditions (4.25, 4.26) are preserved by the flow, and we also have that $\chi = 0$, which means that the deTurck term does not contribute. The remaining flow equations are

$$\dot{A}_t = \frac{u^2 h}{L^2}\partial_u^2 A_t + \frac{u^2}{L^2\alpha^2}\left(\partial_\rho^2 A_t + \frac{1}{\rho}\partial_\rho A_t\right) - p^2 A_t \tag{4.29}$$

$$\dot{A}_\theta = \frac{u^2}{L^2}\partial_u(h\partial_u(A_\theta)) + \frac{u^2}{L^2\alpha^2}\left[\partial_\rho^2 A_\theta - \frac{1}{\rho}\partial_\rho A_\theta\right] - p^2(A_\theta - n) \tag{4.30}$$

$$\begin{aligned}\dot{p} = {} & \frac{u^2}{L^2}\left[\frac{1}{\alpha^2}\left(\partial_\rho^2 p + \frac{1}{\rho}\partial_\rho p\right) + u^2\partial_u\left(\frac{h}{u^2}\partial_u p\right)\right. \\ & \left. - p\left(\frac{-A_t^2}{\alpha^2 h} + \frac{A_\theta^2}{\alpha^2\rho^2} + \frac{L^2 m^2}{u^2}\right)\right].\end{aligned} \tag{4.31}$$

The azimuthal component of the vector potential of the boundary theory can be written [see equation (2.55)] as

$$A_\theta(u) = \frac{B}{2}\rho^2 + J_\theta u + \cdots, \tag{4.32}$$

where $B$ is the magnetic field and $J_\theta$ is an azimuthal current.

### 4.3.2 Solutions to the Gradient Flow

To solve our gradient flow equations we need to proceed numerically, starting from a specified initial configuration for the fields. Since we are particularly interested in studying the flow between two fixed points, we consider the vacuum (hairless black hole) configuration which has a simple analytic form:

$$A_t = \mu(1-u), \quad A_y = Bx, \quad p = 0 \tag{4.33}$$

for the translationally symmetric case, and

$$A_t = \mu(1-u)\,, \quad A_\theta = \frac{B}{2}\rho^2\,, \quad p = 0 \tag{4.34}$$

for the axially symmetric case. It is easy to verify that these configurations are fixed points of the flow. From equations (4.24, 4.32) we see that $B$ is an arbitrary constant external magnetic field. We will start the flow from the vacuum configurations in (4.33) or (4.34) with the addition of a small perturbation of the scalar field, $\delta p$. We employ a simple explicit finite difference method with a forward difference in flow time and centered difference in spatial coordinates. Further details about the numerical method and boundary conditions can be found in Appendix A.

One feature of the gradient flow method is that if our perturbation satisfies $\delta p(u=0) = 0$, then $\dot{A}_\mu(u=0) = 0$. This is true for all of our ansätze and can be seen directly from equations (4.16, 4.21, 4.22, 4.29, 4.30). We have therefore that in the boundary theory, the chemical potential $\mu = A_t(0)$ and magnetic field $B = \partial_x A_y(0,x)$ or $B = \frac{1}{\rho}\partial_\rho A_\theta(0,\rho)$, are specified by our initial configuration and remain constant along the flow.

A more general statement is that using our method the gauge field on the boundary $A_\mu(0,\vec{x})$ and all its derivatives with respect to boundary coordinates are fixed by our initial configuration and unchanged along the flow. This means that the boundary theory does not have a dynamical gauge field, which corresponds physically to the limit where the superconductor is equivalent to a superfluid. It is possible to make the gauge field dynamical by including an additional boundary term in the bulk action and considering a different type of boundary condition on $A_\mu$ [44]. While a dynamical gauge field is important for many superconductor phenomena such as the Meissner effect, a fixed background is sufficient to study how gradient flow in the bulk creates a corresponding flow in the boundary, and the extension of the flow to more complicated systems is

straightforward. We comment that, while $A_\mu(0,\vec{x})$ and its derivatives with respect to boundary coordinates $\partial_x A_\mu(0,\vec{x})$ and $\partial_y A_\mu(0,\vec{x})$ are fixed on the boundary (as explained above), derivatives with respect to the AdS coordinate $\partial_u A_\mu(u,\vec{x})\big|_{u=0}$ are not fixed and give dynamic operators in the boundary theory [see equations (2.53, 4.32)].

We are interested in how the flow alters the condensate operator and the free energy in the boundary theory. With respect to the free energy, the quantity of physical interest is the change in the free energy along the flow relative to the energy of the vacuum state $\Delta E = \mathcal{E} - \mathcal{E}_{\text{vac}}$. Using this normalization we find that when the vacuum solution is unstable the quantity $\Delta E$ moves from an initial value of zero into negative values. This type of behaviour is typical in systems that exhibit spontaneous symmetry breaking, where a false vacuum decays into a more stable (but less symmetric) configuration.

In numerical calculations we will set $L = 1$, which is equivalent to using the AdS radius as a length scale in all dimensional quantities (including the flow parameter). We will also set the chemical potential $\mu = 1$. This is equivalent to defining new $\rho$ (or $x, y$) coordinates and absorbing $\mu$ into the parameter $\alpha$ in the flow equations as follows:

$$A_t \to \tilde{A}_t = \frac{A_t}{\mu} \tag{4.35}$$

$$\rho \to \tilde{\rho} = \mu\rho \tag{4.36}$$

$$\alpha \to \tilde{\alpha} = \frac{\alpha}{\mu} = \frac{4\pi T}{3\mu} \tag{4.37}$$

$$B \to \tilde{B} = \frac{B}{\mu^2}\,. \tag{4.38}$$

In the following we omit the tildes but understand that setting $\mu = 1$ in the solution implies we are in fact referring to the above rescaled quantities in our results. We vary the parameter $\alpha = 4\pi T/3$ (or equivalently the temperature) and the magnetic field $B$.

### 4.3.3 Spatially Independent Solutions

By varying $\alpha = 4\pi T/3$ we can determine the critical value below which the vacuum becomes unstable. Recall from Fig. 4.1(b) that the critical temperature determined is approximately $\alpha_c^2 \approx 0.059$. To study the behaviour along the flow, we start with an initial perturbation of the scalar field given by

$$\delta p(u) = 10^{-3} \times u^2 e^{-(u-1)^2} . \tag{4.39}$$

Figure 4.4 shows how this initial perturbation evolves for two different values of the temperature on either side of the critical value. In Fig. 4.4(a) the bulk scalar field moves away from the (false) vacuum, and in Fig. 4.4(b) we see that at higher temperature the perturbed system returns to the vacuum configuration.

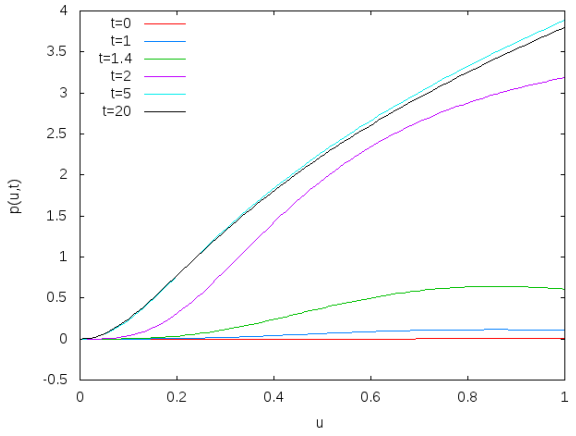


(a) For $\alpha^2 = 0.01$ a perturbation away from $p = 0$ is unstable.

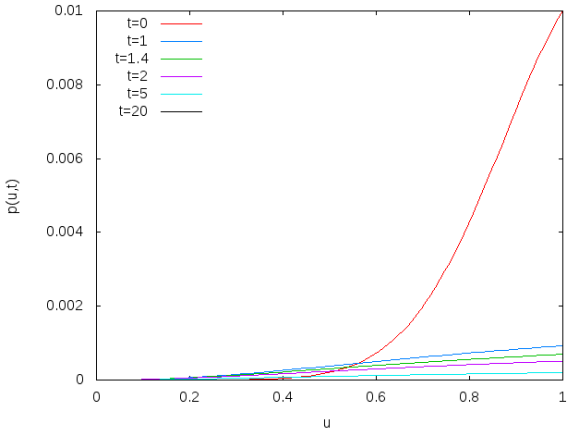


(b) For $\alpha^2 = 0.1$ a perturbation away from $p = 0$ returns to zero.

FIGURE 4.4: The evolution of the scalar field $p(u)$, at several values of $\tau$ along the flow for spatially independent fields.

We also want to study the evolution of physical quantities in the boundary theory as a function of the flow parameter. In Fig. 4.5 we show the evolution of the free energy, charge density, and condensate operator with the flow parameter.

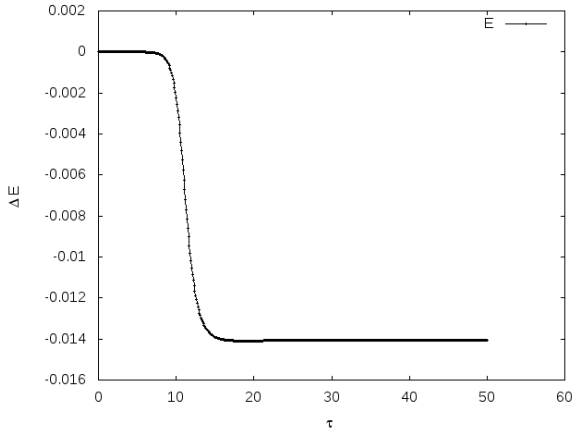


(a) $\Delta E$ as a function of $\tau$ for spatially independent fields

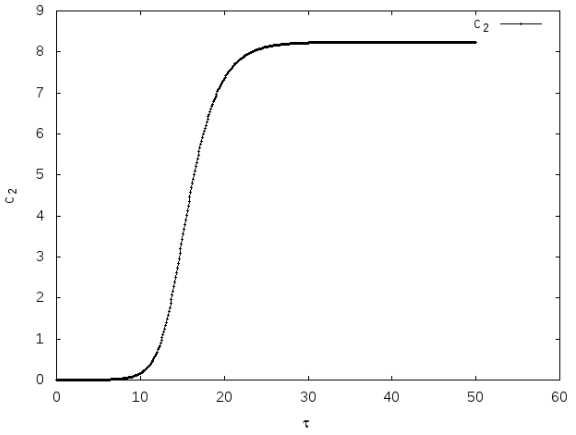


(b) $c_2$ as a function of $\tau$

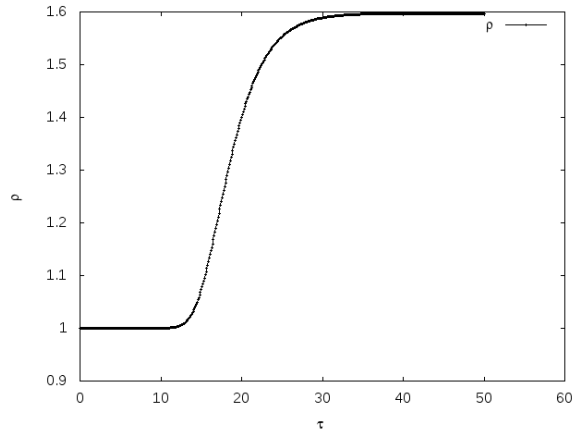


(c) $\bar{\rho}$ as a function of $\tau$

FIGURE 4.5: The flow of quantities in the boundary theory for $\alpha^2 = 0.03$.

Since the energy is a decreasing quantity along the flow between the vacuum fixed point and the scalar hair fixed point, we can look at the quantities in the boundary theory as functions of the bulk free energy instead of the flow parameter, which has no straightforward physical interpretation. Fig. 4.6 shows how the condensate changes as the energy of the system decreases.

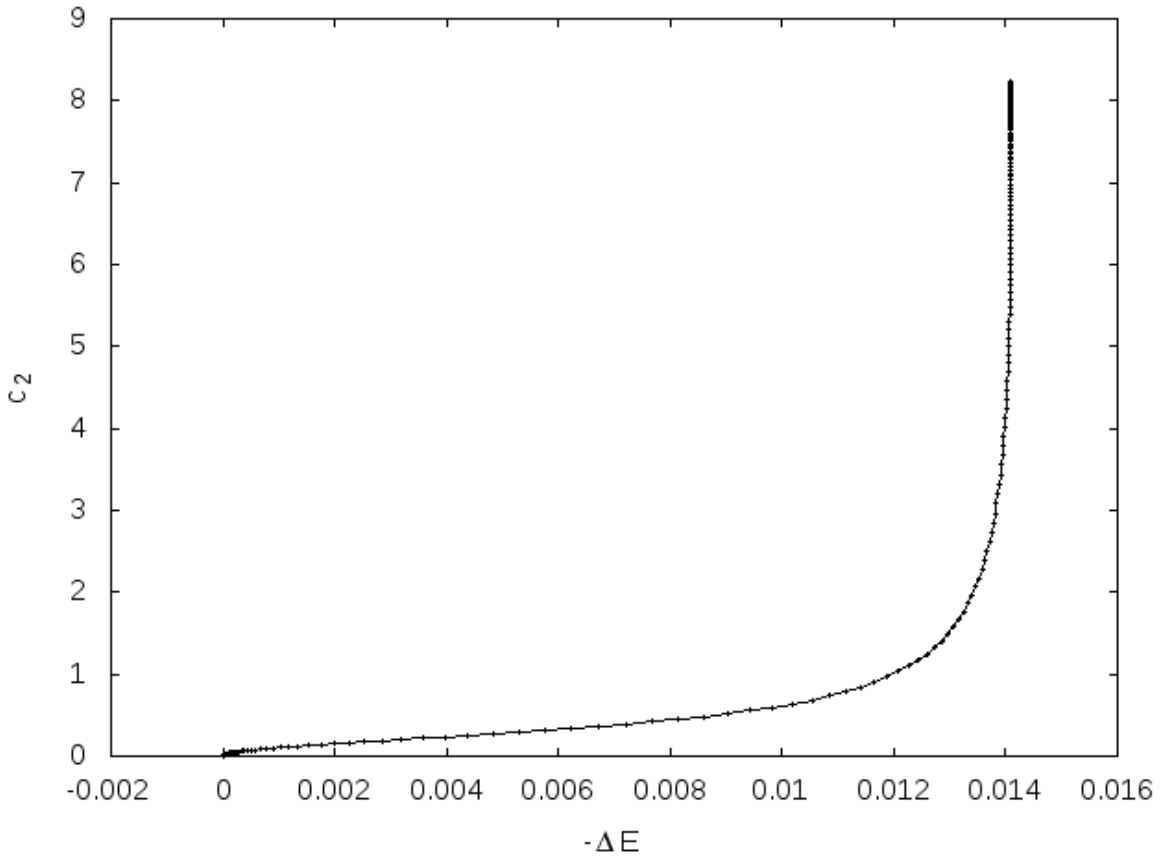


FIGURE 4.6: $c_2$ as a function of $-\Delta E$ for spatially independent fields at $\alpha^2 = 0.03$.

### 4.3.4 Translationally symmetric dark solitons

We notice that the equations used for the spatially independent solutions $p_{\rm si}$ are invariant under the transformation $p \to -p$. This suggests that there may be stable fixed points where $p$ is an odd function of $x$ such that $\lim_{x\to\pm\infty} p(x) = \pm p_{\rm si}$. Such configurations are called 'dark solitons' [43]. We can consider only the portion of the soliton where $p > 0$ by looking at only $x > 0$ and enforcing the condition that $p(u, 0) = 0$. We need to start from a perturbation that satisfies this condition and therefore we choose

$$\delta p(u, x) = 10^{-2} \times u^2 e^{-10(u-1)^2} \tanh(5x). \tag{4.40}$$

This flow can be interpreted as either a full soliton for $-\infty < x < \infty$ where $p$ is antisymmetric around $x = 0$, or as a solution for $x > 0$ where $x = 0$ is an interface with a fixed vacuum solution for $x < 0$. In the boundary theory we can interpret the second case as an interface between a superconductor (for $x > 0$) and a normal material (for $x < 0$). The soliton is the fixed point reached by the flow as $\tau \to \infty$ (see Fig. 4.2(a)).

Although we would like a solution for all $x > 0$, to perform the numerical calculation we need to introduce a cutoff. We would like our cutoff to be large enough that our fields are constant for $x > x_{\max}$. From equation (4.11) we find that for $x_{\max} \approx 5\xi$ we will have $p(x = x_{\max}) > 0.998 \times p(x = \infty)$. We use a cutoff $x_{\max} = 30$ and we find $x_{\max}/\xi > 5.9$ for $T \approx 0.93T_c$. We can calculate the energy density and the boundary

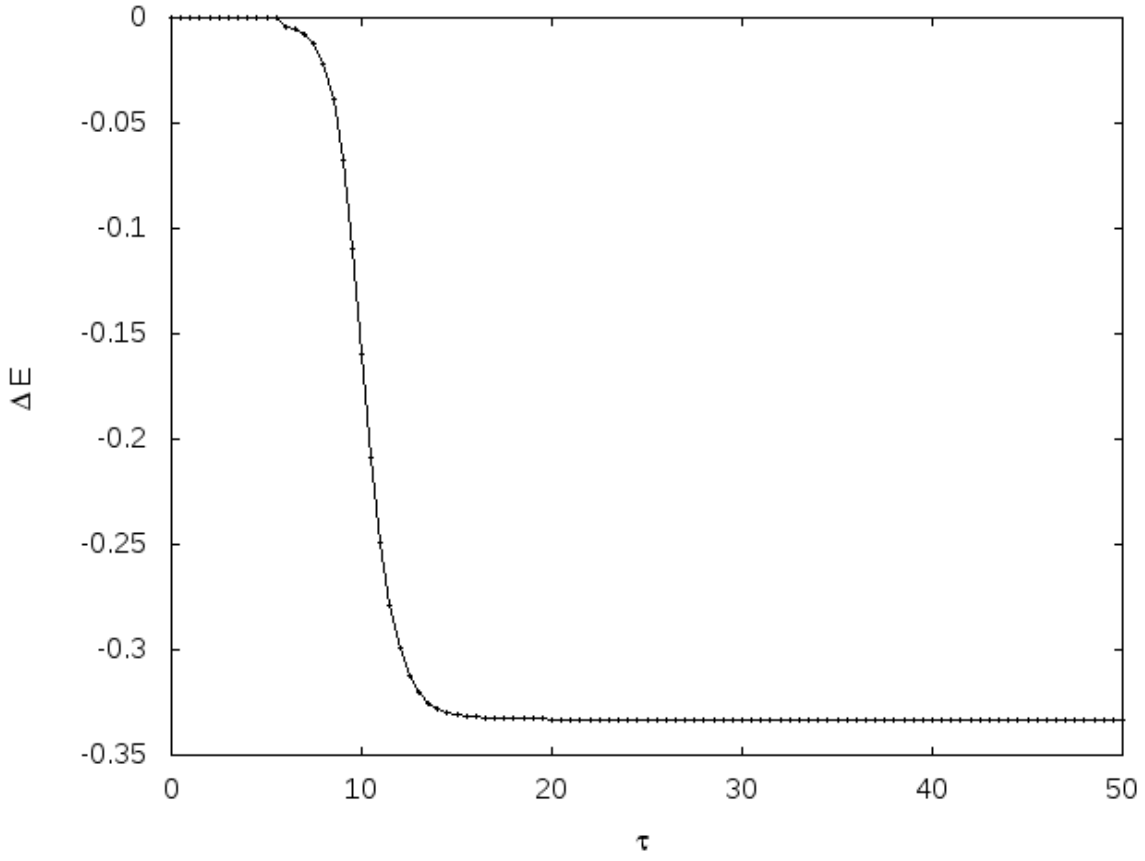


FIGURE 4.7: The free energy ($\Delta E$) as a function of the flow parameter ($\tau$) with $\alpha^2 = 0.03$ for the soliton solution.

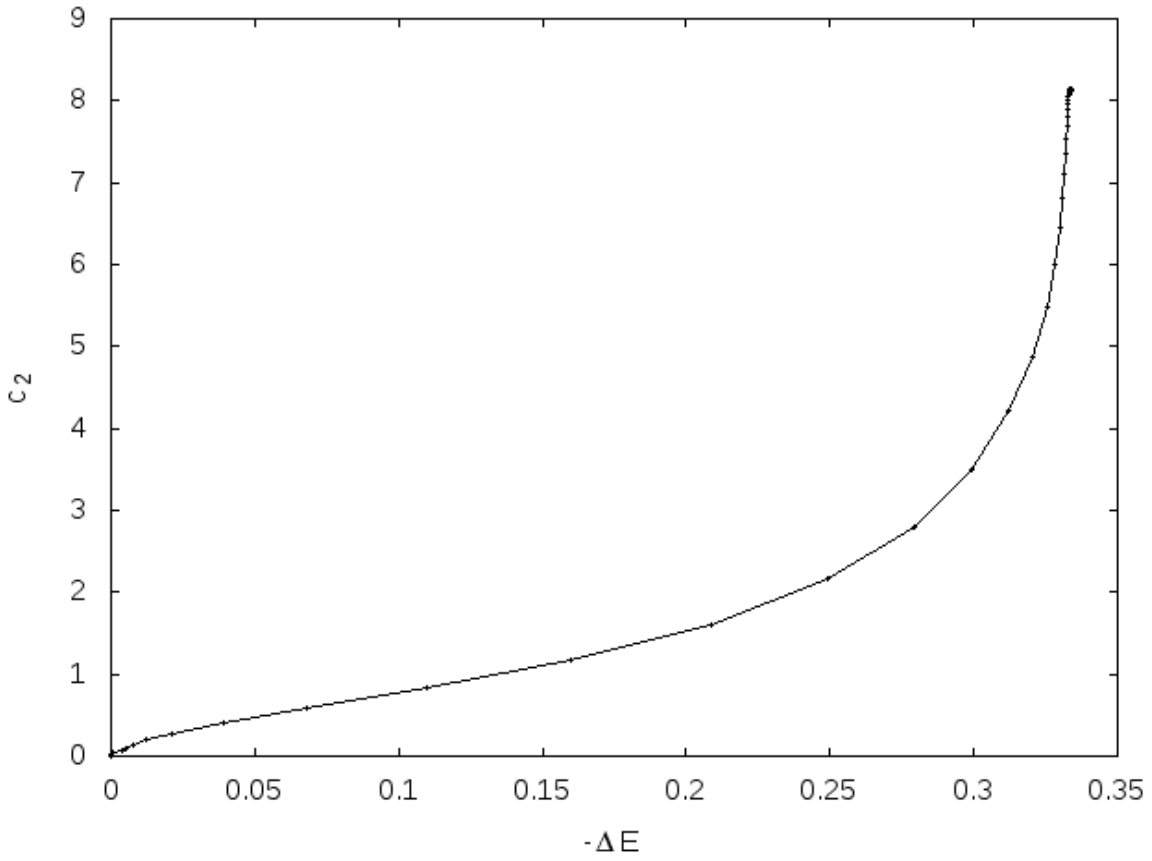


FIGURE 4.8: The operator ($c_2(x = 30)$) as a function of the free energy ($\Delta E$) with $\alpha^2 = 0.03$ for the soliton solution.

operator for the soliton configuration as functions of $x$ and $\tau$. In Fig. 4.7 we show the energy density integrated over $x$ as a function of the flow parameter. Since $\Delta E$ decreases monotonically with $\tau$, we can look at the evolution of the boundary operator as a function of $|\Delta E|$ instead of $\tau$. We have shown that our $x$-cutoff is larger than typical values of the coherence lengths (see Fig. 4.2(b)), which means that field configurations are approximately constant at large $x$ (see for example Fig. 4.2(a)). We therefore expect $c_2(x = x_{\max}) \approx c_2(x \to \infty)$, and that the soliton solution at large $x$ should be close to the spatially independent solution we considered in section 4.3.3. In the soliton case we have $\Delta E_{\text{Sol}} \approx -0.334$, and if we calculate the energy of the spatially independent case on the same interval ($0 \leq x \leq 30$) we find $\Delta E_{\text{Ind}} \approx -0.395$. These energies will depend

on the cutoff ($x_{\max}$), but the difference $\Delta E_{\rm Sol} - \Delta E_{\rm Ind}$ will be independent of the cutoff and can be thought of as a measure of the effect of the soliton.

### 4.3.5 Droplet Solutions

The final case we consider is configurations with non-zero magnetic field. The interesting feature of these solutions is that the magnetic field can limit the formation of the scalar hair/condensate. There is a critical magnetic field $B_c$ above which the boundary operator does not condense. For $B < B_c$ the condensate forms only in a localized region on the boundary, and these localized solutions are called 'droplet' solutions [45]. For the droplet solutions, the initial perturbation does not need to depend on $x$, so we use the perturbation

$$\delta p(u) = 10^{-2} \times u^2 e^{-10(u-1)^2}. \tag{4.41}$$

#### 4.3.5.1 Translationally symmetric droplets

In Fig. 4.9 we show how the magnetic field alters the boundary operator $c_2(x)$. When $B \to 0$ we recover the spatially independent solution (see Fig. 4.5(b)). As $B$ approaches the critical value from below, the droplets become narrower and shorter. In Fig. 4.10(a) we see how the free energy evolves as the flow moves the fields from a small perturbation of the vacuum solution towards a localized droplet of scalar hair. In Fig. 4.10(b) we plot the free energy versus the value of the operator $c_2$ at the center of the droplet. We notice in Fig. 4.10(a) that when $\Delta E$ is small there are noticable fluctuations due to numerical error, which influence the low $\Delta E$ behaviour in Fig. 4.10(b).

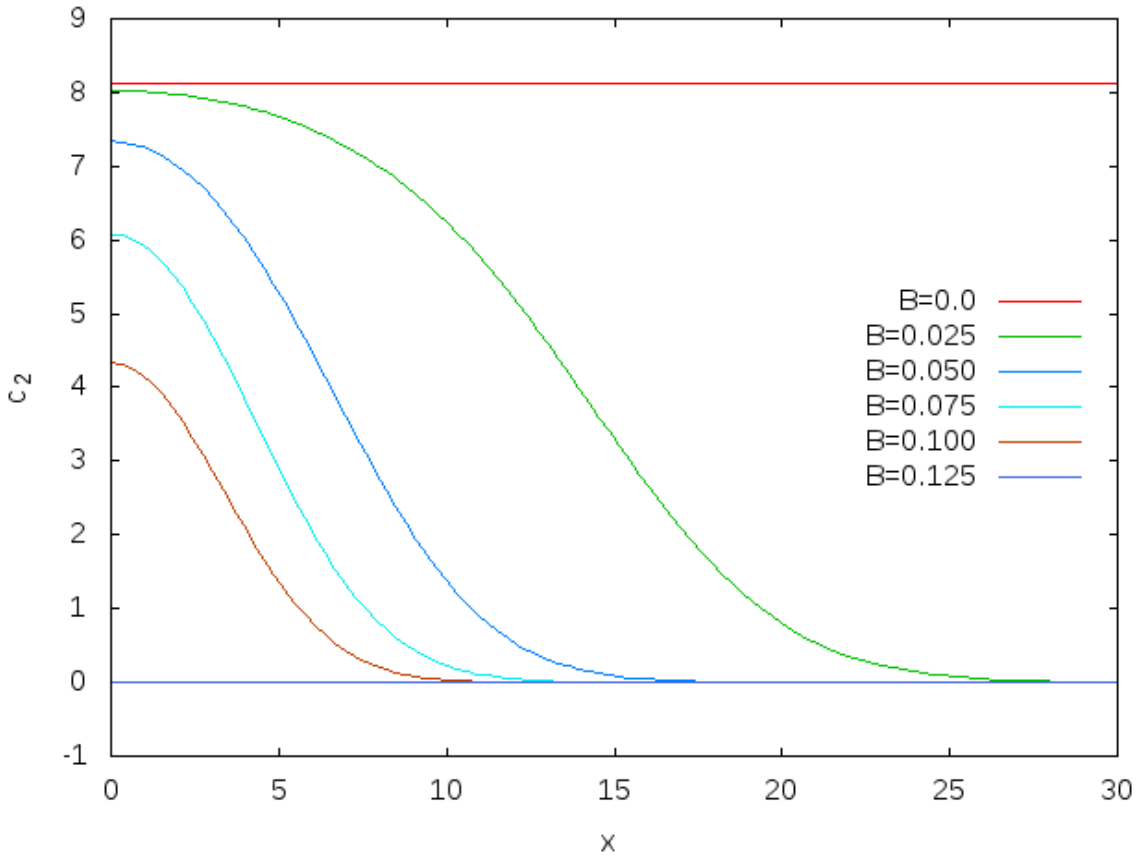


FIGURE 4.9: $c_2(x)$ for several values of the magnetic field, and $\alpha^2 = 0.03$, for a translationally symmetric droplet. As $B$ increases $c_2(x)$ becomes smaller and more localized.

#### 4.3.5.2 Axially symmetric droplet solutions

The droplet solutions do not require translational symmetry. In this section we start from the same initial perturbation but instead enforce axial symmetry along the flow. This leads to droplet solutions that are entirely localized (as condensate in the boundary theory and as scalar hair on the black hole horizon). Our results are similar to those found in [46], with the important difference that we have a constant magnetic field on the boundary. As discussed at the beginning of section 4.3.2, this is a characteristic of the gradient flow method. We will study the flow up to a maximum radius $\rho = 30$, for several different values of the magnetic field. The final configurations for $c_2$ are shown in

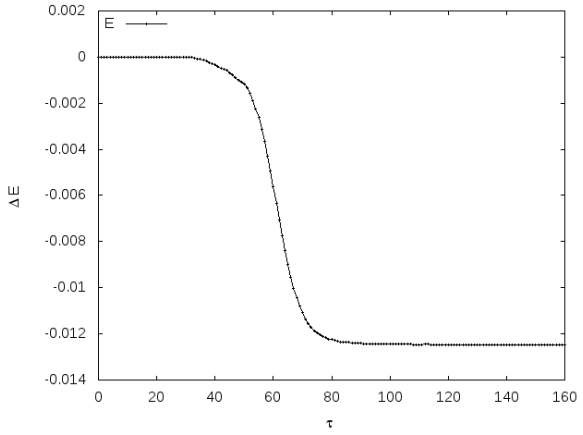


(a) The free energy ($\Delta E$) as a function of the flow parameter ($\tau$) with $\alpha^2 = 0.03$ and $B = 0.075$ for a translationally symmetric droplet.

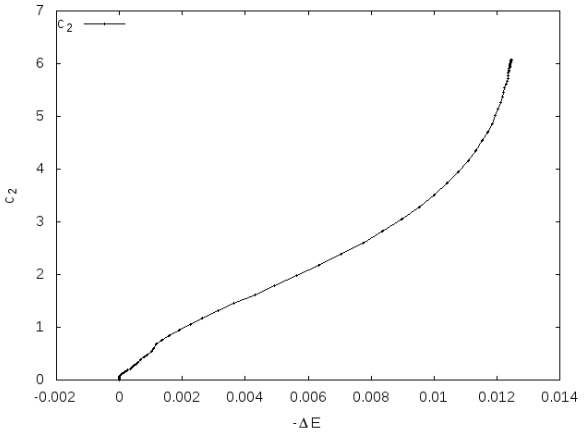


(b) The free energy ($\Delta E$) as a function of the operator at the center of the droplet ($c_2(x = 0)$) with $\alpha^2 = 0.03$ and $B = 0.075$ for a translationally symmetric droplet.

FIGURE 4.10: The formation of a translationally symmetric droplet from the vacuum solution

Fig. 4.11.

In Figs. 4.12(a), 4.12(b) we show the free energy for the case where $\alpha^2 = 0.03$ and $B = 0.1$. In the first figure we show how the free energy evolves as a function of flow time, and in the second we plot the free energy versus the value of the boundary operator at $\rho = 0$.

We can examine other quantites in the boundary theory, namely the charge density $\bar{\rho}$ and the azimuthal current $J_\theta$. Fig. 4.13(a) shows the charge density profile of the droplet. Figure 4.13(b) shows the axial current. We note that the formation of currents at the edge of the superconducting droplets is expected as the superconductor will attempt to expel any magnetic fields.

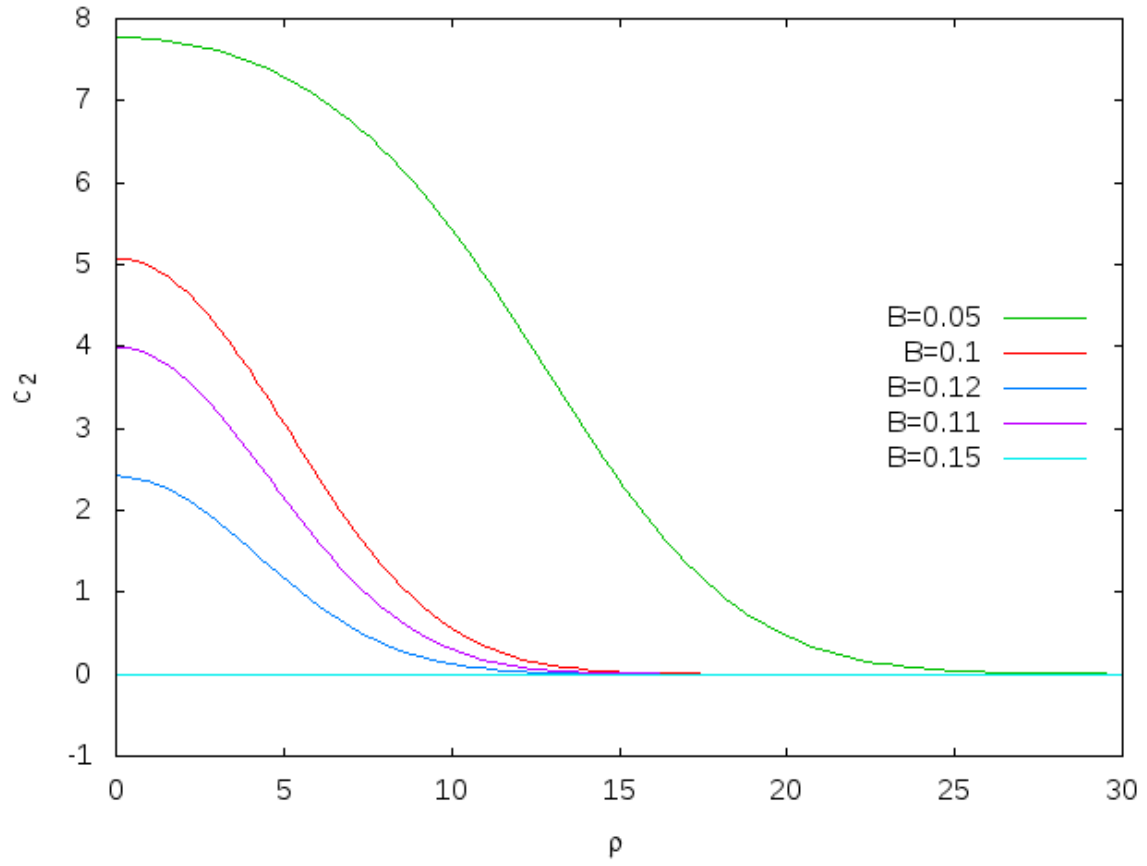


FIGURE 4.11: The operator $c_2(x)$ for several values of the magnetic field, and $\alpha^2 = 0.03$, for an axially symmetry droplet.

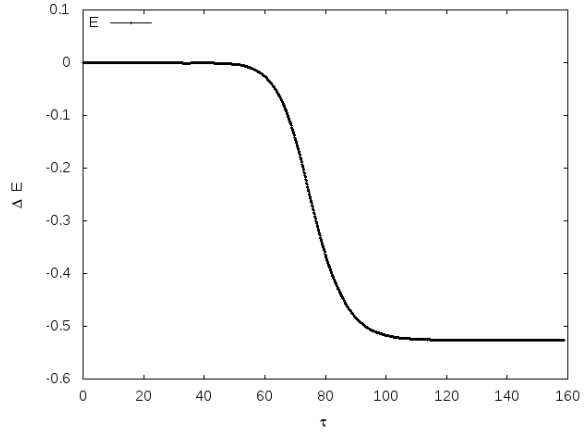


(a) The free energy ($\Delta E$) as a function of the flow parameter ($\tau$) with $\alpha^2 = 0.03$ and $B = 0.1$ for an axially symmetric droplet.

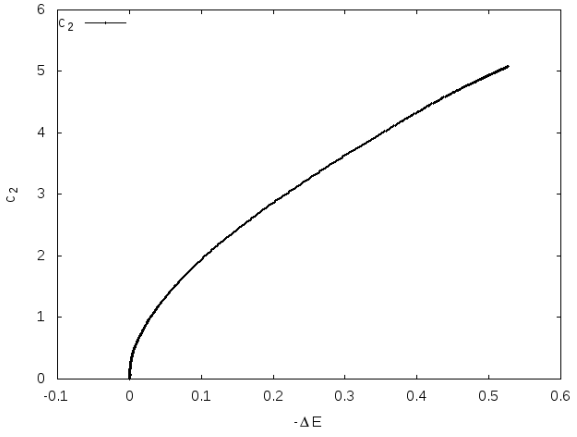


(b) The operator at the center of the droplet ($c_2(\rho = 0)$) as a function of the free energy ($\Delta E$) with $\alpha^2 = 0.03$ and $B = 0.1$ for an axially symmetric droplet.

FIGURE 4.12: The formation of an axially symmetric droplet from the vacuum solution.

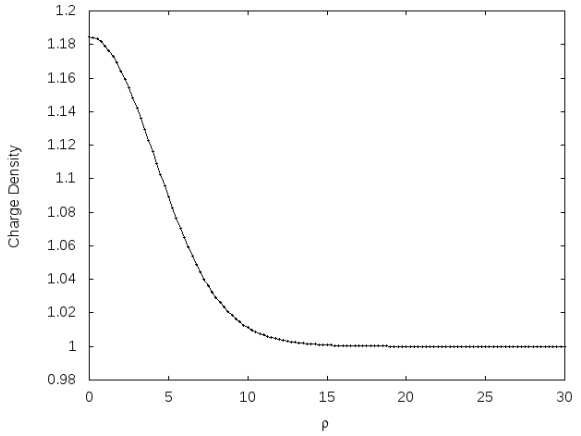


(a) The charge density ($\bar{\rho}$) as a function of the radius ($\rho$) with $\alpha^2 = 0.03$ and $B = 0.1$ for an axially symmetric droplet.

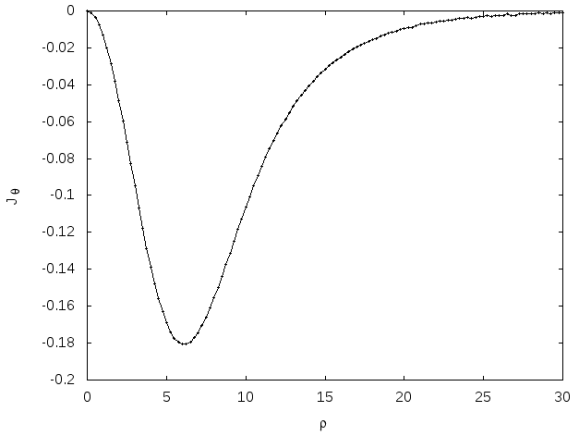


(b) The azimuthal current ($J_\theta$) as a function of the radius ($\rho$) with $\alpha^2 = 0.03$ and $B = 0.1$ for an axially symmetric droplet.

FIGURE 4.13: The charge density and azimuthal current in an axially symmetric droplet, as determined from the asymptotic behaviour of $A_\mu(u \to 0)$.

# Chapter 5

# Conclusions and Future Prospects

## 5.1 Gradient Flow as the TDGL Equations

In Chapter 3 we demonstrated that the gradient flow equations of the Einstein-Maxwell-Higgs action in 3 dimensions are equivalent to the time-dependent Ginzburg-Landau equations. The gradient flow equations were used to study numerically the equilibration of vortices in the Ginzburg-Landau model. The flow equations can be used to numerically find approximate solutions to the GL equations as the endpoint of the flow for any number of vortices at arbitrary locations. While there are better numerical methods to find solutions, the advantage of our method is that we are able to study the dynamical evolution of the flow. The primary focus of our work is a study of the timescales associated with vortex formation and vortex-vortex interactions.

We first studied vortex formation by looking at $n = 1$ vortices centered at the origin. The flow moves towards vortex solutions as expected, with winding number corresponding to that of the initial data. We found that this occurred on relatively short timescales that were largely independent of the initial field configuration. The vortex formation timescale

is proportional to the energy of the vortex, which is a non-linearly increasing function of $\kappa$.

We also considered three different kinds of vortex interactions. We started with configurations that correspond as closely as possible to two or more separated vortex solutions, for various values of $\kappa$. During the early part of the flow the vortex forms rapidly. The flow on longer timescales simulates interactions between the vortices as determined by the time dependent Ginzburg-Landau equations. We were able to model the attraction between vortices in the $\kappa < \kappa_c$ case, and the repulsion in the $\kappa > \kappa_c$ case. We showed that the interaction timescale decreases when $\kappa$ moves away from $\kappa_c$ in either direction. We also showed that vortex anti-vortex interactions are attractive for any values of $\kappa$. Similar results were found in [47] where the authors study the force between vortices by looking at the change in the energy as the separation increases, which is closely related to our gradient flow approach.

Our numerical results raise several interesting issues. The first is related to the fact that the energies in our numerical solutions do not show the $n^2$ scaling for large $\kappa$ that was suggested by approximate solutions in [23] and the heuristic arguments of [37]. In addition, it would be good to understand physically the source of the long and short timescales. The exponential dependence on $\sqrt{t}$ in our fits likely derives from the nonlinear dynamics which affects the early evolution of the far from equilibrium initial configurations. At later times, when the fields are closer to their equilibrium configurations, the dynamics changes qualitatively and linear exponential behaviour is found, as expected.

Several interesting scenarios that have been considered recently using time dependent GL equations of motion could also be studied using a gradient flow approach like the one we have used in this paper. Vortices in three dimensional samples constructed from layers which create anisotropy have been studied in a constant external magnetic field in [48], and the dynamics of vortex loops were studied in [49, 50]. Improved Ginzburg-Landau

models that describe types of multicomponent superconductivity have been studied in [51, 52]. Multiband superconductors [53–55] can exhibit new physics and vortex configurations not found in single band superconductors.

## 5.2 Gradient Flow in Holographic Superconductors

In Chapter 4 we have demonstrated the utility of a gradient flow approach to holographic superconductors. In addition to reliably finding solutions to the equations of motion, we were also able to determine the stability of the solutions in a non-perturbative way. We found stable axially symmetric droplets with a constant background magnetic field, whereas the droplets found in [46] would enhance or weaken the magnetic field at the core depending on the temperature. The gradient flow is a much more general approach to finding droplets as one can consider any magnetic field as a fixed background specified by initial conditions.

Although the flow parameter itself does not have a straightforward physical interpretation, we can exploit its connection with the free energy to gain insight into how the system can undergo the phase change from hairless black hole (normal phase) to a black hole with scalar hair (superconducting phase) in a quasi-static way.

The AdS/CFT correspondence provides an equivalence between the Euclidean on-shell action in the bulk and the free energy of the boundary. This means that at the fixed points of the flow the free energy of the bulk, $\mathcal{E}$, is equivalent to the free energy of the superconductor. Away from the fixed points the AdS/CFT dictionary does not tell us anything about the relationship between the two free energies. However, using the gradient flow method, we can formally link static off-shell configurations in the bulk and in the boundary at the same value of the flow parameter $\tau$. For quasi-static evolution

at least, it may be reasonable to think of this link as an extension of the AdS/CFT correspondence.

There are several straightforward extensions of the work completed in Chapter 4. The first would be to include the additional boundary term in the action as described in [44] in order to include a dynamical gauge field in the boundary theory. This would allow us to construct superconducting vortex solutions, which could be more directly compared to some of the results of Chapter 3. Although in GL theory we were able to model vortex interactions in a 2 dimensional plane, modelling a 2 dimensional holographic superconductor (using a 3 dimensional bulk theory) remains a time intensive task computationally.

Another important extension is relaxing the probe limit and including the gradient flow of the metric. This would allow us to study the system away from the probe limit since the stationary points of the metric flow will be the fully backreacted metric. Although holographic superconductors with metric backreactions have been studied, it is unclear how allowing the metric to change will influence the stability of the scalar hair solutions. The evolution of the metric from the vacuum black hole solution is a physically interesting problem in its own right, and this type of metric curvature flow with source terms is an interesting problem in mathematics.

In addition to the further study of the gradient flow in this particular model of a holographic superconductor, it would be interesting to compare with the flow generated using different background metrics, including those arising from modified theories of gravity. There are also interesting metrics that are not asymptotially AdS, where the dual theory on the boundary does not have conformal symmetry. Most notably, holographic superconductors have been described using Lifshitz black holes [56].

# Appendix A

# Numerical Procedure

## A.1 Time-Dependent Ginzburg-Landau Equations

The computations were done using an explicit finite difference scheme for a $20\xi \times 20\xi$ superconductor discretized into a square grid with spacing $\Delta x = \Delta y = 0.05\xi$. As one check of convergence we confirmed that our results were not affected by further reducing the grid spacing by half. Specifically, the quality of the fits did not change, nor did the values of the fit parameters to the numerical accuracy of the calculation.

As a further check of the numerical results, we compared the asymptotic value of the $\kappa = \kappa_c$ 1-vortex energy in Fig. 3.3(a) to its known analytic value of $\pi$. We found for large times, namely $t = 15$, that $\mathcal{E}(15) = 3.14315391$ and by fitting the long timescale graph we deduced an asymptotic value of energy of $\mathcal{E}(\infty) = 3.14145$. These two values differ from the analytic value $\pi$ by 0.0496% and 0.00454%, respectively.

Data fitting was done using the nonlinear least-squares Marquardt-Levenberg algorithm. In all cases, the $\mathcal{E}(t) \propto e^{-\sqrt{t/T}}$ dependence provided the best fit at the early times, with a reduced chi-squared $\approx 0.01$.

## A.2 Holographic Superconductors

### A.2.1 Grid Spacing

Since our gradient flow equations are analogous to the heat equation we solve them using a simple explicit finite difference scheme with forward differences in flow time and centered differences in our spatial coordinates. Such methods tend to be stable and convergent as long as the time step is proportionally smaller than the square of the space step,

$$d\tau \leq C du^2. \tag{A.1}$$

For a simple one dimensional heat equation it can be shown that $C = 0.5$, but it is difficult to precisely compute the value of $C$ for the type of nonlinear coupled PDEs that we have solved. We typically work with an equal number of grid points in both $u$ and $x$ (or $\rho$). Since $u \in (0, 1)$ and $x \in (0, 30)$, we have $du < dx$ and therefore we do not need to consider a separate convergence condition of the form (A.1) for $dx$.

We found that $d\tau$ obtained from (A.1) with $C = 0.25$ was sufficient for good convergence. For any value of $C$ the computer time required to reach $\tau = 1$ is proportional to $du^{-3}$ for the one dimensional case and $du^{-4}$ for two dimensions. To increase computational speed, we therefore want $du$ to be as large as possible without sacrificing accuracy.

Most of the results presented in this thesis were calculated with a $300 \times 300$ grid. The exception is Figs. 4.5 and 4.6. where we used 2000 grid points. In this case we found that with fewer grid points there was a small but noticeable non-monotonic behaviour in $\Delta E$ which suggested the endpoint of the flow did not minimize the free energy of the system. Figs. A.1(a) and A.1(b) show this behaviour with 300 gridpoints. The non-monotonicity is more noticeable at lower temperatures since $p(u)$ is larger in those cases, and the fact

that it disappears when the grid spacing is reduced (see Figs. 4.5 and 4.6) proves that the effect is numerical.

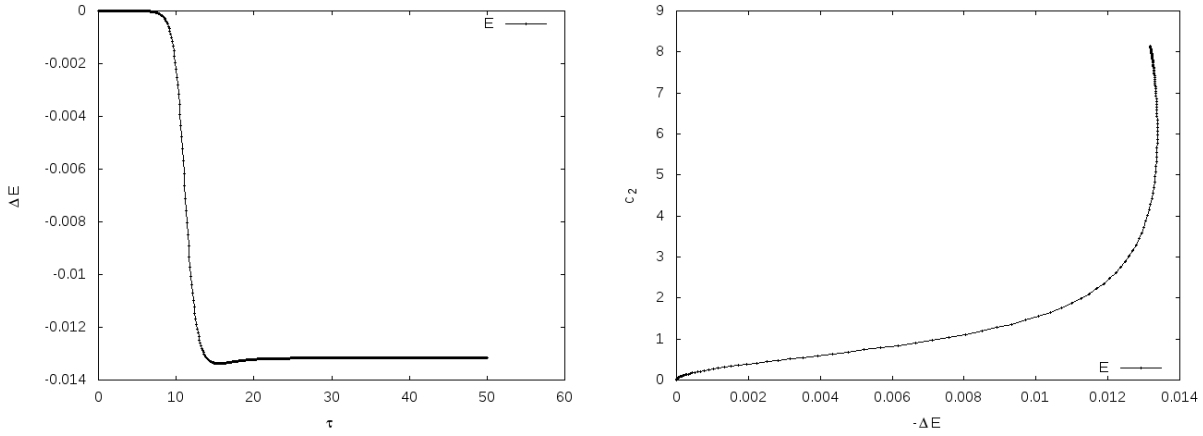


(a) $\Delta E$ as a function of $\tau$ with decreased grid spacing.

(b) The operator $c_2$ as a function of $\Delta E$.

FIGURE A.1: With fewer gridpoints, numerical error leads to non-monotonic behaviour in the energy.

Although we do not see the same behaviour in the spatially dependent cases we instead see smaller fluctuations of the energy, in particular when it is small relative to the grid spacing. These fluctuations are due to the larger error in the spatial derivatives since $dx > du$.

In Fig. A.2 we look at the dependence of $c_2$, $\Delta E$ and $p(u = 1)$ on the number of grid points used (equivalently $du^{-1}$), at the end of the flow for the spatially independent case where the computation time depends least on gridspacing.

The quantities approach a fixed value as the number of grid points increases. Note that the range for the $y$-axis on these plots is roughly a 10% variation for the energy, and 2% for $c_2$ and $p(u = 1)$. The larger error in $\Delta E$ is expected since it is obtained from a numerically computed integral of fields which introduces additional error. The fields themselves and $c_2$ depend mainly on the error in first order finite differences which is proportional to $du$. In Fig. A.2(d) we see that $p(u = 1)$ is linear in $du$, and we can

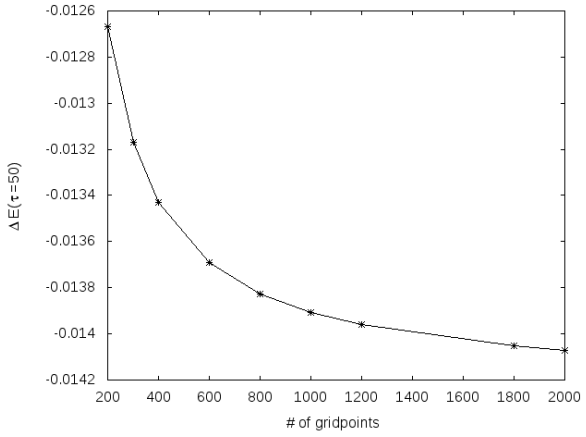


(a) $\Delta E$ as a function of the number of gridpoints for spatially independent fields

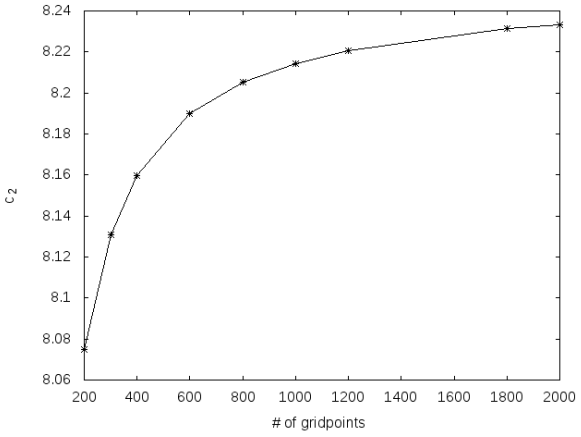


(b) $c_2$ as a function of the number of gridpoints

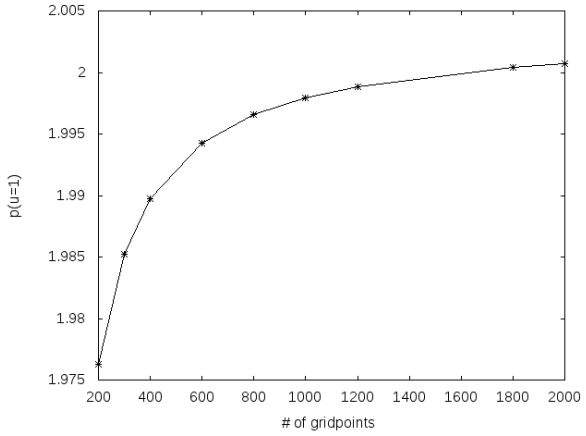


(c) $p(u=1)$ as a function of the number of gridpoints

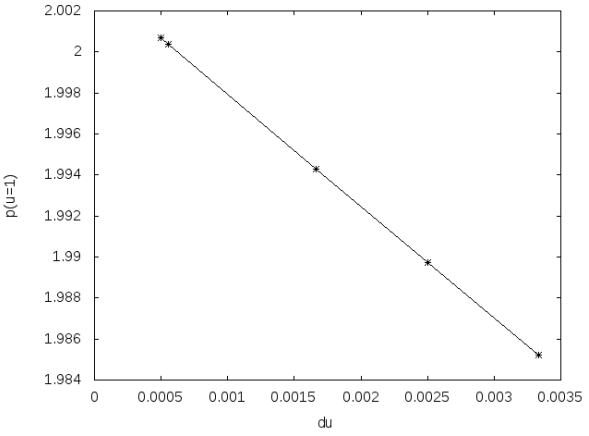


(d) $p(u=1)$ as a function of $du$

FIGURE A.2: The dependence of several quantities on the number of grid points.

extrapolate to $du = 0$ to find that $p(u = 1) \approx 2.0034$ is within 1% of the value obtained using only 300 gridpoints.

### A.2.2 Boundary Conditions

Since we used centered finite differences we need to take special care of the points at the boundaries. For all cases the AdS radial coordinate boundaries $u = 0$ and $u = 1$ were treated in the same way. At the AdS boundary, $u = 0$, all terms with derivatives are

multiplied by a factor $u^2$. We assume that the derivatives of our fields are finite at $u = 0$, which means that any term with a derivative does not contribute to the flow equations. At the horizon, $u = 1$, the factor $h(u)$ goes to zero. We required that $A_t(u = 1) = 0$ in such a way that the ratio $\frac{A_t^2}{h(u)} = 0$ at $u = 1$. Any $u$ derivatives that we needed were calculated using a one-sided finite difference.

For the boundaries at $x_{\max}$ and $\rho_{\max}$ we can usually use one-sided finite differences since typically the fields are approximately constant at this boundary. The one exception is the field $A_\theta$ for which we enforced the condition $\partial_\rho A_\theta(\rho_{\max}) = B\rho$. For a finite superconductor with radius $\rho_{\max}$, this is simply the condition that there is a fixed external magnetic field.

The boundaries at $x = 0$ and $\rho = 0$ were handled by adding a extra gridpoint at $x = -dx$ and calculating centered finite differences as usual. The value of the fields at this point was determined using the symmetry of the configuration. We took $A_t$ to be always symmetric, $A_y$ and $A_\rho$ were always antisymmetric, and $p$ was symmetric except for the soliton case, where it was antisymmetric.

# Appendix B

# Sample Fortran Code

The following code solves the flow equations for multiple vortices in Cartesian coordinates in Chapter 3.

```
program TDGLSOLVE
implicit none

integer, parameter ::  sp = selected_real_kind(6, 37)

real(sp) dt,dx,b,time_start, time_end, time_e1, time_e2
integer i, e, j, k, l, m, n, npos, nneg
integer nt,ntp,nto
real(sp), allocatable, dimension(:,:) :: fr, Bx, By,fc
real(sp), allocatable, dimension(:,:) :: dfr, dBx, dBy, dfc
real(sp), allocatable, dimension(:) :: Inxp, Inyp, Inxn, Inyn, rad
real(sp) Energy, Flux
integer enn, inter
real(sp) x,y,t,tmax,tstep,Hx,Hy,r1,r2,r,phase,CFL,f,temp

open(55,FILE='input.dat',STATUS='OLD')
read(55,*) inter
read(55,*) tmax, tstep
read(55,*) k, l
read(55,*) b
read(55,*) temp
read(55,*) Hx, Hy
read(55,*) CFL
read(55,*) npos, nneg

allocate(Inxp(1:npos),Inyp(1:npos))
allocate(Inxn(1:nneg),Inyn(1:nneg))
allocate(rad(1:nneg+npos))
do e=1,npos
read(55,*) Inxp(e), Inyp(e)
end do
```

```
do e=1,nneg
read(55,*) Inxn(e), Inyn(e)
end do


nt=int(tmax/tstep)

j=0

dx = real(l)/real(k)  !space step size, assumed same for both x and y
dt = CFL*dx**2.
ntp = ceiling(tstep/dt)
write(*,*) dx, dt, k
write(*,*) nt, ntp, ntp*dt, ntp*nt*dt
allocate(fr(-k-1:k+1,-k-1:k+1),Bx(-k-1:k+1,-k-1:k+1),By(-k-1:k+1,-k-1:k+1), &
 fc(-k-1:k+1,-k-1:k+1))
allocate(dfr(-k-1:k+1,-k-1:k+1),dBx(-k-1:k+1,-k-1:k+1),dBy(-k-1:k+1,-k-1:k+1), &
         dfc(-k-1:k+1,-k-1:k+1))

  open(101,FILE='f.dat')
  open(102,FILE='Bx.dat')
  open(103,FILE='By.dat')
  open(104,FILE='w.dat')
  open(105,FILE='FluxEnergy.dat')
  open(1,FILE='params.dat')
  write(1,*) k,nt,dx,b

Bx(:,:)=0.0
By(:,:)=0.0
fr(:,:)=1.0
fc(:,:)=1.0

do e=-k-1,k+1
  do i=-k-1,k+1
    y = i*dx
    x = e*dx
    phase = 0.0

    f=1.
    do j=1,npos
    r= sqrt((x-Inxp(j))**2.+(y-Inyp(j))**2.)
f=f*(1.-exp(-4.*sqrt(b)*r**2.))
phase=phase-atan2(y-Inyp(j),x-Inxp(j))
Bx(i,e)=Bx(i,e)-(y-Inyp(j))*(1.-exp(-r**2.))/(r**2.+1.0d-12)
By(i,e)=By(i,e)+(x-Inxp(j))*(1.-exp(-r**2.))/(r**2.+1.0d-12)
    end do
    do j=1,nneg
    r= sqrt((x-Inxn(j))**2.+(y-Inyn(j))**2.)
f=f*(1.-exp(-4.*sqrt(b)*r**2.))
phase=phase+atan2(y-Inyn(j),x-Inxn(j))
Bx(i,e)=Bx(i,e)+(y-Inyn(j))*(1.-exp(-r**2.))/(r**2.+1.0d-12)
By(i,e)=By(i,e)+(x-Inxn(j))*(exp(-r**2.)-1.)/(r**2.+1.0d-12)
    end do
```

```
    if(inter.eq.0)then
f = 1.
   Bx(i,e) = 0.
By(i,e) = 0.
    endif
    fr(i,e)=f*cos(phase)
    fc(i,e)=f*sin(phase)
    Bx(i,e) = sqrt(temp)*Bx(i,e)
    By(i,e) = sqrt(temp)*By(i,e)
  end do
end do

j=0
i=0
m=1
enn=0.

do while (enn.le.10)

  fr(-k-1,:)  = fr(-k+1,:)
  fc(-k-1,:)  = fc(-k+1,:)
  Bx(-k-1,: ) = Bx(-k+1,: ) - Hy*2.*dx
  By(-k-1,: ) = By(-k+1,: )

  fr(k+1,: )  = fr(k-1,: )
  fc(k+1,: )  = fc(k-1,: )
  Bx(k+1,: ) = Bx(k-1,: ) + Hy*2.*dx
  By(k+1,: ) = By(k-1,: )

  fr(:,-k-1 )  = fr(:,-k+1 )
  fc(:,-k-1 )  = fc(:,-k+1 )
  Bx(:,-k-1 ) = Bx(:,-k+1 )
  By(:,-k-1 ) = By(:,-k+1 ) - Hx*2.*dx

  fr(:,k+1 )  = fr(:,k-1 )
  fc(:,k+1 )  = fc(:,k-1 )
  Bx(:,k+1 ) = Bx(:,k-1 )
  By(:,k+1 ) = By(:,k-1 ) + Hx*2.*dx

  fr(-k-1,-k-1 ) = fr(-k+1,-k+1 )
  fc(-k-1,-k-1 ) = fc(-k+1,-k+1 )
  Bx(-k-1,-k-1 ) = Bx(-k+1,-k+1 )
  By(-k-1,-k-1 ) = By(-k+1,-k+1 )

  fr(-k-1,k+1 ) = fr(-k+1,k-1 )
  fc(-k-1,k+1 ) = fc(-k+1,k-1 )
  Bx(-k-1,k+1 ) = Bx(-k-1,k-1 )
  By(-k-1,k+1 ) = By(-k-1,k-1 )

  fr(k+1,k+1 ) = fr(k-1,k-1 )
  fc(k+1,k+1 ) = fc(k-1,k-1 )
  Bx(k+1,k+1 ) = Bx(k-1,k-1 )
  By(k+1,k+1 ) = By(k-1,k-1 )
```

```
  fr(k+1,-k-1 ) = fr(k-1,-k+1 )
  fc(k+1,-k-1 ) = fc(k-1,-k+1 )
  Bx(k+1,-k-1 ) = Bx(k-1,-k+1 )
  By(k+1,-k-1 ) = By(k-1,-k+1 )

  Call Slope(dfr, dBx, dBy,dfc)

  if(mod(20*j,ntp).le.19)then
    write(105,*) j*dt,Energy,Flux
  endif

  j=j+1

  fr(:,: )  = dfr(:,:)*dt+fr(:,:)
  Bx(:,: )  = dBx(:,:)*dt+Bx(:,:)
  By(:,: )  = dBy(:,:)*dt+By(:,:)
  fc(:,: )  = dfc(:,:)*dt+fc(:,:)
  if(mod(j,ntp).eq.0)then
    if(m.eq.nt)then
      enn=20
      write(101, *) fr(:,: )
      write(102, *) Bx(:,: )
      write(103, *) By(:,: )
      write(104, *) fc(:,: )
      else
      write(101, *) fr(:,: )
      write(102, *) Bx(:,: )
      write(103, *) By(:,: )
      write(104, *) fc(:,: )
      m=m+1
    endif
  endif
end do

contains
subroutine Slope(dfr, dBx, dBy, dfc)
implicit none
real(sp), dimension(:,:), allocatable, intent(inout) :: dfr, dBx, dBy, dfc
real(sp) d2xfr,d2yfr,d2xfc,d2yfc
real(sp) dxyBx,d2yBx
real(sp) dxyBy,d2xBy
real(sp) dxBx,dyBy, dyfr,dxfr, dyfc,dxfc, dxBy, dyBx
real(sp) Pot
Energy = 0.
Flux = 0.
do i = -k,k
  do e = -k,k
    y = i*dx
    x = e*dx

    d2yfr  = (fr(i+1,e )+fr(i-1,e )-2.0d+0*fr(i,e ))/dx**2.
    dyfr   = (fr(i+1,e )-fr(i-1,e ))/(2.*dx)
```

```
    d2xfr  = (fr(i,e+1 )+fr(i,e-1 )-2.0d+0*fr(i,e ))/dx**2.
    dxfr   = (fr(i,e+1 )-fr(i,e-1 ))/(2.*dx)

    d2yfc  = (fc(i+1,e )+fc(i-1,e )-2.0d+0*fc(i,e ))/dx**2.
    dyfc   = (fc(i+1,e )-fc(i-1,e ))/(2.*dx)

    d2xfc  = (fc(i,e+1 )+fc(i,e-1 )-2.0d+0*fc(i,e ))/dx**2.
    dxfc   = (fc(i,e+1 )-fc(i,e-1 ))/(2.*dx)

    dxyBx  = (Bx(i+1,e+1 )+Bx(i-1,e-1 )-Bx(i+1,e-1 )-Bx(i-1,e+1 ))/(4.0*dx**2.)
    dxyBy  = (By(i+1,e+1 )+By(i-1,e-1 )-By(i+1,e-1 )-By(i-1,e+1 ))/(4.0*dx**2.)

    d2xBy  = (By(i,e+1 )+By(i,e-1 )-2.0d+0*By(i,e ))/dx**2.
    dxBx   = (Bx(i,e+1 )-Bx(i,e-1 ))/(2.*dx)
    dxBy   = (By(i,e+1 )-By(i,e-1 ))/(2.*dx)
    d2yBx  = (Bx(i+1,e )+Bx(i-1,e )-2.0d+0*Bx(i,e ))/dx**2.
    dyBy   = (By(i+1,e )-By(i-1,e ))/(2.*dx)
    dyBx   = (Bx(i+1,e )-Bx(i-1,e ))/(2.*dx)

    Pot = temp*b*(fc(i,e)**2.+fr(i,e)**2. - 1.)

    dfr(i,e) = d2xfr+d2yfr-Pot*fr(i,e)-2.*(Bx(i,e)*dxfc+By(i,e)*dyfc) &
               -fc(i,e)*(dxBx+dyBy)-fr(i,e)*(Bx(i,e)**2.+By(i,e)**2.)

    dfc(i,e) = d2xfc+d2yfc-Pot*fc(i,e)+2.*(Bx(i,e)*dxfr+By(i,e)*dyfr) &
               +fr(i,e)*(dxBx+dyBy)-fc(i,e)*(Bx(i,e)**2.+By(i,e)**2.)

    dfr(i,e) = dfr(i,e)/(12.*b)
    dfc(i,e) = dfc(i,e)/(12.*b)

    dBx(i,e) = d2yBx - dxyBy -temp*(Bx(i,e)*(fr(i,e)**2.+fc(i,e)**2.) &
               + fr(i,e)*dxfc - fc(i,e)*dxfr)
    dBy(i,e) = d2xBy - dxyBx -temp*(By(i,e)*(fr(i,e)**2.+fc(i,e)**2.) &
               + fr(i,e)*dyfc - fc(i,e)*dyfr)

    Flux   = Flux + (dxBy-dyBx)*dx**2.
    Energy = Energy + (0.5*(dxBy-dyBx)**2.+0.5*temp*(dxfc**2.+dxfr**2. &
                    +dyfc**2.+dyfr**2.))*dx**2.
    Energy = Energy + 0.25*b*(temp**2.)*((fc(i,e)**2. +fr(i,e)**2.)**2.&
                    -2.*(fc(i,e)**2.+fr(i,e)**2.)+1.)*dx**2.
    Energy = Energy + temp*(dxfc*Bx(i,e)*fr(i,e)-dxfr*Bx(i,e)*fc(i,e) &
                    +dyfc*By(i,e)*fr(i,e)-dyfr*By(i,e)*fc(i,e))*dx**2.
    Energy = Energy + 0.5*temp*(Bx(i,e)**2.+By(i,e)**2.)*(fc(i,e)**2. &
                    +fr(i,e)**2.)*dx**2.
  end do
end do

dfr(k+1,:)=0.
dBx(k+1,:)=0.
dBy(k+1,:)=0.
dfc(k+1,:)=0.

dfr(-k-1,:)=0.
```

```
dBx(-k-1,:)=0.
dBy(-k-1,:)=0.
dfc(-k-1,:)=0.

dfr(:,k+1)=0.
dBx(:,k+1)=0.
dBy(:,k+1)=0.
dfc(:,k+1)=0.

dfr(:,-k-1)=0.
dBx(:,-k-1)=0.
dBy(:,-k-1)=0.
dfc(:,-k-1)=0.

end subroutine slope

end program TDGLSOLVE
```

The following code solves the flow equations for the translationally symmetric case in Chapter 4.

```
program FLOWSOLVE

implicit none

integer, parameter ::  sp = selected_real_kind(6, 37)

real(sp) u, r, du, dr, t, dt, q1, q2, q3, q5, ee
real(sp) tmax,tstep
integer i, j, l, n, ntp, m, nt
integer ku, kr
real(sp), allocatable, dimension(:,:) :: dAy, dAt, dp
real(sp), allocatable, dimension(:,:) :: Ay, At, p
real(sp), allocatable, dimension(:) :: c
real(sp) alph,Mag,Chm
integer FAIL, stp

open(101,FILE='p.dat')
open(102,FILE='Ay.dat')
open(103,FILE='At.dat')
open(105,FILE='c2.dat')
open(104,FILE='params.dat')

open(55,FILE='input.dat',STATUS='OLD')
read(55,*) tmax, tstep
read(55,*) ku, kr
read(55,*) alph
read(55,*) Chm, Mag
read(55,*) n
```

```
du = 1.0d+0/ku
dr = 10.0d+0/kr

allocate(At(0:ku,0:kr),Ay(0:ku,0:kr),p(0:ku,0:kr))
allocate(dAt(0:ku,0:kr),dAy(0:ku,0:kr),dp(0:ku,0:kr))
allocate(c(0:kr))

nt=int(tmax/tstep)
dt=(du**2.0)/4.0d+0
ntp = ceiling(tstep/dt)

m=1
l = 0
j = 0
ee = 1.0d-20
FAIL = 0
stp = 0
write(104,*) nt,ku,kr,du,dr,Mag,Chm,alph

do i=0,kr
  r=i*dr
  do l=0,ku
    u =l*du
    p(l,i)  =  1.0d-2*u**2.0*exp(-1.0d+1*(u-1.0d+0)**2.0)
    At(l,i) =  Chm*(1.0d+0-u)
    Ay(l,i) = Mag*r
  end do
end do

c(:) = (p(2,:)+p(0,:)-2.0d+0*p(1,:))/(2.0d0*du**2.)
write(105,*) (i*dr,i=0,ku)
write(103, *)  At(:,:)
write(102, *)  Ay(:,:)
write(101, *)  p(:,:)
write(105, *)  c(:)


do while (stp.le.10)
  j=j+1

  call slope(dp,dAt,dAy)

  At = dAt*dt+At
  Ay = dAy*dt+Ay
  p  = dp*dt+p
  q1 = Maxval(abs(dAy))
  q2 = Maxval(abs(dp))
  q3 = Maxval(abs(dp/p))
  q5 = Maxval(abs(dAt))
  c(:) = (p(2,:)+p(0,:)-2.0d+0*p(1,:))/(2.0d0*du**2.)

  if(FAIL.eq.1)then
    stp=20
```

```
    elseif (abs(q1).le.ee.and.abs(q2).le.ee) then
    stp=15
    write(103, *)  At(:,:)
    write(102, *)  Ay(:,:)
    write(101, *)  p(:,:)
    write(105, *)  c(:)
    write(104,*)  j*dt

    elseif (q1.ge.(1.0d+4/ee)) then
    stp=25
  endif

  if(mod(j,ntp).eq.0)then
    write(103, *)  At(:,:)
    write(102, *)  Ay(:,:)
    write(101, *)  p(:,:)
    write(105, *)  c(:)
    write(104,*)  q5,q1,q2,q3,j*dt
    write(*,*) q5,q1,q2,q3,j*dt
    FLUSH(101)
    FLUSH(102)
    FLUSH(103)
    FLUSH(104)
    FLUSH(105)

    if(m.eq.nt)then
      stp=35
      else
      m=m+1
    endif
  endif
end do

contains
subroutine slope(dp,dAt,dAy)
real(sp), allocatable, dimension(:,:), intent(inout) :: dp,dAt,dAy
real(sp) d1p,d1Ay,d1At,d2p,d2Ay,d2At
real(sp) d2rp,d2rAy,d2rAt
real(sp) pot,d,h
integer FAIL

d = 2.0d+0*du

do i = 0,kr
  r = i*dr
  do l = 1,ku-1
    u = 0.0d+0 + l*du
    h = 1.0d+0-u**3.0

    d1p  = (p(l+1,i)-p(l-1,i))/d
    d1Ay = (Ay(l+1,i)-Ay(l-1,i))/d
    d1At = (At(l+1,i)-At(l-1,i))/d
    d2p  = (p(l+1,i)+p(l-1,i)-2.0d+0*p(l,i))/du**2.
```

```
  d2Ay = (Ay(l+1,i)+Ay(l-1,i)-2.0d+0*Ay(l,i))/du**2.
  d2At = (At(l+1,i)+At(l-1,i)-2.0d+0*At(l,i))/du**2.
  if(i.eq.0)then
    d2rp  = (2.0d+0*p(l,i+1)-2.0d+0*p(l,i))/dr**2.
    d2rAy = 0.0d+0
    d2rAt = (2.0d+0*At(l,i+1)-2.0d+0*At(l,i))/dr**2.
    elseif(i.eq.kr)then
    d2rp  = (p(l,i)+p(l,i-2)-2.0d+0*p(l,i-1))/dr**2.
    d2rAy = (Ay(l,i)+Ay(l,i-2)-2.0d+0*Ay(l,i-1))/dr**2.
    d2rAt = (At(l,i)+At(l,i-2)-2.0d+0*At(l,i-1))/dr**2.
    else
    d2rp = (p(l,i+1)+p(l,i-1)-2.0d+0*p(l,i))/dr**2.
    d2rAy = (Ay(l,i+1)+Ay(l,i-1)-2.0d+0*Ay(l,i))/dr**2.
    d2rAt = (At(l,i+1)+At(l,i-1)-2.0d+0*At(l,i))/dr**2.
  endif

  pot = ((Ay(l,i))**2.0/alph)-(At(l,i)**2.0/(alph*h))
  dp(l,i)  = (u**2.0)*(d2rp/alph+h*d2p-(u**2.0)*d1p-p(l,i)*(pot)) &
           +(2.0d+0)*(p(l,i)-d1p*u)
  dAy(l,i) = (u**2.0)*(d2rAy/alph+h*d2Ay-3.0d+0*u**2.0*d1Ay) &
            - p(l,i)**2.0*(Ay(l,i))
  dAt(l,i) = (h*u**2.0)*(d2rAt/alph+d2At) - At(l,i)*p(l,i)**2.0

  if(dp(l,i).ne.dp(l,i))then
  FAIL=1
  endif

end do
!~~~~~~Horizon Flow~~~~~~~~~~~~~~~~~~~~
u=1.0d+0
h=0.0d+0
l=ku
if(i.eq.0)then
  d2rp  = (p(l,i)+p(l,i+2)-2.0d+0*p(l,i+1))/dr**2.
  d2rAy = (Ay(l,i)+Ay(l,i+2)-2.0d+0*Ay(l,i+1))/dr**2.
  d2rAt = (At(l,i)+At(l,i+2)-2.0d+0*At(l,i+1))/dr**2.
  elseif(i.eq.kr)then
  d2rp  = (p(l,i)+p(l,i-2)-2.0d+0*p(l,i-1))/dr**2.
  d2rAy = (Ay(l,i)+Ay(l,i-2)-2.0d+0*Ay(l,i-1))/dr**2.
  d2rAt = (At(l,i)+At(l,i-2)-2.0d+0*At(l,i-1))/dr**2.
  else
  d2rp  = (p(l,i+1)+p(l,i-1)-2.0d+0*p(l,i))/dr**2.
  d2rAy = (Ay(l,i+1)+Ay(l,i-1)-2.0d+0*Ay(l,i))/dr**2.
  d2rAt = (At(l,i+1)+At(l,i-1)-2.0d+0*At(l,i))/dr**2.
endif
d1p = (p(ku,i)-p(ku-1,i))/du
d1Ay = (Ay(ku,i)-Ay(ku-1,i))/du
d1At = (At(ku,i)-At(ku-1,i))/du
d2p  = (p(l,i)+p(l-2,i)-2.0d+0*p(l-1,i))/du**2.
d2Ay = (Ay(l,i)+Ay(l-2,i)-2.0d+0*Ay(l-1,i))/du**2.
d2At = (At(l,i)+At(l-2,i)-2.0d+0*At(l-1,i))/du**2.
pot  = ((Ay(l,i))**2.0/alph)
dp(l,i)  = (u**2.0)*(d2rp/alph+h*d2p-(u**2.0)*d1p-p(l,i)*(pot)) &
```

```
           +(2.0d+0)*(p(l,i)-d1p*u)
  dAy(l,i) = (u**2.0)*(d2rAy/alph+h*d2Ay-3.0d+0*u**2.0*d1Ay) &
            -p(l,i)**2.0*(Ay(l,i))
  dAt(l,i) = (h*u**2.0)*(d2rAt/alph+d2At) - At(l,i)*p(l,i)**2.0
  !~~~~~~~Boundary Flow~~~~~~~~~~~~~~~~~~~~~~~~~
  u=0.0d+0
  h=1.0d+0
  l=0
  if(i.eq.0)then
    d2rp  = (p(l,i)+p(l,i+2)-2.0d+0*p(l,i+1))/dr**2.
    d2rAy = (Ay(l,i)+Ay(l,i+2)-2.0d+0*Ay(l,i+1))/dr**2.
    d2rAt = (At(l,i)+At(l,i+2)-2.0d+0*At(l,i+1))/dr**2.
    elseif(i.eq.kr)then
    d2rp  = (p(l,i)+p(l,i-2)-2.0d+0*p(l,i-1))/dr**2.
    d2rAy = (Ay(l,i)+Ay(l,i-2)-2.0d+0*Ay(l,i-1))/dr**2.
    d2rAt = (At(l,i)+At(l,i-2)-2.0d+0*At(l,i-1))/dr**2.
    else
    d2rp  = (p(l,i+1)+p(l,i-1)-2.0d+0*p(l,i))/dr**2.
    d2rAy = (Ay(l,i+1)+Ay(l,i-1)-2.0d+0*Ay(l,i))/dr**2.
    d2rAt = (At(l,i+1)+At(l,i-1)-2.0d+0*At(l,i))/dr**2.
  endif
  d1p  = (p(ku+1,i)-p(ku,i))/du
  d1Ay = (Ay(ku+1,i)-Ay(ku,i))/du
  d1At = (At(ku+1,i)-At(ku,i))/du
  d2p  = (p(l+2,i)+p(l,i)-2.0d+0*p(l+1,i))/du**2.
  d2Ay = (Ay(l+2,i)+Ay(l,i)-2.0d+0*Ay(l+1,i))/du**2.
  d2At = (At(l+2,i)+At(l,i)-2.0d+0*At(l+1,i))/du**2.
  pot  = ((Ay(l,i))**2.0/alph)-(At(l,i)**2.0/(alph*h))
  dp(l,i)  = (u**2.0)*(d2rp/alph+h*d2p-(u**2.0)*d1p-p(l,i)*(pot)) &
           +(2.0d+0)*(p(l,i)-d1p*u)
  dAy(l,i) = (u**2.0)*(d2rAy/alph+h*d2Ay-3.0d+0*u**2.0*d1Ay) &
            -p(l,i)**2.0*(Ay(l,i))
  dAt(l,i) = (h*u**2.0)*(d2rAt/alph+d2At) - At(l,i)*p(l,i)**2.0
end do

end subroutine slope

end program FLOWSOLVE
```

# Bibliography


[1] P. Mikula, M. E. Carrington, and G. Kunstatter. Gradient flow in the Ginzburg-Landau model of superconductivity. *Phys. Rev.*, B94(18):184501, 2016.

[2] P. Mikula, M. E. Carrington, and G. Kunstatter. Nonequilibrium approach to holographic superconductors using gradient flow. *Phys. Rev.*, D, accepted June 2019.

[3] K A Müller and J G Bednorz. The discovery of a class of high-temperature superconductors. *Science (New York, N.Y.)*, 237(4819):1133,1139, 1987.

[4] Yoichi Kamihara, Takumi Watanabe, Masahiro Hirano, and Hideo Hosono. Iron-based layered superconductor la[o(1-x)f(x)]feas (x = 0.05-0.12) with t(c) = 26 k. *Journal of the American Chemical Society*, 130(11):3296,3297, 2008.

[5] J. Bardeen, L. N. Cooper, and J. R. Schrieffer. Theory of superconductivity. *Phys. Rev.*, 108:1175–1204, 1957.

[6] Leonard Susskind. The world as a hologram. *Journal of Mathematical Physics*, 36(11):6377–6396, 1995.

[7] Juan Martin Maldacena. The large N limit of superconformal field theories and supergravity. *Int.J.Theor.Phys.*, 38:1113–1133, 1999.

[8] P. K. Kovtun, D. T. Son, and A. O. Starinets. Viscosity in strongly interacting quantum field theories from black hole physics. *Phys. Rev. Lett.*, 94:111601, Mar 2005.

[9] M. F. Atiyah and R. Bott. The Yang-Mills equations over Riemann surfaces. *Philosophical Transactions of the Royal Society of London. Series A, Mathematical and Physical Sciences*, 308:523–615, 1983.

[10] Grisha Perelman. The entropy formula for the ricci flow and its geometric applications. *arXiv preprint math/0211159*, 2002.

[11] Nir Sochen, Ron Kimmel, and Ravi Malladi. A general framework for low level vision. *IEEE transactions on image processing*, 7(3):310–318, 1998.

[12] Luigi Malagò, Matteo Matteucci, and Giovanni Pistone. Towards the geometry of estimation of distribution algorithms based on the exponential family. In *Proceedings of the 11th workshop proceedings on Foundations of genetic algorithms*, pages 230–242. ACM, 2011.

[13] Romuald A. Janik. *The Dynamics of Quark-Gluon Plasma and AdS/CFT*, pages 147–181. Springer Berlin Heidelberg, Berlin, Heidelberg, 2011.

[14] Thomas Hertog and Kengo Maeda. Stability and thermodynamics of AdS black holes with scalar hair. *Physical Review D*, 71(2):024001, 2005.

[15] Peter Breitenlohner and Daniel Z Freedman. Stability in gauged extended supergravity. *Annals of Physics*, 144(2):249 – 281, 1982.

[16] Igor R Klebanov and Edward Witten. AdS/CFT correspondence and symmetry breaking. *Nuclear Physics B*, 556(1-2):89–114, 1999.

[17] Christopher P Herzog, Pavel Kovtun, Subir Sachdev, and Dam Thanh Son. Quantum critical transport, duality, and m theory. *Physical Review D*, 75(8):085020, 2007.

[18] Sean A Hartnoll, Christopher P Herzog, and Gary T Horowitz. Holographic superconductors. *Journal of High Energy Physics*, 2008(12):015, 2008.

[19] Matthew Headrick and Toby Wiseman. Ricci flow and black holes. *Class. Quant. Grav.*, 23:6683–6708, 2006.

[20] Ryuzo Kato, Yoshihisa Enomoto, and Sadamichi Maekawa. Effects of the surface boundary on the magnetization process in type-ii superconductors. *Phys. Rev. B*, 47:8016–8024, 1993.

[21] G.M. Eliashberg L.P. Gor'kov. Generalization of the Ginzburg-Landau equations for non-stationary problems in the case of alloys with paramagnetic impurities. *Soviet Physics JETP*, 27:328, 1968.

[22] A. Schmid. A time dependent Ginzburg-Landau equation and its application to the problem of resistivity in the mixed state. *Zeitschrift fur Physik B*, 5:302, 1966.

[23] Holger Bech Nielsen and P. Olesen. Vortex line models for dual strings. *Nucl.Phys.*, B61:45–61, 1973.

[24] H. J. de Vega and F. A. Schaposnik. Classical vortex solution of the abelian Higgs model. *Phys. Rev. D*, 14:1100–1106, Aug 1976.

[25] E. B. Bogomolny. Stability of classical solutions. *Sov. J. Nucl. Phys.*, 24:449, 1976. [Yad. Fiz.24,861(1976)].

[26] Arthur Jaffe and Clifford H Taubes. *Vortices and monopoles: structure of static gauge theories*. Birkhäuser, 1980.

[27] D. Stuart. Dynamics of abelian Higgs vortices in the near Bogomolny regime. *Comm. Math. Phys.*, 159(1):51–91, 1994.

[28] Igor Lukyanchuk, VM Vinokur, Andreas Rydh, R Xie, MV Milošević, Ulrich Welp, M Zach, ZL Xiao, GW Crabtree, SJ Bending, et al. Rayleigh instability of confined vortex droplets in critical superconductors. *Nature Physics*, 11(1):21, 2015.

[29] S Wolf, A Vagov, AA Shanenko, VM Axt, A Perali, and J Albino Aguiar. Bcs-bec crossover induced by a shallow band: Pushing standard superconductivity types apart. *Physical Review B*, 95(9):094521, 2017.

[30] A. V. Vagov, A. A. Shanenko, M. V. Milošević, V. M. Axt, and F. M. Peeters. Extended Ginzburg-Landau formalism: Systematic expansion in small deviation from the critical temperature. *Phys. Rev. B*, 85:014502, 2012.

[31] A. A. Shanenko, M. V. Milošević, F. M. Peeters, and A. V. Vagov. Extended Ginzburg-Landau formalism for two-band superconductors. *Phys. Rev. Lett.*, 106:047005, 2011.

[32] A. Vagov, A. A. Shanenko, M. V. Milošević, V. M. Axt, and F. M. Peeters. Two-band superconductors: Extended Ginzburg-Landau formalism by a systematic expansion in small deviation from the critical temperature. *Phys. Rev. B*, 86:144514, 2012.

[33] A. Vagov, A. A. Shanenko, M. V. Milošević, V. M. Axt, V. M. Vinokur, J. Albino Aguiar, and F. M. Peeters. Superconductivity between standard types: Multiband versus single-band materials. *Phys. Rev. B*, 93:174503, 2016.

[34] A. A. Abrikosov. On the magnetic properties of superconductors of the second group. *Sov. Phys. JETP*, 5:1174–1182, 1957. [Zh. Eksp. Teor. Fiz.32,1442(1957)].

[35] S Gustafson and IM Sigal. The stability of magnetic vortices. *arXiv preprint math/9904158*, 1999.

[36] Qi Tang and S Wang. Time dependent Ginzburg-Landau equations of superconductivity. *Physica D: Nonlinear Phenomena*, 88(3-4):139–166, 1995.

[37] Charles P. Poole, Ruslan Prozorov, Horacio A. Farach, and Richard J. Creswick. *Superconductivity*. Elsevier, third edition edition, 2014.

[38] Laurence Jacobs and Claudio Rebbi. Interaction energy of superconducting vortices. *Physical review B*, 19(9):4486, 1979.

[39] V. A. Schweigert and F. M. Peeters. Phase transitions in thin mesoscopic superconducting disks. *Phys. Rev. B*, 57:13817–13832, 1998.

[40] V. A. Schweigert and F. M. Peeters. Flux penetration and expulsion in thin superconducting disks. *Phys. Rev. Lett.*, 83:2409–2412, 1999.

[41] Markus Heusler. No-hair theorems and black holes with hair. *arXiv preprint gr-qc/9610019*, 1996.

[42] Sean A. Hartnoll, Christopher P. Herzog, and Gary T. Horowitz. Building a holographic superconductor. *Phys.Rev.Lett.*, 101:031601, 2008.

[43] Ville Keranen, Esko Keski-Vakkuri, Sean Nowling, and K. P. Yogendran. Inhomogeneous structures in holographic superfluids: I. dark solitons. *Phys. Rev.*, D81:126011, 2010.

[44] Oriol Domènech, Marc Montull, Alex Pomarol, Alberto Salvio, and Pedro J. Silva. Emergent gauge fields in holographic superconductors. *Journal of High Energy Physics*, 2010(8):33, 2010.

[45] Kengo Maeda and Takashi Okamura. Vortex flow for a holographic superconductor. *Phys. Rev.*, D83:066004, 2011.

[46] Tameem Albash and Clifford V. Johnson. Vortex and droplet engineering in holographic superconductors. *Phys. Rev.*, D80:126009, 2009.

[47] Andrey Chaves, F. M. Peeters, G. A. Farias, and M. V. Milošević. Vortex-vortex interaction in bulk superconductors: Ginzburg-Landau theory. *Phys. Rev. B*, 83:054516, 2011.

[48] Chao-Yu Liu, G. R. Berdiyorov, and M. V. Milošević. Vortex states in layered mesoscopic superconductors. *Phys. Rev. B*, 83:104524, 2011.

[49] M. M Doria, A. R. de C Romaguera, M. V Milošević, and F. M Peeters. Threefold onset of vortex loops in superconductors with a magnetic core. *Europhysics Letters (EPL)*, 79(4):47006, 2007.

[50] G. R. Berdiyorov, M. M. Doria, A. R. de C. Romaguera, M. V. Milošević, E. H. Brandt, and F. M. Peeters. Current-induced cutting and recombination of magnetic superconducting vortex loops in mesoscopic superconductor-ferromagnet heterostructures. *Phys. Rev. B*, 87:184508, 2013.

[51] Egor Babaev and Martin Speight. Semi-meissner state and neither type-i nor type-ii superconductivity in multicomponent superconductors. *Phys. Rev. B*, 72:180502, 2005.

[52] A. Chaves, L. Komendová, M. V. Milošević, J. S. Andrade, G. A. Farias, and F. M. Peeters. Conditions for nonmonotonic vortex interaction in two-band superconductors. *Phys. Rev. B*, 83:214523, 2011.

[53] M. V. Milošević and A. Perali. Emergent phenomena in multicomponent superconductivity: an introduction to the focus issue. *Superconductor Science Technology*, 28(6):060201, 2015.

[54] L. Komendová, Yajiang Chen, A. A. Shanenko, M. V. Milošević, and F. M. Peeters. Two-band superconductors: Hidden criticality deep in the superconducting state. *Phys. Rev. Lett.*, 108:207002, 2012.

[55] R. M. da Silva, M. V. Milošević, D. Domínguez, F. M. Peeters, and J. Albino Aguiar. Distinct magnetic signatures of fractional vortex configurations in multiband superconductors. *Applied Physics Letters*, 105(23):232601, 2014.

[56] E J Brynjolfsson, U H Danielsson, L Thorlacius, and T Zingg. Holographic superconductors with lifshitz scaling. *Journal of Physics A: Mathematical and Theoretical*, 43(6):065401, 2010.